

2012-07-23

Approach to ease design criteria of a real-time model used in a VR training system considering constraints of human perception

Widmer, Antoine

Widmer, A. (2012). Approach to ease design criteria of a real-time model used in a VR training system considering constraints of human perception (Doctoral thesis, University of Calgary, Calgary, Canada). Retrieved from <https://prism.ucalgary.ca>. doi:10.11575/PRISM/24980
<http://hdl.handle.net/11023/130>

Downloaded from PRISM Repository, University of Calgary

THE UNIVERSITY OF CALGARY

Approach to Ease Design Criteria of a Real-Time Model Used in a VR
Training System Considering Constraints of Human Perception

by

Antoine Widmer

A DISSERTATION

SUBMITTED TO THE FACULTY OF GRADUATE STUDIES
IN PARTIAL FULFILLMENT OF THE REQUIREMENTS FOR THE
DEGREE OF DOCTOR OF PHILOSOPHY

DEPARTMENT OF ELECTRICAL AND COMPUTER ENGINEERING

CALGARY, ALBERTA

July, 2012

© Antoine Widmer 2012

Abstract

Virtual reality (VR) systems have potential of contributing to the training of medical students in a variety of procedures. This thesis focuses on a design issue related to developing VR training systems for soft tissue (e.g., breast phantom) palpation. In such a VR system, it is paramount to provide a real-time model that simulates physical behavior of an actual breast phantom. However, it is difficult to design such a real-time model with high accuracy due to time and physical constraints. To mitigate this difficulty, I consider constraints of human perception which is insensitive to small discrepancies of objects during real-time interaction. Such consideration could aid to relax design criteria of the real-time model by achieving its accuracy at a certain degree while keeping human perception of object softness unchanged. Therefore, I take a two-step approach to determine visual and haptic (pertinent to force feedback) discrepancies tolerable for this human perception. In the first step, an evaluation method is developed to compute discrepancies of the real-time model for visual displacement and force feedback, compared to its finite element method counterpart featuring physical parameters of a breast phantom. The computation uses statistical analyses which like human perception are insensitive to small discrepancies of datasets. In the second step, two studies are performed to examine the constraints of human perception. The first study reexamined raw data from my MSc work to understand the effect of three popular alignments between a visual display and a haptic device on the human perception of object softness. This study serves to select an alignment producing the least perceptual illusion and physical workload for palpation. Using the evaluation method and the selected alignment, the second study investigates the effect of different discrepancies on the human perception of object softness. It is observed that this perception is insensitive to small discrepancies up to a threshold of 11.0% and 6.3% for visual displacement and force feedback,

respectively. This indicates that a real-time model yielding discrepancies of visual displacement and force feedback below their respective thresholds could be sufficient for simulating a soft tissue (such as a breast phantom) during palpation.

Acknowledgements

I would like to acknowledge to all people who helped me in the past two years during my study and generally in my life. I would like to express my sincere gratitude and acknowledgement to my supervisor, Dr. Yaoping Hu, for trusting my ability of accomplishing the study, for helping me identifying aspects to improve, and for her good advice on both my research and professional development.

I thank the members of my supervisory committee including Dr. Behrouz Far and Dr. Diwakar Krishnamurthy and the members of my examining committee Dr. Vahid Garousi, Dr. Salvatore Federico and Dr. Vincent Hayward for their time and consideration for my research.

In addition, I extend my appreciation to Dr. Qiao Wei, Kan Lo, Simon Ferrari and Chris Millette - my research colleagues. They have always provided me good comment, advice and general knowledge. More importantly, they have provided me with a jovial working environment.

Special thanks go to all my friends in Canada especially Jeremie and Petra Bourqui and in Switzerland (my home country) who have always provided me gracious supports and helps in general.

Finally, I would like to thank all my family: my parents Michel and Monique, my brother Laurent and all his family; my sister Anne and her family and last but not least my girlfriend Michèle Roethlisberger. Without their constant love, support and encouragement, I would not have achieved where I am today.

To my family.

Your support means everything.

God bless you.

Table of Contents

Approval Page	ii
Abstract	iii
Acknowledgements	v
Table of Contents	vii
List of Tables	x
List of Figures	xii
1 Introduction	1
1.1 Research Challenges and Thesis Objective	4
1.2 Contribution and Thesis Organization	6
2 Literature Review	11
2.1 Introduction	11
2.2 Medical VR Training Systems for Palpation	11
2.3 Evaluation of Computational Models	12
2.3.1 Comparison to a FEM Model	13
2.3.2 Comparison to an Actual Object	13
2.3.3 Comparison Metrics	14
2.3.4 Summary	15
2.4 Computational Models	15
2.4.1 Real-Time Models	16
2.4.2 Collision Detection	19
2.4.3 Collision Response	20
2.5 Constraints of Human Perception Constraints	21
2.5.1 Combination of Vision and Touch	22
2.5.2 Effect of Alignments between a Visual Display and an Haptic Device	23
2.5.3 Human Constraints for Perception of Object Softness during Real- Time Palpation	25
2.6 Summary	28
3 Statistical Evaluation of a Real-Time Model	30
3.1 Introduction	30
3.2 Evaluation Method	32
3.2.1 Data Acquisition	33
3.2.2 Data Processing	36
3.3 Case Study	40
3.3.1 Real-Time Model	40
3.3.2 Evaluation Method	49

3.3.3	Results	51
3.3.4	Discussion	54
3.4	General Discussion	56
3.5	Summary	57
4	Effect of the Alignment between a Visual Display and Haptic Device on the Perception of Object Softness	59
4.1	Introduction	59
4.2	Methodology	61
4.2.1	Participants	61
4.2.2	Apparatus	61
4.2.3	Stimuli	62
4.2.4	Procedures	64
4.2.5	Data Analysis	66
4.3	Results and Discussion	67
4.3.1	“Same-location” Alignment	67
4.3.2	Vertical Alignment	70
4.3.3	Horizontal Alignment	74
4.4	General Discussion	77
4.4.1	Subjective Perception versus Objective Measurements	78
4.4.2	Advantage of “Same-Location” Alignment	80
4.4.3	Application	80
4.5	Summary	82
5	Human Constraints for Softness Perception during Real-Time Palpation	83
5.1	Introduction	83
5.2	Variation Computation	84
5.2.1	Real-Time Model	85
5.2.2	Data Acquisition	86
5.2.3	Data Processing	88
5.2.4	Results	90
5.2.5	Discussion	93
5.3	Human Study	94
5.3.1	Methodology	94
5.3.2	Results and Discussion	100
5.4	General Discussion	108
5.4.1	Variation Computation vs. Human Perception	108
5.4.2	Relation to Existing Human Studies	110
5.4.3	Applications	111
5.5	Summary	112
6	Conclusion and Future Work	113
6.1	Summary and Contribution	113
6.2	Future Work	116

6.2.1	Incorporation of Other Human Constraints	116
6.2.2	New Haptic Device for Palpation	116
6.2.3	VR Training System for Clinical Breast Examination	117
6.3	Final Remarks	118
Bibliography		119
A Requirements in VR Systems: The REVIR Approach and its Preliminary Evaluation		132
A.1	Introduction	132
A.2	Abstract	132
B Results of The Second Experiment with Force Application on The Side		134
B.1	Introduction	134
B.2	Variation Computation Results	135
B.2.1	One-Finger Palpation	135
B.2.2	Two-Finger Palpation	137
B.3	Human Study Results	138
B.3.1	Subjective Perception	138
B.3.2	Objective Measurements	142
B.4	Summary	145
C Sample Size for a Within-Subject Human Study		146
D University of Calgary Ethics Approval		147
E Copyright Transfers		149

List of Tables

2.1	Comparison of computational models for matching the criteria of a VR system for palpation training.	18
2.2	Ability of collision detection algorithms to match the criteria for the creation of the VR system for palpation training.	19
2.3	Abilities of algorithms of collision response to match the criteria for the creation of the VR system for palpation training.	20
3.1	Surface parameters extracted from literature.	46
3.2	Inside gel parameters extracted from literature.	46
3.3	Surface parameters for the real-time simulation.	47
3.4	Inside gel parameters for the real-time simulation.	47
3.5	Condition I – Visual displacement comparison [$F^* = F(1, 135199)$]. . . .	52
3.6	Condition I – Force feedback comparison [$F^* = F(1, 9199)$].	52
3.7	Condition II – Visual displacement comparison [$F^* = F(1, 135199)$]. . . .	52
3.8	Condition II – Force feedback comparison [$F^* = F(1, 9199)$].	52
3.9	Condition III – Visual displacement comparison [$F^* = F(1, 135199)$]. . .	53
3.10	Condition III – Force feedback comparison [$F^* = F(1, 9199)$].	53
3.11	Condition IV – Visual displacement comparison [$F^* = F(1, 135199)$]. . .	54
3.12	Condition IV – Force feedback comparison [$F^* = F(1, 9199)$].	54
4.1	Results of one-way ANOVA and Tukey-test for the effects of testing condition on maximum force under “same-location” alignment.	69
4.2	Results of one-way ANOVA and Tukey-test for the effects of testing condition on maximum pressing depth in Experiment I.	70
4.3	Results of one-way ANOVA and Tukey-test for the effects of testing condition on maximum force under vertical alignment.	72
4.4	Results of one-way ANOVA and Tukey-test for the effects of testing condition on maximum pressing depth under vertical alignment.	73
4.5	Results of ANOVA analysis and Tukey-test for the effects of testing condition on maximum force under horizontal alignment.	75
4.6	Results of ANOVA and Tukey-test for the effects of testing condition on maximum pressing depth under horizontal alignment.	76
5.1	Comparisons of visual displacement under one-finger palpation.	90
5.2	Comparisons of force feedback under one-finger palpation.	90
5.3	Comparisons of visual displacement under two-finger palpation.	92
5.4	Comparisons of force feedback under two-finger palpation.	92
5.5	Results of One-Way ANOVA and Pairwise Contrasts for the effect of paired comparison of force distributions on subjective perception under One-Finger palpation.	102
5.6	Results of one-way ANOVA and pairwise contrasts for the effect of testing conditions on subjective perception of object softness under one finger palpation.	102

5.7	Results of one-way ANOVA and pairwise contrast for the effect of force distribution on objective measurement of maximum force under two-finger contact.	106
B.1	Visual displacement comparison computed under one-finger palpation on the side of the phantom.	136
B.2	Force feedback comparison computed under one-finger palpation on the side of the phantom.	137
B.3	Visual displacement comparison computed under two-finger palpation on the side of the phantom.	138
B.4	Force feedback comparison computed under two-finger palpation on the side of the phantom.	138
B.5	Results of One-way ANOVA and pairwise contrasts for the effect of force distributions on subjective perception of object softness palpated under one-finger palpation on the side of the phantom.	139
B.6	Results of One-way ANOVA and pairwise contrasts for the effect of force distribution on subjective perception of object softness palpated under two-finger palpation on the side of the phantom.	140
B.7	Results of One-way ANOVA and pairwise contrasts for the effect of testing conditions on maximum pressing depth palpated under one-finger palpation on the side of the phantom.	142
B.8	Results of One-way ANOVA and pairwise contrast for the effect of testing conditions on maximum pressing depth palpated under two-finger palpation on the side of the phantom.	144
B.9	Results of One-way ANOVA for the effect of force distribution on subjective perception of object softness palpated under two-finger palpation on the side of the phantom.	144

List of Figures

1.1	Breast phantom shaped as a hemisphere and made of silicone gel with two palpating fingers.	2
1.2	Challenges and organization of the thesis.	6
3.1	Flow diagram of the evaluation method.	32
3.2	One-finger contact area (a). Locations (b) and (c) correspond to two different centers of contact force.	34
3.3	Force distributions; (a) Distribution 1 features only one node contact; (b) Distribution 2 involves an uniform force through the contact area; (c) Distribution 3 simulates a finger palpation; (d) Distribution 4 mimics a slanted finger palpation.	35
3.4	Real-time model simulating a breast phantom.	40
3.5	Burger's model used to simulate the surface membrane.	41
3.6	FEM model representing a breast phantom.	46
3.7	Force profile applied to palpate the breast phantom.	47
3.8	Interaction Condition; (a) Condition I features a one-finger contact on the top of the phantom; (b) Condition II involves a two-finger contact on the top of the phantom; (c) Condition III simulates one-finger contact on the side of the phantom; (d) Condition IV mimics a two-finger contact on the side of the phantom.	49
3.9	Two fingers palpation.	50
4.1	The three tested alignments between a visual display and haptic device. (a) "Same-location" alignment; (b) Vertical alignment; (c) Horizontal alignment; (1) Haptic device; (2) Stereoscopic goggle; (3) 3D display; (4) First-surface mirror.	60
4.2	Presentation of deformable balls as visual stimuli. (a) Illustration of viewing angles and pressing areas. (b) A ball at the viewing angle of 0° as reference. (c) A ball at the viewing angle of - 15° for testing.	63
4.3	The correspondence of compliance between the force from the haptic device and the force to deform a ball. [Within the force range of the haptic device from 0.0 N to 3.0 N, the world force was scaled by a factor of 1.2 to match the haptic force. This correspondence was independent of the viewing angle of the ball and the location of the haptic device.]	64
4.4	Definition of objective measurements. (a) Maximum force; (b) Maximum pressing depth.	65
4.5	Objective measurements of maximum force under "same-location" alignment. [Error bars represent standard errors.]	68
4.6	Objective measurements of maximum pressing depth in Experiment I. [Error bars represent standard errors.]	69
4.7	Objective measurements of maximum force under vertical alignment. [Error bars represent standard errors.]	71

4.8	Objective measurements of maximum pressing depth under vertical alignment. [Error bars represent standard errors.]	73
4.9	Objective measurements of maximum force under horizontal alignment. [Error bars represent standard errors.]	75
4.10	Objective measurements of maximum pressing depth under horizontal alignment. [Error bars represent standard errors.]	76
5.1	Representation of a virtual breast phantom and palpation scenarios: (a) side view of the virtual phantom; (b) one-finger palpation using the index finger; (c) two-finger palpation using both index and middle fingers. . . .	86
5.2	Virtual index and middle fingers with shaded finger contact areas (the palm faces to the reader).	87
5.3	Finger position and holding posture on the stylus of the haptic device for palpation. (a) Under one-finger palpation; (b) Under two-finger palpation. . . .	96
5.4	Subjective perception of object softness during one-finger palpation. [Error bars represent standard errors.]	101
5.5	Subjective perception under two-finger palpation. [Error bars represent standard errors.]	103
5.6	Objective measurement of maximum pressing depth under one-finger palpation. [Error bars represent standard errors.]	105
5.7	Objective measurement of maximum force under one-finger palpation. [Error bars represent standard errors.]	105
5.8	Objective measurement of maximum pressing depth under two-finger palpation. [Error bars represent standard errors.]	106
5.9	Objective measurement of maximum force under two-finger palpation. [Error bars represent standard errors.]	106
B.1	Representation of a virtual breast phantom and palpation scenarios: (a) side view of the virtual phantom; (b) one-finger palpation using the index finger; (c) two-finger palpation using both index and middle fingers. . . .	135
B.2	Subjective perception of object softness under one-finger palpation on the side of the phantom. Error bars represent standard errors.	139
B.3	Subjective perception of object softness under two-finger palpation on the side of the phantom. Error bars represent standard errors.	140
B.4	Objective measurement of maximum pressing depth under one-finger palpation on the side of the phantom. Error bars represent standard errors. . . .	141
B.5	Objective measurement of maximum force under one-finger palpation on the side of the phantom. Error bars represent standard errors.	142
B.6	Objective measurement of maximum pressing depth under two-finger palpation on the side of the phantom. Error bars represent standard errors. . . .	143
B.7	Objective measurement of maximum force under two-finger palpation on the side of the phantom. Error bars represent standard errors.	144

Chapter 1

Introduction

For a more than a decade, virtual reality (VR) has provided valuable support for the training of medical students and professionals in a variety of medical procedures [1]. By providing means for simulating real-time visualization of and interaction with organs or body parts (e.g., lungs, breasts), a VR training system can allow surgeons, doctors, etc. to practice medical procedures. Furthermore, VR training systems automatically present a detailed evaluation of user performance during the procedure. Also, computerized VR training systems could save costs that would occur when acquiring physical phantoms of human organs or body parts. Medical VR training systems use stereoscopic displays for real-time visualization of soft tissues and a force feedback (haptic) device for simulating the user's sense of touch by rendering force feedback to the user's hand in real time. For example, a VR training system could provide a good alternative to physical training system for soft-tissue palpation training using a phantom.

Palpation consists of applying force through fingers to assess the health of soft tissues, such as those in the breast [2]. As illustrated in Fig. 1.1, medical students learn breast palpation using hemispheric phantoms made of silicone gels. Using these phantoms, students apply force to a contact area using the distal section of their fingers. Generally, they only use the index finger or both index and middle fingers during palpation [2]. Under the force applied to the contact area, the phantom deforms showing a visual displacement and offers resistance to the finger as force feedback. This combination of visual displacement and force feedback exhibited by the phantom simulates the general mechanical behaviour of a real breast. Unfortunately, such phantoms were found not to be effective in improving the palpation skills of medical students [3]. This is due mainly



Figure 1.1: Breast phantom shaped as a hemisphere and made of silicone gel with two palpating fingers.

to the lack of performance feedback given to the students, such as describing the applied force.

As a suitable alternative, especially with respect to providing adequate performance feedback, a VR training system that can simulate palpation could potentially improve the training of medical students. However, to ensure the learning outcome of such a system, it is important to warrant the physical behavior over time of a computational model capable of simulating the general mechanical behaviour of an actual soft tissue. In the case of a breast phantom, the computational virtual phantom must show softness with viscoelastic and hyperelastic characteristics. These two characteristics replicate the general mechanical behaviour of an actual breast phantom that the user can see and touch in a VR training system. Combining stereoscopic visualization and haptic (force) feedback for interaction, the VR training system is encountered with two different refresh rates for visualization and force feedback, respectively. When using a conventional frame-rendering monitor, the minimum refresh rate to display visual information for both human eyes is 120 Hz, whereas the minimum refresh rate for the haptic device (pertinent to force feedback) is about 1000 Hz [4]. These different refresh rates constrain the development of computational models of soft tissues for real-time interaction. Therefore, most of the research to improve real-time computational models aims at either improving

their accuracy or their rendering speed [5]. The more accurate a model, the more time is needed for its computation. In this thesis, I aim at investigating an approach which would permit to strike a balance between the accuracy and rendering speed of a real-time model, while taking into consideration human perception of object softness. Human perception refers to the process used by humans to gain consciousness of the world around them [6]. This investigation is the first step toward the creation of a VR system for training palpation.

In this context, multiple studies have shown that humans are subject to constraints preventing them from perceiving object softness consistently under various interaction scenarios, especially during interaction with a VR system that includes a visual display and/or force feedback device [7, 8]. These studies observed that humans had difficulties keeping track of object collisions when facing a large number of moving objects [7]; and that they could misjudge object softness when two object of same softness are placed at different vertical locations [8]. This shows the possibility to take into account constraints of human perception for easing the design criteria of a real-time model used for palpation in a VR training system. Some evaluation methods are currently available for assessing the accuracy of computational models that simulate actual soft tissues in a VR system [9, 10]. However, it seems that these methods do not consider any constraints of human perception. The lack of consideration of these constraints can lead to inaccurate perception that possibly affects the learning outcome offered by a VR training system. Therefore, research is needed to investigate a new approach considering constraints of human perception to ease design criteria of a real-time model used in a VR training system without introducing perceptual illusions.

1.1 Research Challenges and Thesis Objective

To carry out this research, the investigation of a new approach that considers human constraints when perceiving object softness needs to address four research challenges.

Challenge I encompasses the development of a new evaluation method to assess spatial and temporal behaviour of a relatively simple real-time model to be used for user interaction in a VR system that considers human constraints. In a VR training system, real-time models must realistically simulate spatial and temporal behaviours of virtual objects based on the behaviour of an actual soft object. Some evaluation methods of real-time models exist to verify the differences of the behaviours of these models compared to their Finite Element Method (FEM) counterparts using physical parameters [9, 10]. Unfortunately, none of these methods takes the approach of considering human constraints when perceiving object softness. Therefore the challenge is to develop an evaluation method that takes into account human constraints during the perception of object softness.

Challenge II focuses on the development of a real-time model to be used as an example to demonstrate the feasibility of the evaluation method. Based on the current state-of-the-art technologies, real-time models still have difficulties to simulate viscoelastic soft tissues with accuracy in a timely manner (100Hz for visual feedback and 1000Hz for force feedback) [4]. This implies that there is a need to provide an alternative solution for developing a real-time model showing viscoelastic behaviour with decreased accuracy measurements and increased rendering speed based on constraints of human perception. Focusing on the human constraints for perceiving object softness, the challenge is to develop a real-time model based on existing technologies that features a fast rendering speed enabled through a reduced model complexity and acceptable model accuracy.

Challenge III and Challenge IV are related to the investigation of human constraints associated to the perception of object softness. The goal of this investigation is to

examine how the development of VR training systems could utilize such constraints. To achieve this goal, two different aspects of human constraints need to be investigated. At first, Challenge III explores the effect of spatial alignment between a visual display and a haptic device on the perception of object softness. In the literature, researchers have used different alignments between a visual display and a haptic device in VR simulations [8, 11, 12]. In meeting this challenge, I have developed a human study to investigate the effect of different alignments between a visual display and a haptic on perception of object softness and physical workload during interaction.

Secondly, using the alignment that is found in meeting Challenge III to produce the least perceptual illusions and physical workload during interacting with soft objects, Challenge IV investigates possible perception insensitivities to subtle variations of visual displacement and force feedback produced by a soft real-time model under palpation. The investigation features two complementary analyses: variation computation and human study. Variation computation quantifies the differences of visual displacement (visual information) and force feedback (haptic information) produced by four different force distributions on a contact area of a palpated soft object. The human study examines the hypothesis that the human perception of object softness is insensitive to some of these theoretical variation levels.

To meet all these challenges, **the objective of this thesis is to investigate a new approach that considers the constraints of human perception of object softness to ease design criteria for real-time models used in VR training systems for palpation.** This investigation could open a new approach of reducing complexity of the real-time models while ensuring no loss in terms of human perception.

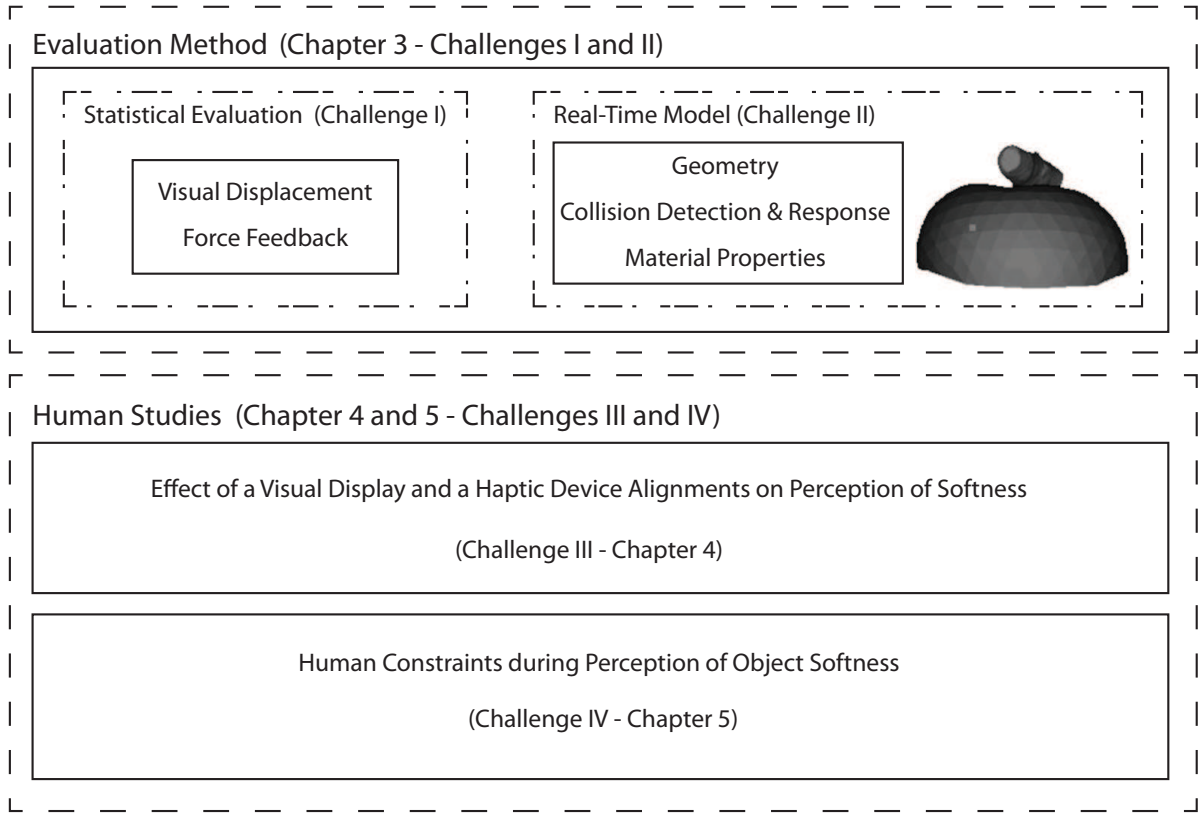


Figure 1.2: Challenges and organization of the thesis.

1.2 Contribution and Thesis Organization

This thesis aims at the investigation of a new approach that considers the constraints of human perception of object softness to ease design criteria for real-time models used in VR systems for training palpation. The thesis outline and the relation of all chapters to research challenges are illustrated in Fig. 1.2. Three major chapters present the contributions of this thesis:

1. **Statistical Evaluation of a Real-Time Model (Chapter 3)** – I proposed a method for evaluating real-time models that take into account constraints occurring in the human perception of object softness (Challenge I). Based upon different interaction scenarios, the evaluation method compared a real-time model with a FEM model featuring physical parameters. The comparison consisted of two statistical tools – Analysis of variance and Bland and Altman agreement method [13]–

to assess the differences between visual displacement and force feedback, respectively. As part of a case study to demonstrate advantages provided by the method, I modified a real-time model based on the one in my previous master's thesis work (Challenge II). The real-time model featured a surface mesh with a state equation simulating a gas encompassed within the surface mesh. This model achieved real-time simulation due to its relative computational simplicity. Compared to a FEM model with physical parameters, the correct match of the real-time model is verified for both visual displacement over time on the entire mesh and force feedback on a contact area, by applying the presented evaluation method. This work has been published in peer-reviewed conference publications as follows:

A. Widmer and Y. Hu, (full-paper submission for review), “Statistical comparison between a real-time model and a FEM counterpart for visualization of breast phantom deformation during palpation,” *Proceedings of the 23rd Canadian Conference on Electrical and Computer Engineering (CCECE)*, 4 pages on CD-ROM, Calgary, AB, Canada, May 2010.

A. Widmer and Y. Hu, (full-paper submission for review), “A viscoelastic model of a breast phantom for real-time palpation,” *Proceedings of the 33rd Annual International Conference of the IEEE Engineering in Medicine and Biology Society (IEEE-EMBC)*, pp. 4546-4549, Boston, MA, USA, August 2011.

A. Widmer and Y. Hu, (full-paper submission for review), “An evaluation method for real-time soft-tissue model used for multi-vertex palpation,” *Proceedings of the IEEE International Conference on Systems, Man, and Cybernetics (IEEE-SMC)*, pp. 127-132, Anchorage, AK, USA, October 2011.

In addition, a journal manuscript of this work has been submitted to a leading journal - the ACM Transactions on Modeling and Computer Simulation and is accepted for publication:

A. Widmer and Y. Hu, (22 single pages submitted on December 22, 2011; reference number #: TOMACS-2011-0142.R1), “An evaluation method for a real-time simulation of a viscoelastic phantom based on constraints of human perception,” ACM Transactions on Modeling and Computer Simulation.

2. **Effects of Hardware Alignments on Human Perception of Object Softness (Chapter 4)** – A critical aspect of VR training systems is to present both visual and haptic information accurately to avoid perceptual illusions (e.g. to properly distinguish the softness of tissues). Using three different hardware alignments between a visual display and haptic device widely used in VR systems, I reanalysed data gathered from a human study to investigate the effect of viewing angles on human perception of object softness during my M.Sc. work. In this chapter, I studied the influence of each alignment on the perception of object softness (Challenge III). To carry out this study, I re-examined raw data from my M.Sc. work for the following dependent measurements: subject perception of object softness and new objective measurements of maximum force and maximum pressing depth. As results, the study showed that a “same-location” alignment offers comparable subjective perception as vertical and horizontal alignments with smaller force magnitude applied (that is, lower physical workload). This observation revealed that a “same-location” alignment facilitates user interaction with soft objects. Part of this work has been published in the flagship IEEE international conference on virtual reality as follows:

A. Widmer and Y. Hu, (full-paper submission for review), “Subjective perception and objective measurements in perceiving object softness for VR surgical systems,” *Proceedings of IEEE Virtual Reality Conference 2009*, pp.267-268, Lafayette, LA, USA, March 2009.

In addition, a journal paper of this study is published in the mainstream journal - IEEE Transactions on Systems, Man and Cybernetics, Part A: Systems and Humans:

A. Widmer and Y. Hu, “Effects of the alignment between a haptic device and visual display on the perception of object softness,” *IEEE Transactions on Systems, Man and Cybernetics, Part A: Systems and Humans*, vol.40, no.6, pp.1146-1155, November 2010.

3. **Human Constraints for Softness Perception during Real-Time Palpation**

(Chapter 5) – An issue of VR training systems for training palpation is to assess contact definitions between the finger(s) and virtual soft tissues (e.g. the breast phantom) during real-time palpation, because contact definitions might affect the softness perception of the phantom. Considering visual and haptic information derived from the phantom, I hypothesized that the human perception of object softness is insensitive to small discrepancies of the information. I conducted two complementary analyses to verify this hypothesis. In the first analysis, I computed variation levels of visual displacement on the meshed nodes of the phantom and force feedback derived from the meshed nodes within a contact area on the phantom, respectively. This computation was conducted among paired comparisons of four force distributions under two contact definitions. In the second analysis, I undertook a human study to determine a variation level of insensitivity under the same force distributions. Both analyses revealed that the perception of object

softness is insensitive up to a variation level of 11.0% for visual displacement and of 6.3% for force feedback. These levels of insensitivities have implications for easing design criteria of real-time models when creating VR training systems for palpation. Part of this work has been published in the mainstream IEEE international conference as follows:

A. Widmer and Y. Hu, (full-paper Accepted on May 25, 2012; paper number #: 91), "Difference of object softness perception during palpation through single-node and multi-node contacts," Proceedings of the 34rd Annual International Conference of the IEEE Engineering in Medicine and Biology Society (IEEE-EMBC), San Diego, CA, USA, August 2012.

In addition, a journal manuscript from this study is submitted to the reputable journal - IEEE Transactions on Haptics:

A. Widmer and Y. Hu, (12 double column pages submitted on June 5, 2012; submission number #: TH-2012-06-0042), "Human Constraints for Softness Perception during Real-Time Palpation," IEEE Transactions on Haptics.

The rest of this thesis is arranged into 5 chapters. Chapter 2 introduces the background information and state-of-the-art that led to the thesis work. Chapter 3 to Chapter 5 describe my contributions to research and the methods used to achieve the objective of this thesis. Chapter 6 summarizes this thesis and presents future work.

Chapter 2

Literature Review

2.1 Introduction

As described in Chapter 1, the objective of this thesis is to investigate a new approach aiming at easing design criteria of a real-time model by considering human constraints when perceiving an object's softness. In the current chapter, I will present the background information and state-of-the-art technologies associated to the four challenges introduced in Chapter 1. First, I will present various VR training systems used for medical applications that use computational models for user interaction. Secondly, I will present different methods used to evaluate real-time computational models and demonstrate the lack of available methods when considering the constraints of human perception. Thirdly, I will discuss computational models available for interaction in a VR training system. These models must be able to simulate the deformation behavior of a soft tissue during palpation in real time. Finally, I will review literature about human constraints when perceiving and interacting with an object's softness using the sense of sight and/or the sense of touch.

2.2 Medical VR Training Systems for Palpation

Offering advantages over current training systems for palpation, VR systems could allow repetitive practice and log the practice for objective assessments of learning. In this context, a few research groups have focused their efforts on the development of VR systems for palpation simulation [14, 15, 16]. Dinsmore *et al.* attempted to create a VR system for simulating human liver palpation [14]. Due to the relatively time-consuming

force computation, they computed the force required to deform the liver offline (before interaction) and rendered the feel of this force through a pair of force feedback gloves. However, there was a lack of extensive testing on the accuracy of the touch; and a temporal delay existed during the interaction of palpating the liver. Chen *et al.* [15] presented a system for real-time visualization of muscle palpation. However, this method cannot be directly applied to viscoelastic soft-tissues such as the breast, because muscles appear to undergo much smaller deformation than a breast during palpation. As a result, it is difficult to transfer their system to simulate breast palpation. Daniulaitis *et al.* [16] developed a system for teaching breast palpation. However, they could not visualize breast deformation in real time without sacrificing the number of vertices on the mesh used for simulating the breast geometry. Consequently, the breast geometry was not realistic enough for visualization.

In short, research efforts have been carried out to develop VR systems for palpation simulation. However, no acceptable VR system for palpation simulation is available due to multiple challenges that prevent real-time interaction from occurring.

2.3 Evaluation of Computational Models

An evaluation method, assessing real-time models by considering the constraints of human perception of object softness, is necessary to warrant the learning outcomes of such VR systems. In particular, evaluation should ensure that the simulation of a real object provides the similar deformation behavior as the real object does under applied force. The evaluation needs to check: (1) the visual displacement (i.e., the deformation) of a virtual object under applied force, and (2) the force feedback computed by a model during the interaction. Many computational models are currently created for applications. It is important to know what model is suitable for a specific application in terms of its accuracy. Some researchers have proposed different methods to address this problem.

This section summarizes some interesting work done on these methods.

2.3.1 Comparison to a FEM Model

On a meshed geometry of an object, current methods usually evaluate computational models by comparing the visual displacement (deformation) of a subset of meshed nodes between the models under study and their offline FEM counterparts [17, 18]. For example, Sedef *et al.* used a Finite Element Method model featuring linear viscoelasticity to compare their real-time model of the human liver. They applied force on a single node and recorded the visual displacement and force feedback from a subset of the meshed nodes that they used to create a cube. Their evaluation only considers single-node contact. However single-node contact does not simulate a normal palpation that applies force on a surface like a finger would. In addition, the results of their evaluation might be misleading as they compared displacement and force feedback on a cube featuring physical parameters of an actual human liver. Using a cube instead of an actual human liver shape could produce different results of visual displacement and force feedback due to different mesh topologies.

2.3.2 Comparison to an Actual Object

Other evaluation methods compare the location of selected nodes on a meshed geometry of an object computed by a real-time model to experimental data acquired from markers carefully positioned on a real counterpart [9, 10]. For example, Kerdok et al. proposed a method that only compared internal displacement in a real-time model simulating a soft-tissue to its physical equivalent [10]. In addition, their method needs expensive equipment to run the comparison. This makes replication of the method difficult.

2.3.3 Comparison Metrics

Some researchers have reported various metrics to compare different models [19, 20]. These metrics are able to evaluate real-time models with respect to a model producing more accurate visual displacement and force feedback using Root Mean Square Errors (RMSE). To predict facial deformation after surgery, Mollemans et al. [19] compared four popular different models (linear Finite Element Model, non-linear Finite Element Model, Mass Spring Model and Mass Tensor Model). The validation process included a computerized portion and a human portion. The computerized validation consisted of the comparison of post-operative data from real patients with the outcomes computed by the four models tested. As a starting point, they created 3D tetrahedral meshes based on pre-surgery data from the same patients. As a comparison metric, they used the distance between nodes computed by each model and actual nodes gathered from the post-operative data. They measured a signed Euclidean distance between nodes computed by the model and nodes measured from their patients. The goal was to compute statistical properties for each model such as the mean, the variance, and the 50%, 90% and 95% percentiles of the distance distribution. As the human validation, they asked surgeons to score the outcome of each model based on the realism and difference with the actual data from the patients. However their goal was to verify only the result of the deformation. Therefore, this method cannot be applied to the evaluation of real-time models.

Marcha *et al.*[20] proposed a unified method to answer two important questions: (1) does the numerical approximation of equations that govern a model provide acceptable results; and (2) does the model provide accurate simulation of the physical behaviour of the simulated object when computation time is limited? As a comparison metric, they consider the “relative energy norm error”. This comparison metric includes the displacement of each node of a meshed object at each time step from the reference model

and from the model under test. The relative energy norm error gives measurements on the whole volume of the model under test. Another comparison metric corresponds to the Euclidean distance between the location of a node computed by the reference model and its counterpart computed by the model under test. The goal of the study was to introduce new metrics, but it was not to link these metrics to their effect on human perception of object softness.

2.3.4 Summary

In summary, the presented methods carry two main problems. The first problem arises from the limited assessment introduced by considering only the visual displacement of a fixed number of selected nodes, or by considering only visual displacement and force feedback produced by a single-node contact. Therefore, these methods cannot evaluate the full mesh of an object governed by a real-time model in term of visual displacement and force feedback. The second problem is that none of the presented methods accommodate human perception as a factor for interaction. As discussed in Chapter 1, human perception of object softness may be significantly affected by external factors such as viewing angles during interaction with a soft object in a VR training system. This might limit the learning experience offered by such training systems.

2.4 Computational Models

Used in most VR systems for training palpation, computational models of soft objects receive attention from researchers due to their time and physical constraints. These computational models are responsible for simulating actual soft objects for user interaction in real time. The responsibilities of such computational models encompass: (1) Control of behavioural deformation (e.g., visual displacement of soft objects and force feedback from soft objects) in real time; (2) Collision detection between such a computa-

tional model of a soft object and a virtual tool/finger moved by a user; and (3) Collision response providing an appropriate deformation response after the collision between the soft object and the tool/finger is detected. This section introduces the state-of-the-art methods and background information related to these three responsibilities.

2.4.1 Real-Time Models

When developing a VR system for palpation training, the model of a soft object used in the VR system is critical because it will affect the visual and haptic (touch) aspects of object deformation during palpation. Minimum features for such models include: (1) real-time rendering to provide visual and haptic feedback without delay; (2) short preprocessing of visual displacement and force feedback to make the deformation of an object quickly available to the user during interaction; (3) realistic deformation to ensure that the computed deformation corresponds to that incurred by a real object; (4) ability to render large deformations caused by palpation (more than 2% of geometrical difference between the object and its deformed state). To create VR systems with different needs, many researchers have investigated computational models to render the real-time deformation of soft objects [21, 22, 23]. Two main categories of models emerge: (1) real-time models suitable for rendering deformation of virtual soft objects in real time and (2) FEM models for taking account material parameters of real soft objects. The real-time models include mass-spring models and mass-tensor models solved using non-FEM numerical methods.

Mass-Spring Models

The real-time models include mass-spring models and mass-tensor models solved using non-FEM numerical methods. Governed by the Hookean law, mass-spring models use a spring constant and a damping factor as material parameters to describe homogenous objects [21, 22]. Mass-spring models are very popular because they provide real-time

rendering, require no preprocessing of visual displacement or force feedback, and handle large deformation in a relatively realistic manner in terms of visual displacement. With additional techniques, such as adding volume springs, the mass-spring models are able to conserve the volume of soft objects during deformation. However, numerical methods used to solve the equation of the Hookean law can cause the models to be unstable [24]. The mapping of the material parameters from real objects to their virtual counterparts is problematic due to the difference in material parameters between those measured on real objects and those used in mass-spring models [24]. Properly determining material parameters of soft objects plays an important role in using such a model to describe their deformation behavior.

Mass-Tensor Models

Differing from the mass-spring models, a mass-tensor model combines advantages of easy implementation and short computation time, and its physical parameters are easily transferable from physical experiments conducted on actual object [25]. However, a mass-tensor model is tuned to handle topologic changes such as cutting soft objects. Therefore, the realism of large deformation is not a key concern in the mass-tensor model. Additionally, the mass-tensor model does not warrant volume conservation.

Non-Linear FEM Model

To overcome the drawbacks of mass-spring and mass-tensor models, researchers investigated models using FEM [23, 26, 27]. FEM solves non-linear and linear constitutive equations using material parameters directly mapped from real objects. Solving non-linear equations produces more accurate results in terms of visual displacement and force feedback but cannot run in real time.

Table 2.1: Comparison of computational models for matching the criteria of a VR system for palpation training.

	Real-Time Models		FEM Models	
	Mass-Spring Model	Mass-Tensor Model	Non-linear	Linear
Computational speed	real-time	real-time	offline	real-time
Preprocessing	no	yes	n/a	yes
Volume conservation	yes	no	yes	yes
Deformation realism	realistic for small and large deformation	realistic for cutting tissue	very realistic	very realistic for small deformation
Large deformation	yes	no	yes	no

Linear FEM Model

Although it is feasible to solve linear equations in real time and to warrant volume conservation of soft objects during deformation, the design of linear FEM models is quite challenging. Consequently, most linear FEM models provide low accuracy when simulating deformation of objects or require time-consuming pre-computation of visual displacement and force feedback [26, 27]. In addition, when resolving linear equations, FEM models show excessive visual distortion when simulating large deformations in objects [28].

Summary

In summary, Table 2.1 compares these 4 types of computational models according to the features deemed important for creating a VR system for palpation training. A computational model alone can describe the behavior of phantom soft object. However collision detection and collision responses are needed to provide interaction with a finger during palpation of the object.

Table 2.2: Ability of collision detection algorithms to match the criteria for the creation of the VR system for palpation training.

	Sphere approximation	BVH	CDC	GJK	VCD
Soft object	yes	yes	no	yes	yes
Shape restriction	no	no	no	concave	no
Multi-node contact	yes	yes	yes	yes	yes
Approximation of distance	yes	no	yes	yes	no

2.4.2 Collision Detection

To be interactive, a computational model needs to detect collision when a finger contacts the geometry of a viscoelastic soft tissue. Therefore, a VR system requires a detection collision algorithm. This algorithm must: (1) consider deformation of soft objects; (2) handle any object shape as soft objects can be both concave and convex, depending on the applied force; (3) include multi-node contact to increase the realism of the collision; (4) rely as little as possible on the approximation of collision distance as it decreases the realism of the collision. Researchers provide many algorithms for collision detection: Sphere approximation uses spheres to detect collision between two objects [15]; Bounding Volume Hierarchies (BVH) use logical trees to store and search the topology of objects when a contact occurs [29, 30]; Continuous Detection Collision (CDC) relies on an approximation of the future object location to detect the collision [31]; The Gilbert-Johanson-Keerthi distance (GJK) algorithm uses Minkowski differences to approximate the collision location [30]; and Voxel-based Collision Detection (VCD) uses location information stored in voxels (small cubical part of an object) [32, 33]. Most of these algorithms were created to handle collision detection of rigid objects. However, Sphere approximation, BVH, GLK and VCD handle collision of soft objects as well. Among these algorithms, BVH seems to be a good candidate to be used to simulate palpation;

Table 2.3: Abilities of algorithms of collision response to match the criteria for the creation of the VR system for palpation training.

	Hertz Contact	Penalty force	Constraint- based force	Impulse force
Visual realism	good	bad	bad	bad
Multi-node contact	yes	yes	no	yes
Realistic collision states	yes	yes	yes	no
Large deformation	no	no	no	no
Collision of soft objects	yes	yes	no	yes

because it is fast (faster than VCD) as it uses logical trees to detect collision, can be applied to any shape, and is easy to implement on a mesh. Table 2.2 summarizes the ability of each algorithm to meet the different criteria required to create a VR system for palpation training.

2.4.3 Collision Response

Once collision is detected, a computational model must provide an appropriate response computed by an algorithm for collision response. Collision response for palpation training requires: (1) visual realism of the response as it affects the perception of object deformation; (2) ability to compute force on a multi-node contact surface; (3) realistic collision outcomes to reflect actual deformation behavior when colliding objects are still in contact; (4) capable to handle large deformation (more than 2% of geometrical difference); (5) ability to response when soft objects are collided. Various algorithms have been used for collision response. For example, the Hertz Contact algorithm uses spheres to approximate a penetration depth and computes forces to separate colliding objects based on this depth [15]. The penalty force algorithm utilizes the penetration

depth of two colliding objects [30], whereas the constraint-based force algorithm applies equations that prevent the objects from interpenetrating. Finally, the impulse force algorithm computes an impulse force that separates the objects each time they collide (summary available in [30]). As shown in Table 2.3, no algorithm seems to encompass all the features I need to develop a VR system for palpation training. Nevertheless, the integration of a computational model for a virtual breast phantom with algorithms of collision detection and response allows the phantom to be fully interactive during palpation - deforming the phantom according to the force applied onto it. To warrant correct visual and force feedback of the phantom, an evaluation method must verify that a real-time model for describing the deformation behavior of the phantom provides appropriate feedback.

2.5 Constraints of Human Perception Constraints

Human perception is the process used by humans to gain consciousness of the world around them [6]. Using the different senses combined by the nervous system, this process is known to be subject to personal learning and memory history [34]. Many illusions associated to all senses affect multiple human perceptions. In the context of visual and haptic (force feedback) perception, several studies have revealed that visual and haptic information can affect each other during object perception, especially in discriminating object softness. For example, Srinivasan *et al.* [35] demonstrated that the discrimination of spring stiffness declined dramatically when visual information about the deformation of the springs did not match with haptic information of the same deformation. Moreover, they discovered that visual information of object displacement had a great influence on the perception of object stiffness of a virtual spring. In certain specific mismatches, they observed that the visual information could even invert the subjects' judgment in a discriminating task of spring stiffness. Wu *et al.* [36] discovered that visual information

such as the 3D perspectives dominated the discrimination of spring stiffness, no matter whether haptic information was present. Furthermore, studies have reported divergence of perception during user interaction within VR systems. In one of my previous studies, I observed concrete evidence that the viewing angle at which a soft object is looked at can influence human perception of object softness [8]. I found that both visual displacement and force feedback of a deformed soft object affect this perception. Also, when studying human perception during real-time simulation, O’Sullivan and Dingliana revealed that subtle visual discrepancies during the simulation can be unnoticed by human perception [7]. To demonstrate this, they performed a human study. Involving only visual simulation, their study focused on the ability of subjects to detect abnormal collisions of many objects, while varying some key aspects such as the speed of the simulation or the number of objects colliding.

Revealing different constraints of human perception, all these studies demonstrate the need to accommodate this perception when assessing a VR system. In particular, the study from O’Sullivan and Dingliana shows that subjects tend to concentrate on a subset of the available visual information when facing large amounts of rapidly changing information [7]. I assume that this tendency also holds when humans interact with soft objects in real time. If this assumption is verified for soft tissue interactions, this will open a new way to develop new VR systems with simplified computational models that can achieve a frame rate of 100Hz or higher, which would be suitable for real-time interaction.

2.5.1 Combination of Vision and Touch

In everyday interaction, both senses of vision and touch supply information about the softness of tissues/organs. These senses always work together to provide a representation of objects for interaction. However, VR systems as artificial environments can easily decouple these senses. To provide realistic simulations of real tissues, it is critical for

VR training systems to display 3D structures of these tissues and to allow interaction with these structures without producing perceptual illusions.

Although the sense of vision is often predominant over the sense of touch, this dominance is not universal [37]. The dominance of the sense of vision seems to be limited when estimating object surface properties, such as its texture [37]. Based on a reliability index of the senses of vision and touch, Ernst and Banks [38] proposed a model to predict the involvement of each sense in integration of visual and haptic stimuli. They discovered that the sense of vision dominates over the sense of touch, only when the variance associated to the estimation of the visual information was smaller than its counterpart of the haptic information. Newer studies on softness perception [39, 40] found that the combination of the visual and touch for softness perception cannot be predicted by the model proposed by Ernst and Bank [38]. Kuschel *et al.* [39] revealed that when both senses disagree, the perceived softness is closer to the harder stimulus given by either the haptic or visual channel. The results from their experiments showed that participants were better at discriminating harder objects. Drewing *et al.* [40] observed that when both visual and haptic information were available, participants tended to trust more the haptic information. Tiest and Kappers [41] demonstrated that participants used mostly deformation of the surface of soft objects as cues to perceive object softness.

In order to minimize perceptual illusion during interaction, all these studies are of interest in building an accurate VR system for palpating a viscoelastic soft tissue. However, the effect of many perceptual illusions is still not clear. Investigating this effect will help understand human perception of object softness and improve such a VR system.

2.5.2 Effect of Alignments between a Visual Display and an Haptic Device

When building VR training systems, it is crucial to display 3D tissues and to allow interaction with them without introducing any perceptual illusion due to patient safety.

However, the integration of visual and haptic information can be problematic in such VR systems due to different representations of both senses of vision and touch [42, 43, 44]. Several studies have revealed that visual and haptic information can intrude with each other in object perception, particularly in discriminating object softness [35, 36, 8]. In addition, I observed that the alignment of a visual display relative to a haptic device affects the perception of object softness [8]. In this study, the haptic device was located directly under the visual display at the same vertical axis (vertical alignment) in one experiment, and was beside the same visual display (horizontal alignment) in another experiment.

There are many other reports on VR systems that have varying alignments between a visual display and haptic device. To develop VR systems, some studies have used a horizontal alignment [45, 12]. A common observation of studies using a horizontal alignment was that the user performance in a virtual environment was inferior to the performance in the real world. Some VR systems use a “same-location” alignment, in which a mirror reflects a visual display onto the spatial location of a haptic device. At one spatial location, this alignment merges the visual information of a visual display with the haptic information provided by a haptic device. This alignment allows the user perception of an object in space to agree with the location of the hand [46]. “Same-location” alignment has been used to provide new 3D tools [47, 48] or to investigate the integration between the senses of vision and touch [49].

Despite the many reported VR systems, only little research exists on investigating the effects of spatial location between visual and haptic information about an object. In a large-scale haptic device (Big SPIDAR), Bouguila *et al.* [50] investigated how the spatial displacement between visual and haptic information about an object affects the depth perception of the object. They found that the user interaction with the object at the same location as the haptic device improved the depth perception. By placing

a haptic device in front of a visual display, Swapp and Loscos [51] examined the effect of spatial displacement between visual and haptic information on user interaction with a 3D object, varying the alignment between a visual display and haptic device. They found that using an alignment similar to the “same-location” alignment improved significantly the accuracy of user interaction for activities that require rapid motion of the hand. By altering the location of the visual display, Wu *et al.* [11] investigated the influence of “same-location” alignment for needle insertion under the guidance of ultrasound displays. The performance of subjects were more accurate using a “same-location” alignment between a needle and the ultrasound displays compared with a conventional alignment of placing the ultrasound displays away from the site of the needle. Although these studies demonstrated the superiority of “same-location” alignment for some tasks, they did not investigate the effects of this alignment on the perception of object softness from a user perspective.

2.5.3 Human Constraints for Perception of Object Softness during Real-Time Palpation

During user interaction with the simulated tissues, computational models are contacted by other objects (e.g. tools) or human users (e.g. fingers). The validation of the contact is paramount for providing realistic experience to the users of VR training systems.

In this thesis, I identified two main contact definitions for interaction: single-node contact and a multi-node contact. The single-node contact definition is commonly used in most current VR simulators. This definition is mainly due to limitations introduced by current stylus-style haptic devices, which render a vector of force feedback at each time step. For example, Gurari *et al.* investigated discrimination of object softness using a real-time spring model with a single-node contact definition [52]. Sedef *et al.* developed a real-time viscoelastic model simulating the human liver [17]. In one of my previous studies, I found that humans are affected by the viewing angle at which they

can see and interact with a soft object when perceiving object softness [8]. In all these studies, the user interaction with the object governed by a real-time model was through a single-node contact definition. However, the single-node contact definition departs from actual user interaction with objects by applying force on a surface (contact area) such as a finger would.

In contrast, a multi-node contact definition covers an area of nodes rather than a single node and thus allows rendering multiple vectors of force feedback (i.e., each vector corresponds to a node). There are reports on utilizing a multi-node contact definition for user interaction. For example, Duriez *et al.* developed a multi-node contact by using the Signorini's model [53]. However, the computation of this contact was not fast enough to permit real-time user interaction. To perceive fabric textures, Manousopoulos *et al.* proposed a contact method for considering the fingertip size of the thumb and index finger [54]. This method demonstrated the advantage of a multi-node contact definition over a single-node contact when pinching a fabric. Moreover, a multi-node contact definition permits the possibility of applying various force distributions over a contact area. As shown in our early study [55], a real-time model of a breast phantom exhibited different displacement and force feedback under the palpation of a single-node or multi-node contact definition with varying force distributions. Nevertheless, the effect of the difference between single-node and multi-node contact definitions on user interaction is currently still unclear.

However, there are some studies to investigate the effect of a single-node contact definition on human perception of object softness. Based on haptic information of objects, Cholewiak *et al.* examined the human ability of discriminating object softness and force magnitude [56]. They observed that the participants in their study could discriminate up to 3 levels of object softness and force magnitude, respectively. This observation implies that humans possess a relatively poor ability of this discrimination when only

relying on haptic information. Using both visual and haptic information, Gurari *et al.* studied human perception of object softness [52]. They observed that some participants used haptic information, whereas others relied on visual information for the perception. That is, the participants subjectively applied strategies to aid their perception of object softness. Kuschel *et al.* proposed a theory to understand how humans perceive object softness using both visual and haptic information [39]. They suggested that humans assign different weights to visual and haptic information for the perception. All these studies used a single-node contact definition for rendering haptic information. A common observation from these studies is that the perception of object softness is affected at certain degrees by both visual and haptic information of the objects.

Similar observation might be present under a multi-node contact definition. There is however little literature reporting such observation. This might result from the lack of haptic devices providing multiple vectors of force feedback on a contact area. Despite of existing glove-style haptic devices (such as a CyberGrasp [4]), this style of haptic devices offers actually a single-node contact definition on each finger by rendering a vector of force feedback on the finger. Current stylus-style haptic devices are for a single-node contact definition to render a vector of force feedback at a spatial location. Such a stylus-style haptic device could be used for examining the human perception of object softness under a multi-node contact definition, because there was no significant difference of perceiving object softness through using a rigid rod (like a single-node contact definition) or a bare finger (as a multi-node contact definition) [57, 35]. Nevertheless, a multi-node contact definition of palpating soft objects would generate visual displacement (visual information) of the objects differently from that under a single-node contact definition, especially when various force distributions is applied to the multi-node contact definition. Such discrepancy of visual displacement might affect the perception of object softness, even under similar haptic information rendered from either single-node or multi-

node contact definitions. This postulation is derived from the observation that visual information of objects plays a certain role in the perception of object softness [52, 56, 39].

2.6 Summary

In recapitulation, VR training systems offer a good alternative for training real critical tasks such as medical procedures. A VR training system for medical procedures must offer a training experience that closely simulates the real tissues that occur during a medical procedure and felt by a trainee. In the case of palpation, a close simulation of largely deformable tissues is needed to achieve this goal. Researchers have already investigated many aspects of deformable tissues to be rendered in real time. Also, some evaluation methods exist to test differences produced by real-time models compared to golden standards, such as FEM models. However, the drawback of those evaluation methods is that they are looking for a perfect physical match rather than looking for a trade-off between rendering speed and accuracy factoring in the constraints of human perception.

To develop an evaluation method factoring in the human constraints when perceiving object softness, my approach integrates statistical methods coupled with human studies. To carry out this approach, I first applied statistical methods to measure the difference between visual displacement and force feedback computed through a real-time model to those computed through a FEM model featuring physical parameters. Chapter 3 presents the methodology of the approach along with a case study demonstrating the application of the method on a virtual breast phantom (as a viscoelastic soft tissue). In addition, Chapter 4 and Chapter 5 present two human studies. Chapter 4 shows the work that investigates the effect of the alignments between a visual display and a haptic device on the human perception of object softness. In Chapter 5, I investigate human constraints for perceiving object softness during real-time palpation using the alignment

that produces the best interaction from Chapter 4.

Chapter 3

Statistical Evaluation of a Real-Time Model*

3.1 Introduction

Soft-tissue palpation plays an important role in diagnosing various diseases. Palpating skills are tedious to learn due to the difficulty of describing the sense of touch in a natural language. Because of its interactive nature, a virtual reality (VR) training system embedded with real-time soft-tissue models may be helpful to teach such skills to medical residents. Studies show that such a VR system impacts human perception during palpating at various levels, largely due to the characteristics of real-time models. In this chapter, I present an evaluation method assessing the behavioral deformation (e.g., visual displacement and force feedback) of a computational model considering human constraints during palpation (Challenge I). I based this preliminary comparison on the rationale that human perception is not sensitive to small discrepancies (less than 5%) during real-time simulations [13]. Similar to human perception, statistical methods are not sensitive to small discrepancies in datasets. Two statistical methods, analysis of

*Parts of this chapter are published:

A. Widmer and Y. Hu, (full-paper submission for review), “Statistical comparison between a real-time model and a FEM counterpart for visualization of breast phantom deformation during palpation,” *Proceedings of the 23rd Canadian Conference on Electrical and Computer Engineering (CCECE)*, 4 pages on CD-ROM, Calgary, AB, Canada, May 2010.

A. Widmer and Y. Hu, (full-paper submission for review), “A viscoelastic model of a breast phantom for real-time palpation,” *Proceedings of the 33rd Annual International Conference of the IEEE Engineering in Medicine and Biology Society (IEEE-EMBC)*, pp 4546-4549, Boston, MA, USA, September 2011.

A. Widmer and Y. Hu, (full-paper submission for review), “An evaluation method for real-time soft-tissue model used for multi-vertex palpation,” *Proceedings of the IEEE International Conference on Systems, Man, and Cybernetics (IEEE-SMC)*, pp. 127-132, Anchorage, AK, USA, October 2011.

A full version of this chapter is under review for publication.

A. Widmer and Y. Hu, (22 single pages submitted on December, 22 2011; reference number #: TOMACS-2011-0142.R1), “An evaluation method for a real-time simulation of a viscoelastic phantom based on constraints of human perception,” *ACM Transactions on Modeling and Computer Simulation*. See Appendix B for copyright transfers.

variance (ANOVA) and a Bland and Altman agreement [13], allow reasonable differences between independent datasets. If ANOVA returns a p -value of less than 5% (e.g., a level generally used as a confidence interval at 95%), the null hypothesis can be rejected as in most studies on human perception [58, 59]; whereas if the Bland and Altman agreement shows that less than 5% of the difference between two datasets is located outside a boundary set by ± 2 standard deviations, both datasets are in agreement with each other [13]. The common practice of using ANOVA for model evaluation is to reject the null hypothesis, because a model is always an approximation to a system to be modeled [60]. Unlike this practice, I use the ANOVA to confirm the null hypothesis under a sufficiently large size of data and a confidence interval at 95% (as in human studies). However, this confirmation does not yield a level of agreement between the datasets, which needs to be computed by using the Bland and Altman agreement.

In this chapter, I use two different contacts as single-node and multi-node contacts with four force distributions. Commonly used in the literature, a single-node contact refers to the usage of only one node to convey the displacement and the force on a discrete mesh used as abstraction of a physical object in a VR system. The discrete mesh is made of multiple nodes connected to each other to form a surface or a 3D representation of a soft tissue. Unfortunately, the single-node contact diverges from the real situation where a whole section of the finger (contact area) touches the phantom of a soft tissue. A multi-node (surface) contact has the advantage to solve this divergence by allowing the application of force on the nodes located on the entire area contacted by the fingers. Also, different force distributions can be simulated by changing distributions of force on a multi-node contact – for example, by applying more force at the tip of the finger to get a different softness perception.

The proposed method aims at assessing a real-time model simulating highly viscoelastic soft tissues. This method took into consideration the constraints of human

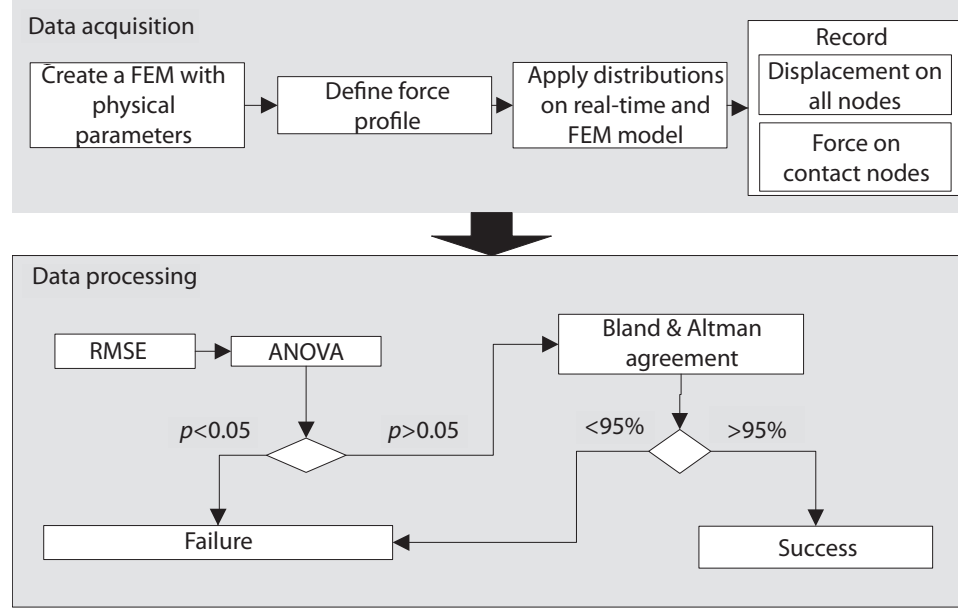


Figure 3.1: Flow diagram of the evaluation method.

perception to evaluate this real-time model. This method has the advantage of ensuring the correct match of the visual displacement over time and the correct force feedback computed by the real-time model on the contact area. To show the benefit of this method, I use a novel real-time model featuring viscoelastic characteristics based on an existing model as a case study (Challenge II). Able to render visual rendering in 10 ms and producing stable haptic interaction, this real-time model simulates a breast phantom during palpation as a case study for the evaluation method.

3.2 Evaluation Method

My evaluation method consists of a data acquisition step and a data processing step, as illustrated in Fig. 3.1. The data acquisition step describes what independent data are needed and how to obtain them. The data processing step presents different statistical methods and their order in undertaking an evaluation of the computational models. Taking a real-time computational model as input, I undertook these two steps based on the assumption that a real-time simulation needs to be evaluated according to the ac-

curacy of its node displacement (visual displacement) and force feedback. The reference model for this evaluation is a FEM counterpart, as reported in literature [17, 18]. In this section, I introduce the tasks of each step.

3.2.1 Data Acquisition

As shown in Fig. 3.1, the data acquisition step includes four tasks. The goal of these tasks is to provide several datasets (visual displacement and force feedback) for the data processing step. The first task involved creating a reference model. The reference model is a non-linear FEM model with the physical parameters (hyperelasticity and viscoelasticity) of the soft object featured in the real-time simulation. The parameters can be taken from the literature or from mechanical experiments. In order to keep a close correspondence to the real object, it is important to partition the FEM model into layers of different materials composing the real object. To facilitate the data processing step, the FEM model and the real-time model should share the same geometric mesh. Thus, the FEM model acting as the reference model is created with parameters from the physical world. Therefore, the real-time model can be assessed against this FEM model.

The second task defines a force profile, i.e., a variation of force magnitude over time. This task aims at imitating the contact surface of the finger and the force applied during palpation. Various force profiles can be used. A step-wise force profile is commonly used for testing viscoelastic materials due to mechanical characteristics of such materials [9, 17]. Other profiles can be used such as a ramping force to simulate an actual palpation procedure [61]. The selection of a suitable force profile is important, as it determines how the models were compared. Therefore, a carefully defined force profile is needed to assess the behavior of a real-time model.

The third task involves the application of a force distribution adjusted with the chosen force profile on both real-time model and FEM model. A force distribution

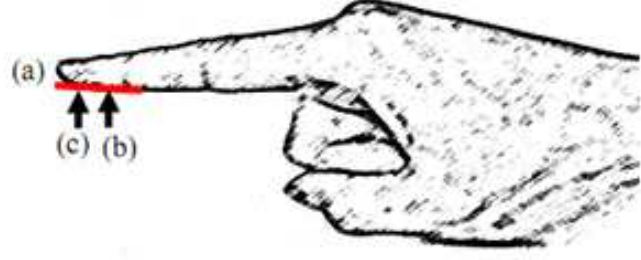


Figure 3.2: One-finger contact area (a). Locations (b) and (c) correspond to two different centers of contact force.

describes how the applied force will be distributed over a surface (a), as in Fig. 3.2. Based on one-finger palpation as depicted in Fig. 3.2, I selected 4 different force distributions to simulate varying cases of palpation as illustrated in Fig. 3.3. As shown in Fig. 3.3a, the first force distribution (Distribution 1) uses a single-node contact centered on the contact area of the finger (b), as in Fig. 3.2, with the amplitude of the force varied by the selected force profile over time. The single node contact is located at the center of the distal section from a virtual finger. This distribution aims at simulating the most common contact paradigm used in the field of haptics. This paradigm is introduced by the usage of a haptic device such as a SensAble PHANToM device. Fig. 3.3b illustrates the second distribution (Distribution 2). This distribution uses a multi-node contact featuring a force evenly distributed among the nodes in the contact area of the finger (area: 5.2 cm^2). This distribution mimics a general contact commonly used in VR simulators [16, 62]. For the third and fourth distributions (Distribution 3 and Distribution 4), I introduced a 2-dimensional (2D) Gaussian distribution. The 2D Gaussian distribution allows the evaluation method to assess complex force distributions. Since little literature describes how the fingertip contacts a deformable object (such as a breast phantom), the use of a 2D Gaussian distribution could take account the curve and deformable surfaces of both human fingertip and object. Distribution 3 and Distribution 4 had contact force, $f(x, y)$ at the position (x, y) of a 2D Gaussian function as depicted in Eq. (3.1):

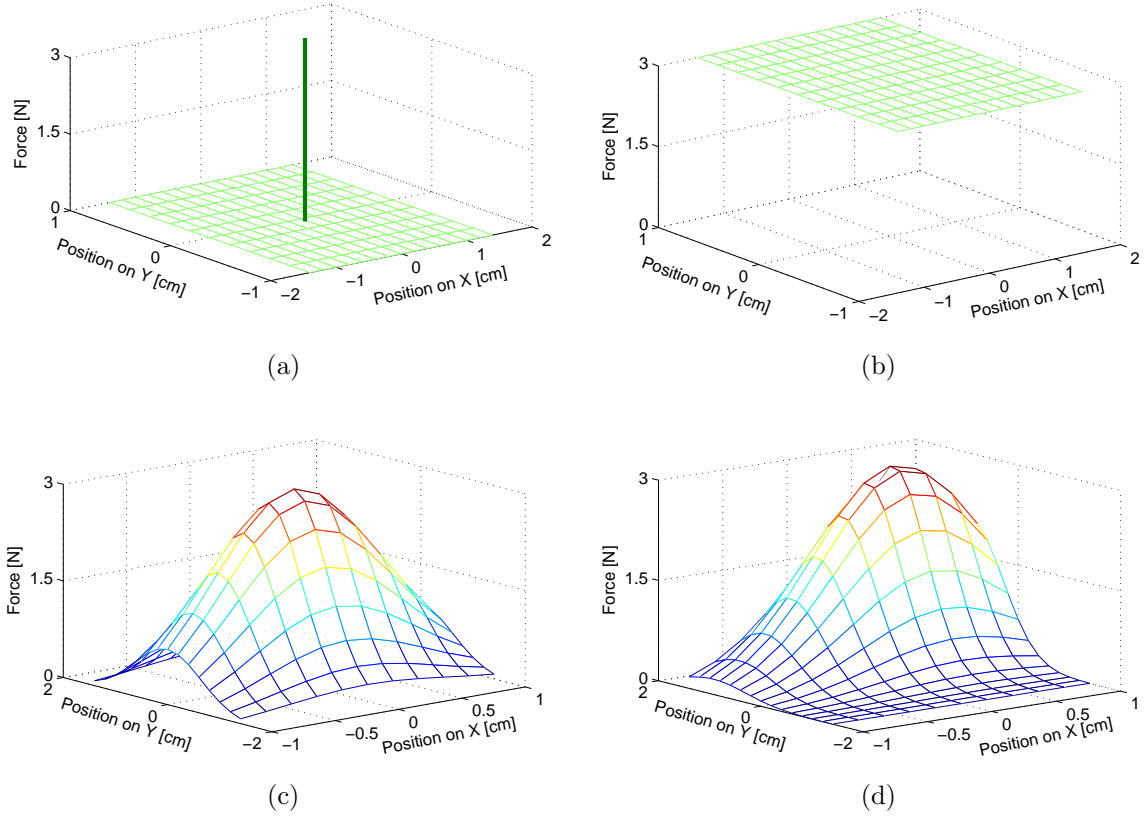


Figure 3.3: Force distributions; (a) Distribution 1 features only one node contact; (b) Distribution 2 involves an uniform force through the contact area; (c) Distribution 3 simulates a finger palpation; (d) Distribution 4 mimics a slanted finger palpation.

$$f(x, y) = Ae^{-((\frac{(x-x_0)^2}{2\sigma^2} + \frac{(y-y_0)^2}{2\sigma^2}))}, \quad (3.1)$$

where A is the amplitude of the force, (x_0, y_0) is the position of the maximum amplitude of the force, and σ means the variance of the amplitude. As illustrated in Fig. 3.3c, Distribution 3 uses a centered 2D Gaussian distribution simulating a common palpation technique in which the practitioner holds his/her finger flat on the palpated tissue [2]. Therefore, the position (x_0, y_0) corresponds to the center of the contact area, (b), as in Fig. 3.2. As shown in Fig. 3.3d, Distribution 4 uses a non-centered 2D Gaussian distribution simulating another common palpation technique in which the practitioner holds his/her finger slanted over the palpated tissue [2]. Therefore, the maximum amplitude position (x_0, y_0) is situated at the tip of the finger, (c), as depicted in Fig. 3.2.

The fourth task focuses on the collection of data. The collected data includes the displacement of all surface nodes and the force feedback computed by the nodes within the contact area. I collected these data at every time step of the force profile for both real-time and FEM models, respectively. At the end of the task, the data sets are independent and ready to be analyzed by the step of data processing to verify if both models have a statistical agreement with each other.

3.2.2 Data Processing

Three tasks compose the step of data processing. To enable the comparison with other evaluations, the first task uses a root mean square error (RMSE) analysis [63]. The RMSE measures the average difference (a scalar value) of two datasets between the real-time model and its FEM counterpart. This analysis with a correlation coefficient constitutes a commonly used approach for model evaluation [64, 17]. The correlation coefficient usually computes the “goodness” of a linear relationship between two datasets [63]. I did not use this coefficient due to the postulate of Bland and Altman [13], explaining the difficulty of the coefficient to verify the agreement between two datasets. Nonetheless, I provided the RMSE for each force distribution in order to keep a comparison metric with other methods in the literature [64, 17].

In the second task, I used an ANOVA statistical analysis. This analysis appears useful to show whether or not different means exist in independent datasets that each follows a normal distribution. The ANOVA analysis is not sensitive to small discrepancies in datasets, alike human perception reported in literature [7]. My two hypotheses to be tested by ANOVA were the following: (1) “My real-time model computes differently the displacement of nodes than its FEM counterpart” and (2) “my real-time model computes differently the force feedback on the contact nodes than its FEM counterpart”. To analyze the first hypothesis, ANOVA compared the displacement of nodes yield by the real-time model with that computed by its FEM counterpart. In addition, to verify

the second hypothesis, ANOVA compared the force feedback yield by both real-time and FEM models on nodes in contact. As part of the analysis for both hypotheses, an F -value and a p -value were calculated for each comparison. Derived from an F -test, the F -value is given by the ratio of two mean square values [65]. The numerator value of the ratio expresses a between-dataset variability to indicate an explained variance between the datasets; whereas the denominator value of the ratio is a within-dataset variability to depict an unexplained variance among the datasets. If an F -value is much greater than 1.0, the variability between datasets is dominated over the variability within the datasets. This would yield a meaningful p -value. In this case, the p -value represents the probability that an explained variance is equal to or greater than the variance yielded by chance. If $p < 0.05$, the confidence interval is equal to or larger than 95%. Thus, for $p < 0.05$, ANOVA indicates a statistically significant difference among the datasets. Given a very large population of nodes to represent a geometry, a subset of the nodes could be used for the ANOVA analysis if the size of this subset is large enough as determined by a size computation [66]. Nevertheless, using all nodes of the geometry for the ANOVA analysis would be realistic, if the population of the nodes is in a reasonably countable size.

Practically, to test the first hypothesis, I computed the location of nodes governed by the real-time model and the FEM model, respectively, at each time step (e.g., a sample). For each model, Eq. (3.2) converts the Cartesian coordinates, (x_i, y_i, z_i) , of a node i into an Euclidean distance, D_i , between the node i to the fixed reference of a geometry (the origin of the Cartesian coordinate system of the geometry) by:

$$D_i = \sqrt{x_i^2 + y_i^2 + z_i^2}. \quad (3.2)$$

That is, the Euclidean distance, D_i , represents the displacement of the node i at a time step. Here, the geometry and its Cartesian coordinate system for the real-time model are same as those for the FEM model. Thus, the test of the first hypothesis examines

different means between two independent datasets of the Euclidean distance: one for the real-time model and another for the FEM model. Given the geometry of N nodes under a force profile for L time steps, there are a total of $N \times L$ data points in each displacement dataset. To analyze the second hypothesis, I obtained the force feedback data from using a technique similar to the one applied to get displacement data. I focused only on forces computed by the nodes touched by the contact area of the finger. Moreover, I considered only the magnitude of the force along the same direction as a force vector is applied in each model. Therefore, I computed the magnitude through the dot product between the vector of the applied force in its opposite direction and the force feedback vector computed by the model. Given M nodes for the contact area of the finger, applying the force profile for L time steps yields a total of $M \times L$ data points in each force dataset. In the equations below, I use G to represent the node number N (or M) for visual displacement (or force feedback).

From these data, two ANOVA analyses were carried out: one evaluating the Euclidean distance data (visual displacement) and another comparing the magnitude of force feedback. In the two analyses, I compared the data from the real-time model to the data from the FEM model. As ANOVA input data, each model was represented by a one-dimensional array, whose size is $G \times L$. The array is sorted as a chunk of G nodes in the order of the time steps. In each time step, the order of the G nodes has the same sequence. The ANOVA compared both input arrays for each hypothesis and returned the probability whether the two models were different. In the case that both arrays did show significant differences, I concluded that the real-time model did not approximate the FEM model well enough. Alternatively, if ANOVA does not show a significant difference, it does not mean that both models are in agreement. In this case, I continue the analysis with the third task.

The third task includes the agreement analysis to verify if the real-time model ap-

proximated its FEM counterpart. Introduced by Bland and Altman [13], this analysis tests the agreement between two sets of data. Assuming the normal distribution of the differences between datasets. Assuming the normal distribution of the differences between the two datasets, the analysis indicates the agreement when at least 95% of the data in each dataset lie within ± 2 standard deviations (SD) of mean differences between corresponding data of these datasets. The value of 95% is set as the confidence interval of the hypothesis, alike in the ANOVA analysis [7, 58, 59]. In this way, I would accept the real-time model to be enough as an alternative to its FEM counterpart. Based on the mean difference and standard deviation of differences, the agreement analysis computes the size of difference likely to occur between two independent datasets. I applied this analysis to both data of visual displacement and force feedback, respectively. For the visual displacement, I computed the mean difference \bar{d} using Eq. (3.3):

$$\bar{d} = \sum_{i=1, j=0}^{G, L} \sqrt{(x_{i,j,m} - x_{i,j,a})^2 + (y_{i,j,m} - y_{i,j,a})^2 + (z_{i,j,m} - z_{i,j,a})^2 / GL}, \quad (3.3)$$

where G is the total number of nodes in consideration, L is the total number of time steps, $(x_{i,j,m}, y_{i,j,m}, z_{i,j,m})$ are the Cartesian coordinates of the node i at the time step j in the real-time model, and $(x_{i,j,a}, y_{i,j,a}, z_{i,j,a})$ are the FEM counterparts of $(x_{i,j,m}, y_{i,j,m}, z_{i,j,m})$. Relatively, data processing for force feedback datasets follows the same equation as described by Eq. (3.3) to compute the mean difference. For the force feedback, I replaced the parameter $(x_{i,j,m}, y_{i,j,m}, z_{i,j,m})$ by the components of the force vector computed by the real-time model and the parameters $(x_{i,j,a}, y_{i,j,a}, z_{i,j,a})$ by the force vector computed by the FEM model. The standard deviation, SD , of the difference is then computed using Eq. (3.4):

$$SD = \sqrt{\frac{\sum_{i=1}^{G \times L} (d_i - \bar{d})^2}{GL}}, \quad (3.4)$$

where d_i is either the Euclidean distance or force magnitude at the node i . Under both analyses, I computed the percentage of data lying within $\pm 2SD$ for visual displacement



Figure 3.4: Real-time model simulating a breast phantom.

and force feedback, respectively.

3.3 Case Study

To demonstrate the effectiveness of the evaluation method, I created a simple real-time simulation of a breast phantom based on a viscoelastic real-time model, as illustrated in Fig. 3.4. Forces were applied to the real-time model to mimic multi-node contact during palpation.

3.3.1 Real-Time Model

My goal was to provide a real-time simulation governed by the real-time model to offer the visual displacement and force feedback in agreement with an offline FEM model. In the current study, I was interested to mimic the breast phantom in real time as illustrated in Fig. 3.4. For simplification, I simulated a breast phantom instead of physical breasts. A virtual breast phantom with a radius of 4.0 cm is composed of the same triangularly meshed geometry as I used in our previous study [61], including a surface membrane of 338 nodes and an inside gel without any node. However, two major modifications have to take place in this current case study to approximate the high viscoelastic behavior of the breast phantom. First, the equation governing the surface membrane has to

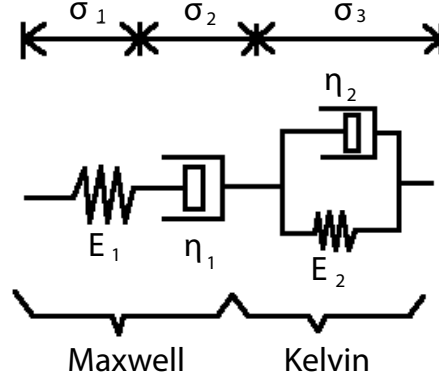


Figure 3.5: Burger's model used to simulate the surface membrane.

accommodate high viscoelasticity. Second, the state equation featuring the inside gel has to simulate a viscoelastic and incompressible gel.

As the first step, I developed the model governing the surface membrane to simulate viscoelastic features of its real counterpart. To achieve this simulation, I linked each node of the surface membrane to its neighbours through an assembly of dashpots and springs as illustrated in Fig. 3.5. As reference, I based the selection of this assembly on the observations made by Sridhar and Insana [67]. Using ultrasonic measurements, they highlighted three important mechanical characteristics relevant for simulating breast tissues. The first characteristic featured the observation that breast tissues have a linear behavior in response of up to 5 N of applied force. The second characteristic involved a creep-relaxation strain response lasting 200 s from an in-vivo breast. They observed that when a force of 4 N was applied during the first 90 seconds, the breast was not back to its original shape after 200 s. The third characteristic was a two-term Prony series with a quickly and sharply rising displacement followed by a time independent displacement. According to Moheesin [68], a Burger's material including a Maxwell material in series with a Kelvin material (illustrated in Fig. 3.5) can simulate all these characteristics. To simulate a Burger's material, I use Eq. (3.5) to describe the behavior of the surface

membrane [68]:

$$\sigma + \left(\frac{\eta_1}{E_1} + \frac{\eta_1}{E_2} + \frac{\eta_2}{E_2}\right)\dot{\sigma} + \frac{\eta_1\eta_2}{E_1E_2}\ddot{\sigma} = \eta_1\dot{\varepsilon} + \ddot{\varepsilon}, \quad (3.5)$$

where σ is the stress of the material, $\dot{\sigma}$ and $\ddot{\sigma}$ are the first and second time derivatives of the stress respectively, η_1 and η_2 represent the damping coefficients of the two dashpots, E_1 and E_2 represent the levels of stiffness of the two springs, $\dot{\varepsilon}$ and $\ddot{\varepsilon}$ are the first and second time derivative of the strain ε , respectively. To isolate the strain, I assumed that the Burger's material was under a constant force or no force at the time step 0. Therefore, the strain ε is governed by 3.6 [68]:

$$\varepsilon(t) = \frac{\sigma}{E_1} + \frac{\sigma}{E_2}(1 - e^{-E_2/T\eta_1}) + \frac{\sigma}{\eta_2}T, \quad (3.6)$$

where T is the time in a continuous form. In order to replace the exponential term with a differential term better suited for a real-time simulation, I use the exponential decay derivation. This allows the model to approximate the response of the breast phantom in each current time step with values computed in previous time steps. For this real-time simulation, I implemented Eq. (3.7) as the discrete form of Eq. (3.6) to compute the displacement of a node.

$$u(t) = \frac{F(t)}{E_1} + \frac{F(t)}{E_2} - \frac{F(t)}{E_2} \cdot \frac{E_2}{\eta_1} \cdot \frac{du(t)}{dt}, \quad (3.7)$$

where t is the discrete time step, u is the displacement and F is the force in the Burger material. In addition to the displacement computation, the Burger's material is expected to compute force feedback.

In terms of force feedback from the Burger material, I based the computation on studies reporting that the stress is the same in both Maxwell and Kelvin materials [17, 68]. For faster computation, I chose to use the Maxwell part of the Burger's material to compute force feedback. Stress computation of the Maxwell material was governed by Eq. (3.8) [68]:

$$\sigma(t) = \varepsilon_0 E(e^{-E/T\eta} + 1), \quad (3.8)$$

Similarly to the strain equation Eq. (3.7), the time T in Eq. (3.8) is not discretized and the exponential function in Eq. (3.8) is replaced with a differential term using an exponential decay derivation. I also modified it to accommodate two free nodes a and b as shown in the following constitutive equation:

$$F_{surface,a}(t) = \frac{E_1}{\eta_1} \left(\frac{du_a(t)}{dt} - \frac{du_b(t)}{dt} \right) + E_1 (\|u_a(t) - u_b(t)\| - \|r\|), \quad (3.9)$$

where t represents the discrete time step, $F_{surface,a}$ is the force computed from one link attached to the node a , $du_a(t)/dt$ is the velocity of the node a , $du_b(t)/dt$ is the velocity of the node b at the other end of the link, $u_a(t)$ and $u_b(t)$ are the vector position of the node a and node b at the time step t respectively, and $\|r\|$ is the resting distance between these two nodes when the force between them is null. Due to the presence of two different materials for the surface membrane and inside gel, the force computed by the Burger's material was only a part of the force computed by the model. Without internal node, the inside gel material was responsible for the rest of the force maintaining the shape of the virtual phantom.

As the second step, I used a state equation required to keep the shape of the breast phantom consistent. In order to simulate a high viscoelastic gel and keep the volume of the phantom stable, I derived a new differential equation. This equation was preceded by a simple ideal gas law:

$$F_{inside}(0) = \frac{P}{V}, \quad (3.10)$$

where $F_{inside}(0)$ is the force setting the shape of the phantom stable at the time step 0. P represents the pressure inside the phantom and V is the initial volume of the phantom computed through the divergence theorem [69]. The ideal gas law equation computed the initial internal force needed to set the volume of the phantom equal to its real counterpart. For each following time step t , the internal force was computed

through the following constitutive equation:

$$F_{inside}(t) = F_{inside}(t-1) - F_{inside}(t-1) \frac{V(t) - V(t-1)}{V(t-1)} a_1 - a_2 V(t)/dt + a_3 F'_{inside}(t)/\delta t, \quad (3.11)$$

where $F_{inside}(t)$ is the force keeping the shape of the phantom stable, $F_{inside}(t-1)$ and $V(t-1)$ represent the internal force and the volume of the phantom at the time step $t-1$, respectively, a_1 , a_2 and a_3 are factors applied to the different elements of the equation and are modifiable to change the behavior of the inside material, δt is the change of a time step and $F'_{inside}(t)$ represents the first derivative of the force keeping the shape of the phantom stable. The force computed by Eq. (3.11) was transferred on each triangle of the surface mesh based on its individual geometric size. The force was furthermore equally distributed to the 3 nodes forming each triangle. Because a node was included in more than one triangle, each node's internal force was a summation of the force distributed by each triangle formed by the particular node.

The combination of the force distributed from the surface mesh and the force computed from the inside gel on each node yielded a stable virtual phantom mimicking the geometry of a physical counterpart. An external force can be applied to any nodes of the virtual phantom. On each node in contact with the external force, I summed the external force with the surface force and the internal force using Eq. (3.12):

$$F_i(t) = F_{inside,i}(t) + F_{surface,i}(t) + F_{applied,i}(t), \quad (3.12)$$

where $F_i(t)$ is the total vector force at the node i at the time step t , $F_{inside,i}(t)$ and $F_{surface,i}(t)$ represent the vector force computed by the state equation and the surface mesh respectively at the node i at the time step t . Finally, $F_{applied,i}(t)$ is the vector force externally applied on the node i at the time step t . The aggregation of a surface mesh with an inside gel has the advantage of being faster to compute than 3D mesh simulation due to the reduced number of nodes to be computed, and allows the simulation to be stable and close to the behavior of its physical counterpart when the constitutive

parameters are carefully approximated.

The approximation of the parameters for both constitutive equations, Eq. (3.9) and Eq. (3.11), was of paramount importance for closely simulating a breast phantom. Following my assumption that a breast phantom is a generalization of a physical breast mimicking its real mechanical properties, I based my approximation on two different reports studying the viscoelasticity and hyperelasticity parameters from real breasts and breast phantoms [67, 70]. With help of ultrasonic measurement, the first report describes the viscoelastic behavior of an in-vivo breast under the application of force at 4 N during a period of 90 seconds. From this report, I extracted a two-term Prony series Eq. (3.13) [71]:

$$C_{ij}^R(t) = C_{ij}^0 \left(1 - \sum_{k=1}^2 g_k^P (1 - e^{t/\tau_k}) \right), \quad (3.13)$$

where g_k^P and τ_k are the k -th Prony constants and the k -th Prony retardation time constants, respectively, t is the current time step and C_{ij}^0 is the Neo-Hookean hyperelastic parameter. After a manual test on a physical breast phantom, I reduced the recovery time (time needed to have the phantom back to its original shape) to 1 second. Therefore both retardation time constants were significantly reduced. The second report describes the hyperelastic parameters governing a breast phantom using a Neo-Hookean equation [70]. Eq. (3.14) controls the surface membrane and inside gel components [71]:

$$U = C_{10}(\bar{I}_1 - 3) + \frac{1}{D_1}(J^{el} - 1)^2, \quad (3.14)$$

where U represents the strain energy per unit of reference volume, C_{10} and D_1 are material parameters, J^{el} is the elastic volume ratio of the original volume of the breast phantom over it deformed volume, \bar{I}_1 is the average first invariant of left Cauchy-Green deformation tensors. Under the assumption of volume conservation, J^{el} should be always equal to 1. Tables 3.1 and 3.2 indicate the proper values for the modified Prony series and Neo-Hookean parameters for membrane and inside gel, respectively.

My customized real-time model did not allow the direct use of the parameter values



Figure 3.6: FEM model representing a breast phantom.

Thickness	2 mm			
Density	950 kg/m ³			
Neo-Hookian parameters	C_{10}	700.3 kPa	D_1	0.001
Prony Series	g_1^p	0.9	τ_1	0.002
	g_2^p	0.9	τ_2	0.002

Table 3.1: Surface parameters extracted from literature.

Density	950 kg/m ³			
Neo-Hookian parameters	C_{10}	10.3 kPa	D_1	0.001
Prony Series	g_1^p	0.9	τ_1	0.002
	g_2^p	0.9	τ_2	0.002

Table 3.2: Inside gel parameters extracted from literature.

collected in the two reports [67, 70]. Therefore, I approximated the parameters for the real-time model from the behavior produced by these collected parameters in the reports. I accomplished this by creating a FEM model as shown in Fig. 3.6. This FEM model shared two features of the real-time model: the outside geometry used in the real-time model and the usage of surface membrane and inside gel as materials. The geometry of both real-time and FEM models are identical to have the same number of nodes and the same Cartesian coordinate system.

Based on these two reports, I utilized the same two-term Prony series to simulate the viscoelastic component for both materials. Using the parameters from Table 3.1 and

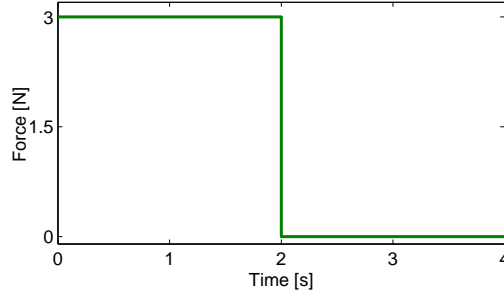


Figure 3.7: Force profile applied to palpate the breast phantom.

Burger's model parameters	Elasticity of the 1st spring	E_1	0.6 N/cm
	Elasticity of the 2nd spring	E_2	0.01 N/cm
	Viscosity of the 1st dashpot	ε_1	0.49 N×s/cm
	Viscosity of the 2nd dashpot	ε_2	0.01 N×s/cm

Table 3.3: Surface parameters for the real-time simulation.

Pressure	Initial value	P	10 N/cm ²
Viscoelasticity factors	Change of velocity between two time-steps	a_1	120
	1 st derivative of velocity	a_2	0.01
	2 nd derivative of force	a_3	0.001

Table 3.4: Inside gel parameters for the real-time simulation.

3.2, Eq. (3.13) and Eq. (3.14) governed the FEM model under applied force. Following the standard procedure of a creep followed by a relaxation to test viscoelastic response [9, 17], I created a 4-second step-wise force profile as depicted in Fig. 3.7. During the first 2 seconds, a force of 3 N (maximum force sustained for a period of time by the haptic device PHANTOM 1.5/6DOF) was applied on the top node without ramping to observe the creep response. During the last 2 seconds, no force was applied to observe the relax response – the recovery of the phantom. From this 4-second force profile, I focused on the displacement of the top node and manually set the ranges of values for the different parameters. A naive optimization algorithm of testing every value within the ranges selected the value that produced the minimal difference of displacement between the real-time model and its FEM counterpart. Tables 3.3 and 3.4 show the parameters to mimic the phantom in real time used in Eq. (3.9) and Eq. (3.11), respectively. With

these parameters, the real-time simulation was updated at 100 Hz computing visual displacement and force feedback on a DELL Precision 690 (with 2 dual-core processors at 3.2GHz and 4 GB of RAM). That is, a time step of simulation governed by the real-time model is 10 ms long. Thus, the 4-second stepwise force profile yields 400 time steps for both real-time and FEM models. At each time step, the simulation governed by the FEM model requires however 22.5 s on the same computer. This great difference of the computational time between the real-time and FEM models offers an incentive to consider the real-time model as an alternative candidate to its FEM counterpart, once the real-time model is evaluated as acceptable.

To create a real-time model for palpation training, algorithms of collision detection and collision response must have the following features: to provide multi-node contact, to handle soft objects, and to accommodate varying types of shapes. For collision detection, I used the Axis Aligned Bounding Box (AABB) algorithm [72] because it offers all of the features needed for the simulation as introduced in Chapter 2. The AABB algorithm is part of BVH algorithms, as described in Chapter 2. I implemented two AABB trees: a dynamic AABB tree to describe the virtual breast phantom with a hemispherical shape and a diameter of 8.0 cm and a static AABB tree to depict an irregular rigid object (such as a finger). A coarse mesh of 338 nodes comprised the whole breast phantom. A fine mesh with 1587 nodes formed the whole finger. The contact area of the finger had about 120 nodes whereas the contact area on the virtual phantom had 23 nodes. The fine mesh of the finger permits the computation necessary to contact and deform the breast phantom. When the finger contact area collided to the breast phantom, a standard algorithm of tree searching checked upon contacting faces and returned two sets of contacted mesh faces (one set for the breast phantom and another set for the finger contact area).

Based upon the returned two sets of contacted mesh faces, I coded an algorithm

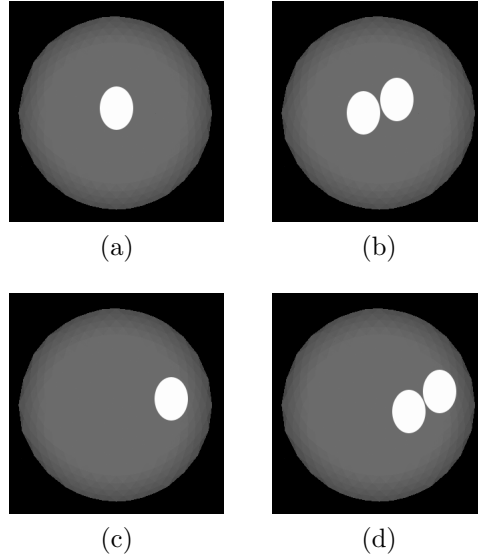


Figure 3.8: Interaction Condition; (a) Condition I features a one-finger contact on the top of the phantom; (b) Condition II involves a two-finger contact on the top of the phantom; (c) Condition III simulates one-finger contact on the side of the phantom; (d) Condition IV mimics a two-finger contact on the side of the phantom.

of collision response. This algorithm has three steps. In the first step, the algorithm finds the normal of a closest contact face from the set of the finger contact area for each contacted vertex of the breast phantom. In the second step, the algorithm moves each contacted vertex of the phantom to separate the phantom and the finger contact area. In the third step, the algorithm updates the phantom deformation with the new locations of all vertices of the phantom.

3.3.2 Evaluation Method

Applying the evaluation method described earlier, I started the evaluation of the real-time model with the data acquisition step. As the first task of the data acquisition, I took the same FEM model as used to approximate the real-time parameters earlier. The second task involves the definition of a force profile. In this case study, I used the same 4-second stepwise force profile as illustrated in Fig. 3.7. For the third task, I created four different testing conditions as depicted in Fig. 3.8. In each condition,

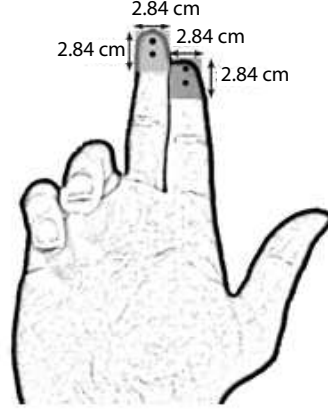


Figure 3.9: Two fingers palpation.

I tested the four force distributions shown in Fig. 3.3 in sequence. Fig. 3.8a shows Condition I. This condition tested the most trivial case in which the user palpates the top of the phantom with only the distal section of an index finger as shown in Fig. 3.2(a). Condition II, depicted in Fig. 3.8b, assessed the usage of the same finger positioned on a selected node located off-center on the phantom. This condition aimed to evaluate the dispersion of the force from a randomly selected node. The Condition III and Condition IV investigated the usage of a large, realistic contact area during palpation. Under these two conditions, I took the distal section of the index and middle finger as the contact area, as illustrated in Fig. 3.9. Each force distribution was applied simultaneously on both distal sections of the fingers. Condition III and Condition IV tested the contact area created by both sections on the top of the phantom, in Fig. 3.8c, and on the same location as in Condition II, in Fig. 3.8d, respectively. The size and shape of both fingers matched the mean measurements taken on some male personnel of the U.S. Army [73].

For all force distributions in each testing condition, the fourth task involves data recording. At each time step of the force profile, I recorded datasets on the real-time model and the FEM model. One dataset included the visual displacement of all surface nodes whereas another dataset accumulated the force feedback computed on the contact area. Computing values for every node on the hemisphere, the real-time model required

each time step for 10 milliseconds whereas the FEM model needed 22.5 seconds for each time step. For each force distribution, I collected a set of 135,200 data points (338 nodes - all nodes composing the geometry - in 400 time steps) for the dataset of visual displacement and a set of 23 nodes - all nodes within the contact area - in 400 time steps per finger for the dataset of force feedback.

Using all displacement data and only force feedback data located in the contact area, the step of data processing starts with the RMSE computation, followed by ANOVA analyses. When the p -value is higher than 0.05, this means that the datasets cannot be differentiated. However, the ANOVA analysis in this case does not denote that the datasets agree with each other. Consequently, the Bland and Altman agreement analysis [13] is implemented to reveal agreement between these two datasets when more than 95% of the data is located within $\pm 2SD$.

3.3.3 Results

The results here follow the organization of the evaluation method described in the previous subsection. I focused on two different aspects. The first aspect validates the real-time model to mimic an actual breast phantom. The second aspect assesses differences in agreement among the four force distributions. To undertake these two aspects, I started with Condition I and Condition II, as shown in Fig. 3.8a and Fig. 3.8b, involving the palpation performed by the distal section of the index finger located on the top and on the side of the phantom. For Condition I, Table 3.5 and Table 3.6 present the results of the comparison for visual displacement and force feedback, respectively; whereas Table 3.7 and Table 3.8 show the results of the comparison for visual displacement and force feedback, respectively, for Condition II. I observed that each force distribution yields p -values from ANOVA well above the significance threshold of 0.05 and an agreement over 95%.

For the second aspect, I looked at agreement levels and SD values in these four

	RMSE [cm]	ANOVA		Bland and Altman Agreement	
		F^*	p	SD [cm]	Agree [%]
Distr. 1	0.08	1.45	0.21	0.16	98.6
Distr. 2	0.16	1.92	0.18	0.21	97.3
Distr. 3	0.15	1.43	0.25	0.17	96.2
Distr. 4	0.21	1.98	0.15	0.32	95.2

Table 3.5: Condition I – Visual displacement comparison [$F^* = F(1, 135199)$].

	RMSE [N]	ANOVA		Bland and Altman Agreement	
		F^*	p	SD [N]	Agree [%]
Distr. 1	0.06	0.15	0.85	0.01	99.2
Distr. 2	0.10	0.28	0.68	0.09	96.1
Distr. 3	0.14	0.35	0.51	0.19	95.2
Distr. 4	0.16	0.84	0.32	0.28	95.1

Table 3.6: Condition I – Force feedback comparison [$F^* = F(1, 9199)$].

	RMSE [cm]	ANOVA		Bland and Altman Agreement	
		F^*	p	SD [cm]	Agree [%]
Distr. 1	0.17	2.37	0.12	0.27	95.2
Distr. 2	0.21	1.52	0.36	0.29	95.0
Distr. 3	0.26	1.69	0.32	0.32	95.3
Distr. 4	0.32	0.96	0.48	0.33	96.5

Table 3.7: Condition II – Visual displacement comparison [$F^* = F(1, 135199)$].

	RMSE [N]	ANOVA		Bland and Altman Agreement	
		F^*	p	SD [N]	Agree [%]
Distr. 1	0.05	0.12	0.86	0.01	98.6
Distr. 2	0.12	1.20	0.31	0.12	96.3
Distr. 3	0.26	1.93	0.29	0.21	95.8
Distr. 4	0.32	2.02	0.21	0.25	95.3

Table 3.8: Condition II – Force feedback comparison [$F^* = F(1, 9199)$].

tables. As illustrated in Table 3.5 and Table 3.7, all distributions yield similar levels of agreement with varying SD values for visual displacement. This observation was similar for force feedback as shown in Table 3.6 and Table 3.8. The main difference appeared between Distribution 1 (single-node contact) and the other Distributions 2 to 4 (multi-node contact). This was mainly due to the smaller number of data points

	RMSE [cm]	ANOVA		Bland and Altman Agreement	
		F^*	p	SD [cm]	Agree [%]
Distr. 1	0.19	1.31	0.21	0.20	97.7
Distr. 2	0.23	1.25	0.25	0.29	96.2
Distr. 3	0.34	1.50	0.35	0.35	94.0
Distr. 4	0.35	1.52	0.36	0.36	93.5

Table 3.9: Condition III – Visual displacement comparison [$F^* = F(1, 135199)$].

	RMSE [N]	ANOVA		Bland and Altman Agreement	
		F^*	p	SD [N]	Agree [%]
Distr. 1	0.08	0.21	0.72	0.05	98.1
Distr. 2	0.15	1.01	0.21	0.21	92.5
Distr. 3	0.25	1.21	0.15	0.28	89.2
Distr. 4	0.26	1.23	0.14	0.29	87.1

Table 3.10: Condition III – Force feedback comparison [$F^* = F(1, 9199)$].

for Distribution 1 (1 data point per time step) than for the other distribution (23 data points per time step for one finger).

I continued the investigation with Condition III and Condition IV. During palpation, these two conditions have the same contact area of fingers (46 data points per time step). The contact area (46 data points per time step) was formed by the distal section of the index and middle fingers. For Condition III, Table 3.9 and Table 3.10 exhibit the comparison results of visual displacement and force feedback, respectively. The results of the same comparison for Condition IV are shown in Table 3.11 and Table 3.12, respectively. The validation of the real-time model as a candidate for mimicking an actual phantom did not produce similar results as in Condition I and Condition II. For visual displacement, Table 3.9 shows that only Distribution 1 (single-node contact) and Distribution 2 (multi-node contact with uniform force) yielded an agreement value over the 95% threshold in Condition III, whereas Table 3.12 has only Distribution 1 over that threshold in Condition IV. Similarly, force feedback data comparison (Table 3.10 and Table 3.12) displays only Distribution 1 as over the agreement threshold in both conditions. This shows the limit of the real-time model due to a larger number

	RMSE [cm]	ANOVA		Bland and Altman Agreement	
		F^*	p	SD [cm]	Agree [%]
Distr. 1	0.16	1.50	0.49	0.30	95.0
Distr. 2	0.25	1.70	0.35	0.21	93.2
Distr. 3	0.32	1.82	0.35	0.36	92.5
Distr. 4	0.35	1.72	0.42	0.35	90.1

Table 3.11: Condition IV – Visual displacement comparison [$F^* = F(1, 135199)$].

	RMSE [N]	ANOVA		Bland and Altman Agreement	
		F^*	p	SD [N]	Agree [%]
Distr. 1	0.10	0.25	0.65	0.05	97.5
Distr. 2	0.19	0.99	0.46	0.21	92.1
Distr. 3	0.27	1.27	0.23	0.35	88.2
Distr. 4	0.29	1.31	0.21	0.38	86.5

Table 3.12: Condition IV – Force feedback comparison [$F^* = F(1, 9199)$].

of contact nodes in Distributions 2 to 4. Nevertheless, differences of agreement among the four force distributions revealed important details. As illustrated in Table 3.10 and Table 3.12, force feedback agreement was more sensitive to the complexity of the force distribution than its visual displacement counterpart. The difference between the best agreement (Distribution 1) and the worst agreement (Distribution 4) was about 10% in Condition III and Condition IV. In contrast, this difference was only about 5% in visual displacement for both Condition III and Condition IV.

3.3.4 Discussion

The results of my case study have implications for using the real-time model as a candidate to simulate a highly viscoelastic soft tissue. These implications can be explored from three different perspectives. The first perspective investigates the difference among force distributions within a testing condition. This point of view has the potential to determine the usability of the different force distributions for user interaction. The evaluation assesses not only single-node contact, but also multi-node contact. In most testing conditions, I observe a generally decreasing trend of the level of agreement from

Distribution 1 to Distribution 4. This holds not only for visual displacement but also for force feedback. These observations confirm that the complexity of the contact force plays a role in the level of agreement between the real-time model and its FEM counterpart. Because multi-node contacts simulate more closely palpation than a single-node contact, a trade-off between the level of agreement and realism might become a suitable compromise to provide users with the best interaction. However, a human study is needed to verify if a trade-off is possible and which distribution would produce the most intuitive interaction.

The second perspective looks at the difference among the testing conditions at the top and side locations. The aim is to verify whether the location of the applied force plays a role in the level of agreement between the real-time model and its FEM counterpart. My observations indicate only slight differences in visual displacement and force feedback between these two locations. Although no significance tests are performed for confirmation, the location of the applied force does not seem to affect the level of agreement for visual displacement and force feedback.

The third perspective focuses on the difference between the one-finger and two-finger contacts. I examined whether the real-time model is able to keep a reasonable agreement with its FEM counterpart when the contact area is enlarged by a second finger applying force. In the one-finger contact, my case study reveals that using one-finger contact along with multiple-node contact area could reduce modeling complexity while keeping a high level of agreement and good realism. However this observation is not as clear-cut for the two-finger contact. Only Distribution 1 (single-node) shows a level of agreement over 95% in visual displacement and force feedback comparison, whereas all other multi-node contacts (Distributions 2 to 4) display various levels of agreement, but never below 86.5%. Although being below the 95% threshold set in this study, lower levels of agreement might still be enough to prevent humans from noticing a difference

due to the just-noticeable difference threshold of 10%-15% for softness discrimination [36].

In summary, the real-time model seems to handle very well the contact force generated by the one-finger contact under all force distributions. However for two-finger contact, the real-time model becomes less reliable and fails the statistical analysis. Nevertheless, studies are needed to verify if humans could perceive the deformation of the real-time model correctly.

3.4 General Discussion

In the present study, I proposed an evaluation method for assessing real-time models for multi-node contact of palpation. This method was based on the rationale that human perception seems to be less than perfect at many levels [74, 7, 36]. I demonstrated the practicality of this method for investigating both visual displacement and force feedback in various force conditions for palpation. This method was formalized to provide a standard procedure to assess models of soft tissues in real-time simulations.

Based on a more precise assessment than state-of-the-art evaluation methods comparing output at selected time steps [9, 64], my method of evaluation compares both visual displacement and force feedback at every time step with varying applied force. This difference allows warranting that the real-time model closely follows its FEM counterpart over the whole force profile. Moreover, my method of evaluation is highly customizable, since it permits changes in force distributions, locations and contact areas while still keeping the same evaluation procedure.

Because of imperfect human perception, achieving an excellent match between a real-time model and its physical counterpart suggests a superfluity for developing VR real-time systems. Therefore, from a perspective of user interaction, I selected a lower level of agreement at 95% for both visual displacement and force feedback under each

force distribution. This particular level of agreement is derived from statistical methods assuming less than 5% offset data, as well as from the observed limitation of human perception [7]. Removing the need for excellent match that requires a lot of computational power, human perception limitation can be an important factor in providing fast and relatively less complex real-time model sufficient for user interaction. Nevertheless, further studies are presented in the following chapters to confirm this notion.

3.5 Summary

This chapter presented an evaluation method designed to assess the behavior of a real-time model in comparison with an offline FEM model. Based on evidence that human perception is not very sensitive to small differences in a real-time simulation, this evaluation takes a statistical approach to check the level of agreement between the real-time model and its FEM counterpart. To show the benefit of this evaluation, I applied it to a breast phantom real-time model used in a VR palpation training system. The main innovations introduced in this chapter are: (1) the evaluation considering this limitation of human perception, (2) the comparison of visual displacement and force feedback at all time steps of a quantized force profile, (3) the usage of force distributions in different testing conditions involving one or two fingers, and (4) the modification of a real-time model to simulate an highly viscoelastic soft tissue.

In this chapter, the real-time model shows an agreement level over 95% for all distributions in the two conditions involving only one-finger contact. However, the agreement level is not as high when using a two-finger contact. Nevertheless, it is not clear at the moment if the levels of agreement found in this study are sufficient for adequate human interaction. The next chapters of this thesis will describe two human studies to investigate the effect of levels of agreement on human interaction. In particular, Chapter 4 presents a human study exploring the effect of alignment between a visual display and

a haptic device on perception of object softness. The goal of this study is to find the alignment that provides interaction introducing a minimum physical workload.

Chapter 4

Effect of the Alignment between a Visual Display and Haptic Device on the Perception of Object Softness*

4.1 Introduction

As introduced in Chapter 2, the integration of haptic and visual information can be problematic in VR systems for palpation training, due to different representations by the two senses of touch and vision [75, 43, 44]. Several studies have revealed that haptic and visual information can interfere with each other in object perception, particularly in discriminating object softness [35, 36, 76]. While working for my master's degree, I investigated the effect of viewing angle on the perception of object softness using three different alignments. During this investigation, I observed that the alignment of a visual display relative to a haptic device appeared to have some effect on the perception of object softness [76]. Furthermore, I was unable to find other reports on the effect of such alignments on the perception of object softness. The investigation of such effect is important for providing a right alignment of a VR training system for palpation. This alignment needs to have a limited impact on user interaction and perception of object softness. Therefore, in the current chapter, I conducted a study to investigate

*Part of this chapter is published.

A. Widmer and Y. Hu, "Subjective Perception and Objective Measurements in Perceiving Object Softness for VR Surgical Systems," *IEEE VR 2009*, pp.267-268, Lafayette, Louisiana, 14-18 March 2009.

A full version of this chapter is published in IEEE transactions.

A. Widmer and Y. Hu, "Effects of the alignment between a visual display and haptic device on the perception of object softness," *IEEE Trans. on Syst, Man and Cyber., Part A*, vol.40, no.6, pp.1146-1155, Nov. 2010. See Appendix B for copyright transfers.

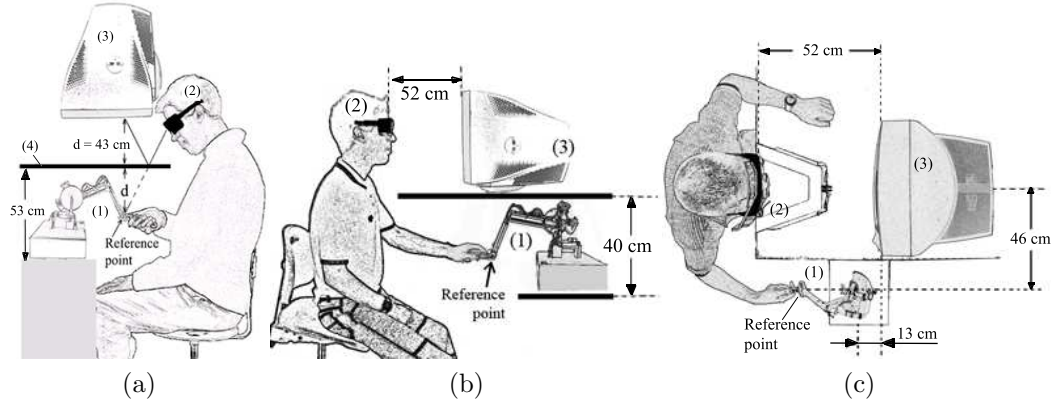


Figure 4.1: The three tested alignments between a visual display and haptic device. (a) “Same-location” alignment; (b) Vertical alignment; (c) Horizontal alignment; (1) Haptic device; (2) Stereoscopic goggle; (3) 3D display; (4) First-surface mirror.

how three popular alignments affect the perception of object softness. From raw data partially collected for my master’s work, I re-examined the data to compare dependent measurements – as subjective perception of object softness and objective measurements of maximum force and pressing depth – in three alignments (independent variables) between a visual display and haptic device. The three alignments are illustrated in Figs. 4.1a, 4.1b and 4.1c, respectively.

Fig. 4.1a depicts the VR setup for Experiment I - a “same-location” alignment. This alignment is obtainable via a first-surface mirror, which reflects the visual display of deformable balls to meet the reference point of the haptic device. This alignment merges the senses of touch and vision at one spatial location. Experiment II used a vertical alignment between a visual display and haptic device, as shown in Fig. 4.1b. In this alignment, the haptic device is located directly under the visual display. This alignment introduces a vertical offset between the senses of vision and touch. I used a horizontal alignment between a visual display and haptic device in Experiment III, as illustrated in Fig. 4.1c. In this alignment, the haptic device is beside the visual display, introducing a horizontal offset between the senses of touch and vision.

4.2 Methodology

For providing information connected to data analysis, subsections 4.2.1, 4.2.2, 4.2.3 and 4.2.4 below re-introduce experimental methodology of participants, apparatus, stimuli and procedure, respectively. This information was based upon the three experiments undertaken for my master’s work, Data analysis (subsection 4.2.5) re-examined the raw data of this master’s work to include objective measurements for comparing the effect of the different alignments on the perception of object softness.

4.2.1 Participants

A total of 45 participants (25 males and 20 females, aged between 20 and 30 years old) participated in the study. They were randomly divided into three groups of 15; participants in one group palpated a virtual soft ball using the “same-location” alignment, vertical alignment or horizontal alignment. They were all naive to the purpose of the study and had normal or corrected-to-normal vision (including normal abilities of recognizing colours), with a stereo acuity at least 40” of arc as determined by the Randot Stereotest (Stereo Optical, Inc). All participants were strongly right handed, as determined by a modified version of the Edinburgh handedness inventory [77]. Their participation followed an ethical clearance approved according to the Canadian Tri-Council Ethics Guidelines.

4.2.2 Apparatus

Three types of alignment between a visual display and haptic device were considered in this study.

- “Same-location” Alignment – As illustrated in Fig. 4.1a, the visual display faced down to a first-surface mirror which was placed at 43 cm underneath the monitor. The haptic device was located in a way that its reference point matched the ball

displayed in the mirror during each trial. The participant manipulated the haptic device underneath the mirror and viewed the balls reflected in the mirror. The participant placed his/her head on a fixed chin rest to constrain the position and orientation of his/her head and could not view his/her hand during each trial. The chin rest warranted the consistent location and orientation of the eyes of all participants.

- Vertical Alignment – As illustrated in Fig. 4.1b, the haptic device was positioned 22.0cm underneath the base of the monitor and exactly at the vertical from the middle line of the visual display. The participant placed his/her head on a chin rest to constrain the position and orientation of his/her head and could not view his/her hand during each trial.
- Horizontal Alignment – As illustrated in Fig. 4.1c, the haptic device was always placed on the right side of the visual display during the experiment, in order to accommodate the dominant hand of the participants. The haptic device was 16.5 cm lower than the base of the visual display for the comfort of resting the arm and hand. The reference point of the haptic device was located horizontally 46 cm from the middle line of the display. The participant placed his/her head on a chin rest to constrain the position and the orientation of his/her head. I placed a cache between the display and the haptic device to prevent the participant from viewing his/her hand during the experiment.

4.2.3 Stimuli

As shown in Fig. 4.2, the visual stimuli of the study were two virtual deformable balls[†] of the same size (8 cm in diameter) presented one after another on the same vertical axis.

[†]Due to the sequence of the work during my PhD study, these virtual deformable balls and their governing equations (described later) were different from the virtual breast phantom and its viscoelastic governing equations used in Chapter 3 and Chapter 5.

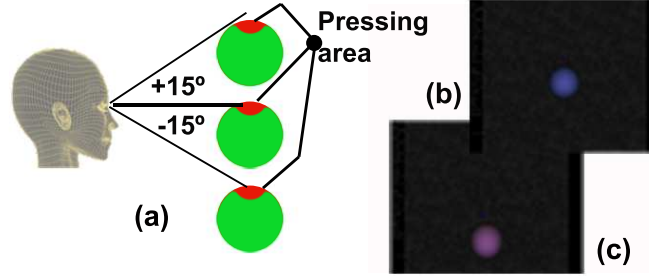


Figure 4.2: Presentation of deformable balls as visual stimuli. (a) Illustration of viewing angles and pressing areas. (b) A ball at the viewing angle of 0° as reference. (c) A ball at the viewing angle of -15° for testing.

Combined with a pair of StereoGraphics Crystal Eyes, a CRT monitor with a refresh frequency of 120 Hz and a resolution of 1024x768 pixels displayed the visual stimuli in 3D stereoscopy. In each trial, these two balls had randomly assigned two colors (purple and blue), respectively. The participant could interact with any ball via a virtual probe, which had a shape of a match stick with a red sphere attached to a blue rod. The red sphere of the virtual probe corresponded to the reference point of the 6 DOF haptic device (see Fig. 4.1a). The virtual probe moved freely in the 3D space of the balls via the haptic device. When the participant interacted with a ball by placing the virtual probe on the top of the ball via the haptic device, the ball turned into green. While one of the balls was the reference with its viewing angle always at 0° , another was the testing ball varied its viewing angle from -15° , -7.5° , 0° , 7.5° , to 15° . Each trial was either a testing trial to record the participant's interaction with the balls or a catching trial to distract the participant. All trials were randomly ordered. In all testing trials, both reference and testing balls were identical in softness (compliance = 2.1 mm/N). In catching trials, the softness of the reference ball was same as their counterparts in testing trials, whereas the testing ball had softness either with compliance = 3.8 mm/N or compliance = 0.9 mm/N. Thus, the relative compliances between the testing ball and its reference counterpart was larger than 15% – the just noticeable difference [57] – to allow this difference easily identifiable. The participant pressed (via the haptic device)

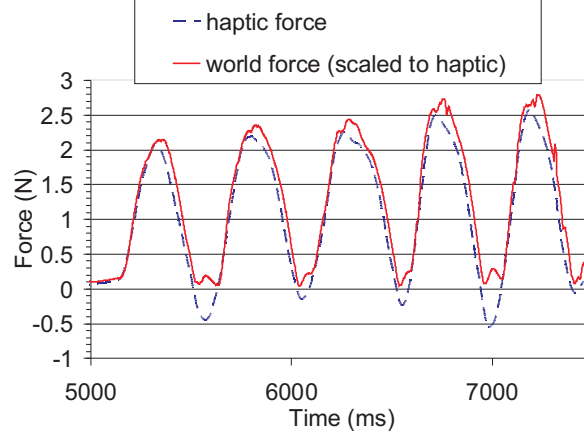


Figure 4.3: The correspondence of compliance between the force from the haptic device and the force to deform a ball. [Within the force range of the haptic device from 0.0 N to 3.0 N, the world force was scaled by a factor of 1.2 to match the haptic force. This correspondence was independent of the viewing angle of the ball and the location of the haptic device.]

only within a pressing area – on the top of a ball where its viewing angle was defined. Using a mass-spring model [78], I simulated the softness of a ball in real time. This model used the ideal gas law to calculate the inflating pressure inside the ball to keep the volume of the ball constant during pressing and the Hookean linear law to compute spring force with damping. I applied a simple model [78] as a numerical method to solve this model. According to the deformation of the ball, the real-time solution of this model provided a proper amount of force via the haptic device back to the participant’s hand as illustrated in Fig. 4.3. Thus, the deformation of the ball visualized on the CRT monitor matched the force feedback delivered by the haptic device.

4.2.4 Procedures

Before each experiment, each participant was aware of that the haptic device had a safety threshold of force. In each experiment, the participant was instructed to select the harder ball between the two deformable balls in each trial - a common paradigm of two alternative forced choices for perceiving object softness [35]. The participant took

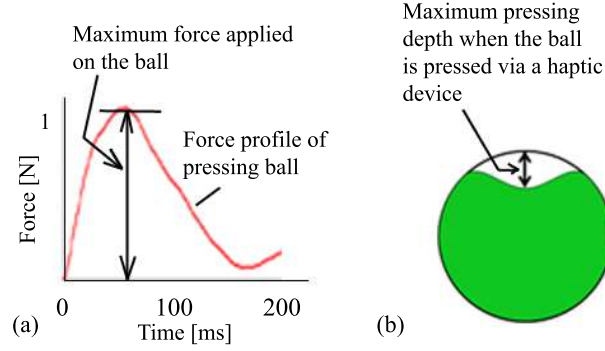


Figure 4.4: Definition of objective measurements. (a) Maximum force; (b) Maximum pressing depth.

part in all following three experimental conditions:

- V+H – Both visual and haptic information are available at the same time. During pressing a ball, the participant could view the deformation of the ball and feel the force feedback via the haptic device simultaneously.
- Vonly – Only visual information is available. The participant manipulated the haptic device in the same way as under the two conditions V+H and Honly. He/she could view the deformation of a ball without feeling the force feedback during pressing the ball.
- Honly – Only haptic information is available. During pressing a ball, the participant could feel the force feedback via the haptic device but the view of the ball was concealed.

Under each condition, a practicing session of 10 trials was prior to a testing session of 25 trials (4 testing trials and 1 catching trial for each viewing angle), allowing the participant to familiarize the condition in testing. All trials were randomized in both practicing and testing sessions in each experiment. The practicing session lasted less than 30 minutes. The testing session was about 1 hour. The order of the three conditions was counterbalanced for all participants in each experiment.

4.2.5 Data Analysis

For each experiment, I used in each trial two types of data as dependent measurements: subjective perception and objective measurements. The subjective perception was the recorded participant's selection of the harder one between the two deformable balls. The objective measurements included maximum force and maximum pressing depth applied by the participant on each ball. I computed these measurements from the recorded vertex displacements on each ball under pressing. As illustrated in Fig. 4.4a, the maximum force corresponds to the peak value of the force that the participant applied to a deformable ball in a trial. When the ball deforms under force within its pressing area, the maximum pressing depth is the longest distance between the depressed surface and its original counterpart, as shown in Fig. 4.4b. The maximum force and pressing depth are not directly correlated to each other due to the damping factor of the mass-spring model [78]. Under the condition V+H, there were both maximum force and pressing depth computed. Although the participant could not view the deformed ball under the condition Honly, the maximum pressing depth existed because the participant could feel force feedback from the ball. The maximum force was always zero under the condition Vonly, due to the absence of force feedback to the participant's hand.

For each experiment, I processed these data in all testing trials and discarded those in all catching trials. Applying the statistical method of two-way within-subject-design ANOVA (analysis of variances)[79], I examined the effect of both testing condition and viewing angle on subjective perception and objective measurements, respectively. When the two-way ANOVA analysis demonstrated a statistical significance on either testing condition or viewing angle, I employed one-way ANOVA (within subject-design) followed by a post-hoc Tukey test of HSD (honestly significant difference) to further investigate this significance.

4.3 Results and Discussion

4.3.1 “Same-location” Alignment

Subjective Perception

In my master’s work, I examined the effect of testing condition and viewing angle on subjective perception of object softness. A two-way ANOVA analysis revealed that subjective perception of object softness had no significant difference among all testing conditions [$F(2, 14) = 2.47, p > 0.05$]. In contrast, the viewing angle significantly affected this subjective perception [$F(4, 14) = 9.09, p < 0.001$], even though the balls at the extreme viewing angles of -15° and $+15^\circ$ had similar softness under both conditions V+H and Vonly. Further analysis using one-way ANOVA indicated that subjective perception of object softness exhibited significant difference among viewing angles under each condition. As well, a post-hoc Tukey test found that subjective perception of object softness differed when two viewing angles were apart at least 15° for all 5 significant pairs of viewing angles.

Using a “same-location” alignment between a visual display and haptic device, subjective perception of object softness was under the influence of viewing angles. Although there was a common significant pair of viewing angles ($-7.5^\circ, +7.5^\circ$) under both conditions Vonly and Honly, this pair was not significant under the condition V+H. This indicates that there is a subtle difference of subjective perception among all conditions. Nevertheless, the effect of viewing angle as observed in my master’s work - “the larger the viewing angle was, the harder the ball was perceived” - was valid only within the interval of viewing angles from -7.5° to $+7.5^\circ$ under all conditions. Considering that all testing balls at varying viewing angles were identical in softness, these results demonstrate that subjective perception of object softness is under a perceptual illusion under all conditions, even though the effect of this illusion is not equal under each condition. In short, viewing angle affects subjective perception of object softness, whereas testing

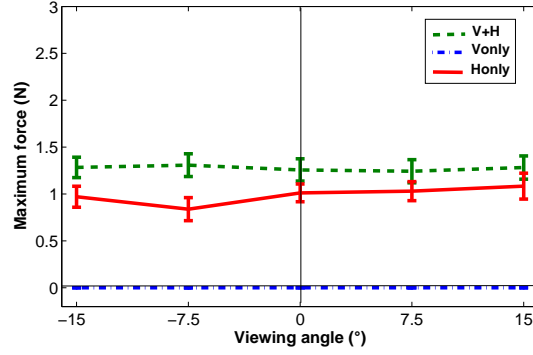


Figure 4.5: Objective measurements of maximum force under “same-location” alignment. [Error bars represent standard errors.]

condition does not.

Objective Measurements

As extension, I re-examined the raw data of my master’s work to investigate the effect of testing condition and viewing angle on objective measurements of maximum force and pressing depth. A two-way ANOVA analysis discovered that all three testing conditions had a significant difference of effects on objective measurements of maximum forces [$F(2, 14) = 155.08, p < 0.0001$] and pressing depth [$F(2, 14) = 15.06, p < 0.001$], respectively. These results contrast to the above observations related to subjective perception of object softness.

As shown in Fig. 4.5 and Table 4.1, further analysis using one-way ANOVA revealed that objective measurements of maximum force among three testing conditions had a significant difference at each viewing angle. A post-hoc Tukey test (see the last column in Table 4.1) found that objective measurements of maximum force exhibited significant differences between the conditions V+H and Vonly (as well between conditions Vonly and Honly) for all viewing angles. The same observations were true between the conditions V+H and Honly for two viewing angles of -15° and -7.5° , even though the mean of the maximum force (1.33 N) under the condition V+H was larger than its counterpart (1.11 N) under the condition Honly, as illustrated in Fig. 4.5. The mean of the maximum

Table 4.1: Results of one-way ANOVA and Tukey-test for the effects of testing condition on maximum force under “same-location” alignment.

	One-way ANOVA	Tukey-test HSD	
-15°	$F = 55.20 \ p < 0.0001$	V+H to Honly	$p < 0.001$
		V+H to Vonly	
		Vonly to Honly	
-7.5°	$F = 44.01 \ p < 0.0001$	V+H to Honly	$p < 0.001$
		V+H to Vonly	
		Vonly to Honly	
0°	$F = 57.83 \ p < 0.0001$	V+H to Vonly	$p < 0.001$
		Honly to Vonly	
7.5°	$F = 51.86 \ p < 0.0001$	V+H to Vonly	$p < 0.001$
		Honly to Vonly	
15°	$F = 41.57 \ p < 0.0001$	V+H to Vonly	$p < 0.001$
		Honly to Vonly	

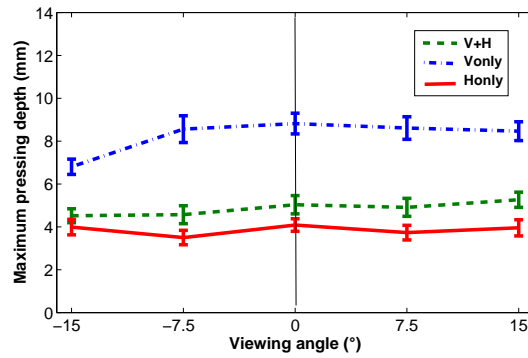


Figure 4.6: Objective measurements of maximum pressing depth in Experiment I. [Error bars represent standard errors.]

force was 0.0 N under the condition Vonly, because no force was rendered.

For objective measurements of maximum pressing depth, there were similar observations resulted from the analyses of a one-way ANOVA and a post-hoc Tukey-test, as shown in Fig. 4.6 and Table 4.2. The exception is that there was no difference of maximum pressing depth between the conditions V+H and Honly, although the mean of the maximum pressing depth under the condition V+H was constantly larger than its counterpart under the condition Honly. The mean of the maximum pressing depth was 4.98 mm under the condition V+H and 4.06 mm under the condition Honly. Without force rendering, the mean of the maximum pressing depth was 8.13 mm under the

Table 4.2: Results of one-way ANOVA and Tukey-test for the effects of testing condition on maximum pressing depth in Experiment I.

	One-way ANOVA	Tukey-test HSD	
-15°	$F = 18.48 \ p < 0.0001$	V+H to Vonly	$p < 0.01$
		Honly to Vonly	
-7.5°	$F = 31.44 \ p < 0.0001$	V+H to Vonly	$p < 0.001$
		Honly to Vonly	
0°	$F = 37.77 \ p < 0.0001$	V+H to Vonly	$p < 0.001$
		Honly to Vonly	
7.5°	$F = 34.25 \ p < 0.0001$	V+H to Vonly	$p < 0.001$
		Honly to Vonly	
15°	$F = 34.96 \ p < 0.0001$	V+H to Vonly	$p < 0.001$
		Honly to Vonly	

condition Vonly - almost twice higher than those under the conditions V+H and Honly.

In contrast, viewing angle did not have the same effects as testing condition on objective measurements of maximum force [$F(4, 14) = 0.22, p > 0.05$] and pressing depth [$F(4, 14) = 2.13, p = 0.0782$], respectively. Noticed that the effect of viewing angle on maximum pressing depth was at the border of significance ($p < 0.05$), I conducted further a one-way ANOVA analysis and found that this effect was only significant under the condition Vonly. A post-hoc Tukey-test revealed that this significance was only between two viewing angles of -15° and 0°.

In short, testing condition significantly affects objective measurements of maximum force and pressing depth. However, viewing angle does not influence maximum force under all conditions. Under the condition Vonly, viewing angle has a significant effect on maximum pressing depth only between viewing angles of -15° and 0°.

4.3.2 Vertical Alignment

Subjective Perception

In my master's work, I examined the effect of testing condition and viewing angle on subjective perception of object softness. As revealed by a two-way ANOVA analysis, testing condition do not affect the subjective perception of object softness [$F(2, 14) = 0.59,$

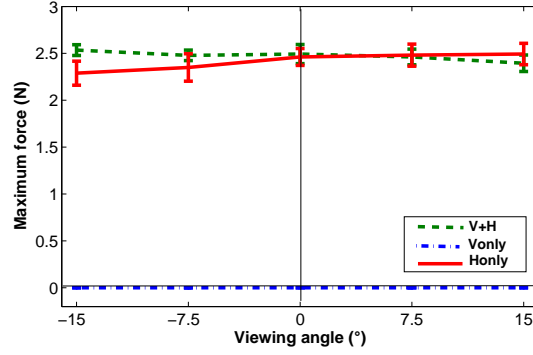


Figure 4.7: Objective measurements of maximum force under vertical alignment. [Error bars represent standard errors.]

$p > 0.05$]. Viewing angle, however, significantly influenced this subjective perception [$F(4, 14) = 21.46$, $p < 0.0001$]. A one-way ANOVA analysis on the effect of viewing angle further revealed that, under each testing condition, the larger the viewing angle was the harder the ball was perceived to be. As well, a post-hoc Tukey test revealed that all 12 significant pairs of viewing angles were at least 15° apart. Although these observations are in agreement with those made with the “same-location” alignment, the numbers of significant pairs of viewing angles found under vertical alignment is much more than that under “same-location” alignment. This indicates that vertical alignment has unique characteristics to show subtle different effects on the subjective perception of object softness from “same-location” alignment, even though both alignments has the same general effect of viewing angle.

Objective Measurements

As part of my doctoral work, I examined the effect of testing condition and viewing angle on objective measurements of maximum force and pressing depth on the basis of the raw data derived from my master’s work. A two-way ANOVA analysis revealed that testing condition had a significant effect on objective measurements of maximum forces [$F(2, 14) = 196.05$, $p < 0.0001$] and pressing depth [$F(2, 14) = 5.61$, $p < 0.0001$], respectively. As indicated in Fig. 4.7 and Table 4.3, further analysis using one-way

Table 4.3: Results of one-way ANOVA and Tukey-test for the effects of testing condition on maximum force under vertical alignment.

	One-way ANOVA	Tukey-test HSD	
-15°	$F = 294.80 \ p < 0.0001$	V+H to Vonly	$p < 0.001$
		Honly to Vonly	
-7.5°	$F = 237.83 \ p < 0.0001$	V+H to Vonly	$p < 0.001$
		Honly to Vonly	
0°	$F = 330.97 \ p < 0.0001$	V+H to Vonly	$p < 0.001$
		Honly to Vonly	
7.5°	$F = 292.90 \ p < 0.0001$	V+H to Vonly	$p < 0.001$
		Honly to Vonly	
15°	$F = 288.27 \ p < 0.0001$	V+H to Vonly	$p < 0.001$
		Honly to Vonly	

ANOVA revealed that objective measurements of maximum force among three testing conditions had a significant difference at each viewing angle. A post-hoc Tukey test (see the last column in Table 4.3) found that this difference exhibited between the conditions V+H and Vonly (as well between conditions Vonly and Honly). No significant difference existed between the conditions V+H and Honly, indicating that participants applied the similar amount of maximum force at each viewing angle under both conditions. The means of the maximum force were 2.45 N and 2.41 N under the conditions V+H and Honly, respectively. The mean of the maximum force was 0.0 N under the condition Vonly, as no force was rendered. The general observations are same as those made with the “same-location” alignment. However, the means of maximum pressing depth under three conditions under vertical alignment are about twice times larger than their counterparts under the “same-location” alignment.

In contrast, a one-way ANOVA and a post-hoc Tukey test revealed different results for objective measurements of maximum pressing depth. As shown in Fig. 4.8 and Table 4.4, difference of maximum pressing depth between the conditions V+H and Honly existed for the two negative viewing angles -15° and -7.5°. The mean of the maximum pressing depth under the condition Vonly was larger than its counterpart under the conditions V+H and Honly. At the two positive viewing angles +7.5° and +15°, no testing condition

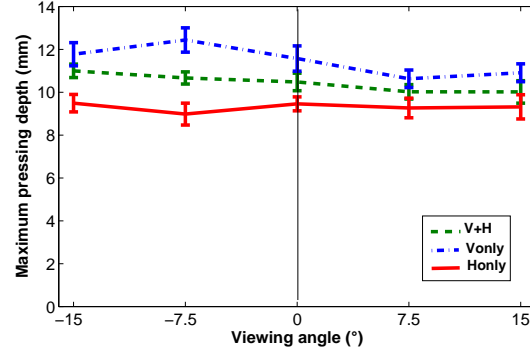


Figure 4.8: Objective measurements of maximum pressing depth under vertical alignment. [Error bars represent standard errors.]

Table 4.4: Results of one-way ANOVA and Tukey-test for the effects of testing condition on maximum pressing depth under vertical alignment.

	One-way ANOVA	Tukey-test HSD	
-15°	$F = 7.29 \ p < 0.005$	V+H to Honly	$p < 0.001$
		Vonly to Honly	
-7.5°	$F = 13.55 \ p < 0.0001$	V+H to Honly	$p < 0.001$
		V+H to Vonly	
		Vonly to Honly	
0°	$F = 5.39 \ p < 0.005$	Honly to Vonly	$p < 0.05$
7.5°	$F = 2.86 \ p > 0.05$	—	—
15°	$F = 2.49 \ p > 0.05$	—	—

was significantly different from the other. The means of the maximum pressing depth were 11.03 mm and 9.56 mm under the conditions V+H and Honly, respectively. The mean of the maximum pressing depth was 11.6 mm under the condition Vonly. This mean was close to its counterpart under the condition V+H, although being much higher than that under the condition Honly. This observation indicates that, in the absence of maximum force under the condition Vonly, the participants used the similar maximum pressing depth for perceiving object softness as that under the condition V+H with the feedback of both maximum force and pressing depth. In disagreement with observations made using the “same-location” alignment, the means of maximum pressing depth under three conditions under vertical alignment are about 1.5 to 2 times larger than their counterparts under the “same-location” alignment.

To exam the effect of viewing angle on the objective measurements of maximum force and pressing depth, I conducted atwo-way ANOVA analysis too. The analysis revealed that viewing angle did not have the same effects as testing condition on objective measurements of maximum force [$F(4, 14) = 0.17, p > 0.05$] and pressing depth [$F(4, 14) = 1.74, p > 0.05$], respectively. These results are in agreement with those observed under “same-location” alignment.

4.3.3 Horizontal Alignment

Subjective Perception

In agreement with the results observed under the “same-location” alignment and under the vertical alignment as described in my master’s work, a two-way ANOVA analysis demonstrated that testing condition did not influence the subjective perception of object softness [$F(2, 14) = 1.61, p > 0.05$]. In contrast, viewing angle significantly affected this subjective perception [$F(4, 14) = 15.53, p < 0.0001$]. A one-way ANOVA analysis on viewing angle found that the relationship between viewing angle and perceived object softness - the larger the viewing angle was, the harder the ball was perceived - was still valid as observed in the other alignments. A post-hoc Tukey test revealed that all 8 significant pairs of viewing angles were at least 15° apart. These observations are same as those found under “same-location” and vertical alignments. Nevertheless, the horizontal alignment yields different significant pairs of viewing angles from those found under “same-location” and vertical alignments. That is, the horizontal alignment between a visual display and haptic device has subtle different effects on the subjective perception of object softness from the other two alignments (“same-location” and vertical alignments).

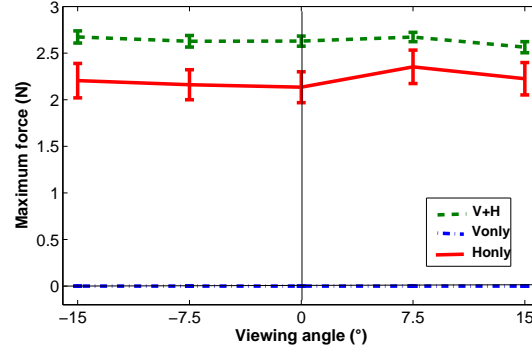


Figure 4.9: Objective measurements of maximum force under horizontal alignment. [Error bars represent standard errors.]

Table 4.5: Results of ANOVA analysis and Tukey-test for the effects of testing condition on maximum force under horizontal alignment.

	One-way ANOVA	Tukey-test HSD	
-15°	$F = 159.98 \ p < 0.0001$	V+H to Vonly	$p < 0.001$
		V+H to Honly	
		Honly to Vonly	
-7.5°	$F = 197.52 \ p < 0.0001$	V+H to Vonly	$p < 0.001$
		V+H to Honly	
		Honly to Vonly	
0°	$F = 191.93 \ p < 0.0001$	V+H to Vonly	$p < 0.001$
		V+H to Honly	
		Honly to Vonly	
7.5°	$F = 183.99 \ p < 0.0001$	V+H to Vonly	$p < 0.001$
		Honly to Vonly	
15°	$F = 171.75 \ p < 0.0001$	V+H to Vonly	$p < 0.001$
		Honly to Vonly	

Objective Measurements

Based on the raw data of my master's work, I investigated the effect of testing condition and viewing angle on objective measurements of maximum force and pressing depth, as part of my doctoral work. A two-way ANOVA analysis revealed that all three testing conditions had significant effects on objective measurements of maximum forces [$F(2, 14) = 119.25, p < 0.0001$] and pressing depth [$F(2, 14) = 9.43, p < 0.0001$], respectively. These observations are in agreement with those found under the “same-location” alignment and vertical alignment. As illustrated in Fig. 4.9 and Table 4.5, one-way

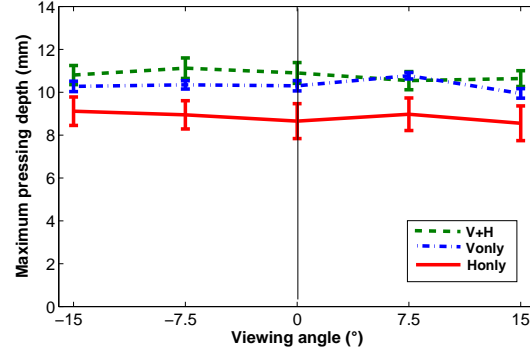


Figure 4.10: Objective measurements of maximum pressing depth under horizontal alignment. [Error bars represent standard errors.]

Table 4.6: Results of ANOVA and Tukey-test for the effects of testing condition on maximum pressing depth under horizontal alignment.

	One-way ANOVA	Tukey-test HSD	
-15°	$F = 3.19 \ p < 0.05$	V+H to Honly	$p < 0.05$
-7.5°	$F = 5.20 \ p < 0.01$	V+H to Honly	$p < 0.01$
0°	$F = 4.26 \ p < 0.05$	V+H to Honly	$p < 0.05$
7.5°	$F = 3.69 \ p < 0.05$	Vonly to Honly	$p < 0.05$
15°	$F = 4.03 \ p < 0.05$	V+H to Honly	$p < 0.001$

ANOVA analysis revealed the same trend as observed under the “same-location” alignment that objective measurements of maximum force among three testing conditions had a significant difference at each viewing angle. A post-hoc Tukey test (see the last column in Table 4.5) found that objective measurements of maximum force exhibited significant differences between the conditions V+H and Vonly (as well between conditions Vonly and Honly) for all viewing angles. The same observations were true between the conditions V+H and Honly for three viewing angles of -15°, -7.5° and 0°. In agreement with observations made under the “same-location” alignment, the mean of the maximum force under the condition V+H was constantly larger than its counterpart under the condition Honly, as illustrated in Fig. 4.9. The mean of the maximum force was 2.68 N and 2.35 N under the conditions V+H and Honly, respectively. The mean under the condition Vonly was 0.0 N as no force was rendered. The observation of these means is similar as that under vertical alignment.

In contrast, a one-way ANOVA and post-hoc Tukey test revealed different results for objective measurements of maximum pressing depth, as shown in Fig. 4.10 and Table 4.6. At any viewing angle, the maximum pressing depth under the condition Honly was significantly different under the condition V+H, except for the viewing angle $+7.5^\circ$. Under both conditions V+H and Vonly, there was no significant difference of the maximum pressing depth. The mean of the maximum pressing depth under the condition V+H was larger than its counterpart under the condition Honly. The mean of the maximum pressing depth was 11.03 mm and 9.05 mm under the conditions V+H and Honly, respectively. The mean of maximum pressing depth was 10.55 mm under the condition Vonly. This value was close to the mean computed in the condition V+H. These means are in the same scale as those computed under vertical alignment. As well, the participants used the similar maximum pressing depth under the condition Vonly (in the absence of maximum force) as that under the condition V+H (with the feedback of both maximum force and pressing depth). This observation agrees with that found under vertical alignment.

I conducted a two-way ANOVA analysis to investigate the effect of viewing angle on the objective measurements of maximum force and pressing depth. The analysis revealed that viewing angle did not have the same effect as testing condition on objective measurements of maximum force [$F(4, 14) = 0.32, p > 0.05$] and pressing depth [$F(4, 14) = 0.39, p > 0.05$], respectively. These results are in agreement with those observed in under “same-location” and vertical alignments.

4.4 General Discussion

In all three different alignments between a visual display and haptic device, ANOVA analyses revealed that subjective perception of object softness differed significantly for varying viewing angles under all testing conditions. This is in agreement with the results

found in an early work [8]. However, ANOVA analyses of the objective measurements of maximum force and pressing depth indicate that testing condition affects these two objective measurements significantly, whereas viewing angle does not. These results reveal that subjective perception of object softness is not correlated with objective measurements of maximum force and pressing depth. Furthermore, the effect of subjective perception and objective measurements are not equal among these three alignments. These observations carry implications for creating accurate VR surgical systems.

4.4.1 Subjective Perception versus Objective Measurements

In all alignments, participants applied an force (see Fig. 4.3) to a virtual deformable ball on a visual display, in order to determine its softness. The number of oscillations needed was $4 \sim 12$ for pressing each ball. This number is twice as large as the $2 \sim 6$ times for finger touching an object via a softness display device in discriminating object softness[80]. This difference might be due to the different ways of interacting with objects in this current study versus the study described in [80]. In this study, the participants pressed virtual deformable balls under both (or either) visual and haptic information, whereas in the study of [80], the participants depressed actual objects via a softness display device.

After applying oscillating force on each of two deformable balls at varying viewing angles, participants were able to select the harder ball. As subjective perception of object softness, this selection was under a perceptual illusion - the larger the viewing angle, the harder the ball is perceived. This is true for all alignments between the visual display and haptic device. Vertical alignment has the largest number of significant pairs of viewing angles that exhibits this perceptual illusion; whereas “same-location” alignment has the least number of significant pairs. This implies that the “same-location” alignment produces in general relatively consistent subjective perception of object softness among the three compared alignments. Under the condition V+H when both visual and haptic

information were available, data collected under horizontal alignment reveal only one significant pair of viewing angles (-15° to $+15^\circ$), compared to those collected under “same-location” and vertical alignments. Under this condition, data collected under horizontal alignment show stable subjective perception of objective softness at viewing angles from -7.5° to $+7.5^\circ$.

Objective measurements of maximum force and pressing depth give precision about the information underlying the subjective perception of object softness, although maximum force and pressing depth are not directly correlated to each other due to the damping factor of the mass-spring model [78]. Under all alignments, objective measurements of maximum force were indistinguishable for varying viewing angles under all three conditions. Objective measurements of maximum pressing depth had a significant difference only under “same-location” alignment among the viewing angles under the condition Vonly. Similar results were not found under both conditions Honly and V+H. This is true under all conditions using both vertical and horizontal alignments.

The above observations indicate that there seems to be a division between subjective perception of object softness and objective measurements of maximum force and pressing depth for all alignments. This is in agreement with that observed by Bergmann *et al.*[41] for perceiving object roughness. They reported that there was no correlation between an object’s perceived roughness (subjective perception) and its physical roughness (objective measurement). Furthermore, these observations seem to follow the distributive nature of haptic information for object perception, proposed by Bracewell *et al.*. [81]. When only haptic information was available, I observed no significant difference among viewing angles for objective measurements of maximum force and pressing depth. However, subjective perception of object softness demonstrated a significant difference given this same haptic information.

4.4.2 Advantage of “Same-Location” Alignment

Among the three alignments, an interesting observation from objective measurements is the different means of maximum force and pressing depth under all conditions [there is no force under the condition Vonly]. The means of maximum force and pressing depth under vertical and horizontal alignments had similar values, but were nearly twice as large as their counterparts under “same-location” alignment. This difference indicate that the “same-location” alignment offers similar subjective perception as the vertical and horizontal alignments, but with less physical effort as described by force and pressing depth. This implies an advantage of “same-location” alignment over the vertical and horizontal alignments.

This observation confirms the notion that a “same-location” alignment facilitates user interaction with objects. For example, Wu *et al.*[11] studied the effect of their “same-location” alignment for merging the site of ultrasound visualization with the site of action during needle insertion in a VR surgical system. They discovered that participants were more accurate using their “same-location” alignment compared to a conventional ultrasound alignment by placing a monitor away from the site of action. Swapp and Loscos[51] reported that their “same-location” alignment of placing a haptic device in front of a visual display improved significantly the accuracy of user interaction that requires rapid hand motions. These studies, together with the current study, reveal the advantage of a “same-location” alignment for user interaction.

4.4.3 Application

Based on the different observations of subjective perception and objective measurements, this current study reveals two factors that have implications for creating accurate simulation and interaction in VR surgical systems. This accuracy is crucial in VR surgical system due to the requirement for patient safety. The first factor is the perceptual illu-

sion of object softness under viewing angles-the larger the viewing angle is, the harder the ball is perceived. To avoid this perceptual illusion, VR surgical systems should place their cameras in such a way that the cameras have a range of viewing angle that is less than 15° with respect to an organ/tissue in interaction. Because viewing angle does not affect the objective measurements of maximum force and pressing depth-as observed in the current study, placing the cameras within this range of viewing angle eases the alignment between a haptic device and visual display for accurate simulation and interaction in VR surgical systems.

The second factor is the advantage of the “same-location” alignment between a visual display and haptic device (as illustrated in Fig. 4.1a) over the vertical and horizontal alignments. This “same-location” alignment gives a relatively consistent subjective perception of object softness over a range of viewing angles between -7.5° and $+7.5^\circ$ with less physical effort. In creating accurate simulation and interaction in VR surgical systems, this allows reduction of fatigue associated with the use of force feedback devices. Presumably, a surgeon would feel less tired using less effort to interact with organs/tissues. Consequently, he/she could interact with virtual organs/tissues in the same way as if they were under an actual surgical procedure.

As observed in the operating room, surgeons often use their fingers to touch and press specific organs/tissues for assessing their softness (i.e. disease sites within the organs/tissues). They make this assessment by closing their eyes while touching and pressing the organs/tissues [personal communication with surgeons]. That is, surgeons try to acquire precise information on disease sites by removing their visual context. Starting from this observation, I enquired whether there are separate effects of visual and haptic information on the perception of object softness. As revealed in this study, visual and haptic information together affect this perception when both are available. However, haptic information (under the condition Honly) and visual information (under

the condition Vonly) influence objective measurements of maximum force and pressing depth in different ways. This carries an implication for creating accurate VR systems of surgical simulation, in which it would be difficult to accommodate physical constraints of a haptic device and a visual display for the perception of object softness. The different influences of haptic and visual information on objective measurements enable possibilities of simulating organs/tissues to reflect the objective measurements and thus to separately meet the physical constraints of the visual display and haptic device. Further studies are needed to examine how to undertake this simulation for creating accurate VR surgical systems.

4.5 Summary

This chapter presented a study investigating the effect of three different hardware alignments on human perception of object softness. Although the three different alignment yielded similar subjective perceptions of object softness, this study showed the advantage of the “same-location” alignment in both subjective and objective measurements. This particular alignment allows a user to have the same subjective feeling of object softness while using less force to discriminate object softness. The next chapter presents a study investigating the effect of interaction styles on human perception of softness during real-time palpation using the “same-location” alignment.

Chapter 5

Human Constraints for Softness Perception during Real-Time Palpation*

5.1 Introduction

In this chapter, I present my work aiming at investigating the insensitivity of human perception during perceiving object softness. The investigation featured two complementary analyses: variation computation and human study. Variation computation quantified the differences of visual displacement (visual information) and force feedback (haptic information) among four different force distributions on a contact area of a palpated soft object. The contact area was considered as a single-node or multi-node contact definition. The palpation under these force distributions had a same applied force profile. The analysis was based upon statistical approaches, which are not very sensitive to small variations in datasets. This analysis computed, among the force distributions, theoretical variation levels for visual displacement and fore feedback, respectively.

This study examined the hypothesis that the human perception of object softness is insensitive to some of these theoretical variation levels. Using a stylus-style haptic device, human participants palpated a soft object and discriminated the softness of the object among the four force distributions. The palpation was under

*Parts of this chapter is accepted for a conference.

A. Widmer and Y. Hu, (full-paper accepted on May 07, 2012; paper number #: 91), "Difference of object softness perception during palpation through single-node and multi-node contacts," *Proceedings of the 34rd Annual International Conference of the IEEE Engineering in Medicine and Biology Society (IEEE-EMBC)*, San Diego, CA, USA, August 2012.

A full version of this chapter is under review in IEEE transactions.

A. Widmer and Y. Hu, (12 double column pages submitted on June 5 2012; submission number #: TH-2012-06-0042), "Human Constraints for Softness Perception during Real-Time Palpation," *IEEE Transactions on Haptics* .

a single-node or multi-node contact definition. For comparing each pair of force distributions, I analyzed the following parameters: subjective perception of object softness and objective measurements of maximum force and pressing depth. The observation of the study indicated that the human perception of object softness is affected by a certain variation level for visual displacement, whereas this perception is insensitive to any computed variation level for force feedback.

Together, both analyses revealed, (a) there is a difference in perceiving object softness between a single-node and multi-node contact definitions; and (b) the human perception of object softness is insensitive to a variation level up to 11.0% and 6.3% for visual and haptic information, respectively. The analyses were performed on the two same locations as described in Chapter 3 (top and side). However, only results for application of forces on the top of the phantom are presented in this chapter. Due to close similarities, results for application of force on the side of the phantom are presented in Appendix B.

5.2 Variation Computation

The analysis of variation computation took an approach of using statistical tools such as the Analysis of Variance (ANOVA) and Bland and Altman's (B&A) agreement method [13]. This approach is similar to that in my previous work described in Chapter 3 of confirming the behavioural agreement between a real-time viscoelastic model of a breast phantom and its counterpart model based on the Finite Element Method (FEM). Based upon this real-time model, the analysis of variation computation quantified variation levels of both visual displacement and force feedback among four force distributions, under the single-node and multi-node contact definitions. These force distributions simulated different palpation cases. The following context presents briefly the real-time model used in this analysis, and then details two phases of the analysis: data acquisition and data processing.

5.2.1 Real-Time Model

Based upon a viscoelastic model of a soft object, CPU-based computation has difficulties to achieve a simulation of the object, which has accurate behavioural deformation (e.g., visual displacement and force feedback) for real-time user interaction. For simulating the deformation of a breast phantom, my previous work modified a viscoelastic model of the phantom to increase its computational speed for a real-time rendering as described in Chapter 3. However, this increase was at a cost of decreasing the accuracy of the deformation, when compared to a FEM model featuring physical parameters of the phantom. Based on the virtual breast phantom (a hemisphere of 8 cm in diameter) as depicted in Fig. 5.1, the real-time model nevertheless yielded both visual displacement and force feedback in 10 ms under a CPU-computation. This is true for both common types of palpation: one-finger palpation and two-finger palpation. The real-time model consisted of a surface membrane and an inside gel. The surface membrane was a mesh of 338 nodes connected by a Burger element between a pair of nodes as introduced in Chapter 3, the Burger element included a Kelvin element in series with a Maxwell element and considered viscoelastic characteristics of the membrane. The inside gel, without any node, was governed through a state equation featuring a modified gas law equation and took into account viscoelasticity of the gel.

Physical parameters for both surface membrane and inside gel were derived from literature about actual breast phantoms; and then were manually fitted for palpation of the virtual breast phantom as shown in Chapter 3. Under one-finger palpation as shown in Fig. 5.1b, the real-time viscoelastic model achieved an agreement level over 95% with its FEM counterpart for both visual displacement and force feedback. However, this agreement level dropped to 90.2% and 86.5% for visual displacement and force feedback respectively, under two-finger palpation as illustrated in Fig. 5.1c. All these agreement levels were evaluated through the B&A agreement method introduced in Chapter 3.

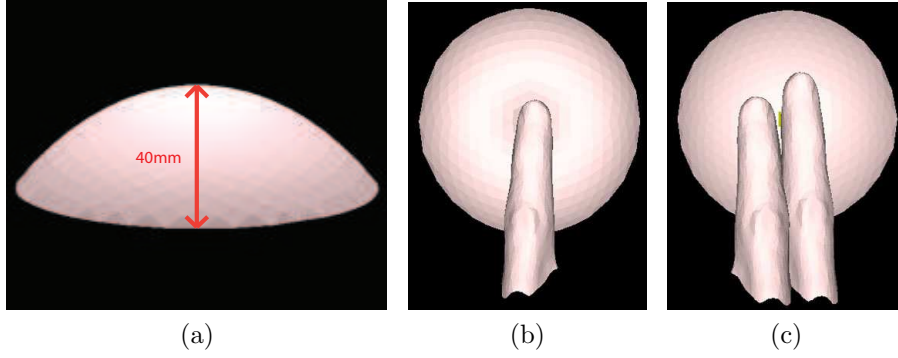


Figure 5.1: Representation of a virtual breast phantom and palpation scenarios: (a) side view of the virtual phantom; (b) one-finger palpation using the index finger; (c) two-finger palpation using both index and middle fingers.

5.2.2 Data Acquisition

Based on this real-time viscoelastic model, the current analysis of variation computation departed from the work done in Chapter 3 that compared behavioural deformation governed by this model and its FEM counterpart. Indeed, this analysis computed respective variations of visual displacement and force feedback under applying four different force distributions for palpation. The first phase of this analysis is data acquisition.

As illustrated in Fig. 5.1, the palpation was represented as a finger (or two-finger) applied force over a contact area on the top of the virtual breast phantom. The location of the contact area was to maximize a pressing depth under palpation. Similar to the study in chapter 3, the contact area covered 23 nodes on the surface membrane and had the size of $2\text{ cm} \times 2.84\text{ cm}$ for one-finger palpation. This size corresponded to the average area of the distal section for a male index (or middle) finger [73]. For two-finger palpation, the contact area on the surface membrane had 46 nodes to occupy twice of this size. For each finger, the same force distributions as those used in Chapter 3 were considered as follows:

- Single-node contact (Distribution 1): As shown in Fig. 3.3a, force was applied to only one node at the centre (a circle as illustrated in Fig. 5.2) of the contact

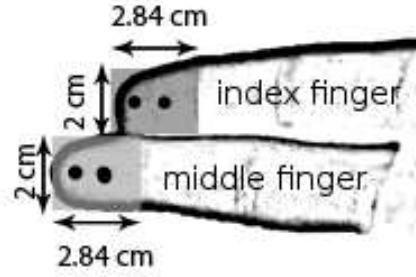


Figure 5.2: Virtual index and middle fingers with shaded finger contact areas (the palm faces to the reader).

area (a shaded area in Fig. 5.2). This mimics a common contact used in a VR simulator with a stylus-style haptic device.

- Homogenous multi-node contact (Distribution 2): As depicted in Fig. 3.3b, identical force was applied to each meshed node of the contact area. This contact describes a scenario of applying force evenly over the virtual breast phantom with respect to its base.
- Centred 2D Gaussian multi-node contact (Distribution 3): As illustrated in Fig. 3.3c, force was applied to each meshed node of the contact area, following a 2D Gaussian distribution with its peak at the center of the contact area. This contact represents a possible scenario of applying force by a finger over the curved surface of the breast phantom.
- Off centred 2D Gaussian multi-node contact (Distribution 4): As displayed in Fig. 3.3d, force was applied to each meshed node of the contact area, following a 2D Gaussian distribution with its peak at the distal tip (a dot in Fig. 5.2) of the contact area. This contact simulates the scenario of applying force by an inclined finger over the breast phantom for palpation.

Each force distribution had a maximum force identical of 3 N and followed a profile lasting a period of 4 seconds. This profile was stepwise, with a force of 3 N during

the first half period of 2 seconds and 0 N during the last half period of 2 seconds, to mimic the finger motion of pressing on a palpated surface and then releasing the pressure. Using the real-time viscoelastic model of the breast phantom described in Chapter 3, I computed one dataset of visual displacement from each meshed node on the virtual phantom, except those within the contact area covered by the finger; and another dataset of force feedback from each meshed node within the contact area to the finger. The dataset of force feedback did not include force computed from meshed nodes located outside of the contact area, due to their non-contact to the finger. Visual displacement of each node was the spatial resultant of its 3D position with respect to the base center (the origin of a Cartesian coordinate) of the hemispheric phantom. Force feedback of each node possessed the resultant of its 3D force vector. Visual displacement or force feedback of a node was computed at each time step. On a CPU-based computer (Dell Precision 690 with 2 dual-core processors at 3.2 GHz and 4 GB of RAM), this computation took 10 ms for one time step and lasted 400 steps for the period of the force profile.

Under one-finger palpation, the dataset of visual displacement totaled 126,000 samples ($400 \text{ time steps} \times 315 \text{ nodes}$) by excluding the invisible 23 nodes within the contact area. This dataset was 116,800 samples ($400 \text{ time steps} \times 292 \text{ nodes}$) under two-finger palpation by discarding 46 nodes beneath two fingers. In contrast, the dataset of force feedback aggregated per finger 9,200 samples ($400 \text{ time steps} \times 23 \text{ nodes}$) within the contact area. Both datasets were recorded under each force distribution for data processing below.

5.2.3 Data Processing

As the second phase of the analysis, data processing compared a pair of force distributions for visual displacement and force feedback, respectively. Consequently, the paired comparison yielded respective variations of visual displacement and force feed-

back. Among all force distributions, there were six pairs of comparison for each of visual displacement and force feedback. All paired comparisons were performed separately under each type of palpation: one-finger palpation and two-finger palpation.

Each paired comparison involved three computations: the Root Mean Square Error (RMSE), the p -value computed by the ANOVA and an agreement level calculated by the B&A agreement method [21]. The RMSE between one pair of datasets indicates their Euclidean distance. Because most investigations on comparing two object models used this computation for assessing behavioral difference between the models, I kept this computation in compliance with these investigations. The p -value smaller than or equal to 0.05 (with 95% confidence) implies that the pair of datasets is significantly different from each other. That is, the datasets are separable without agreement. In case of the p -value larger than 0.05, the ANOVA suggests that the two datasets in one pair cannot be differentiated from each other. However, the ANOVA in this case does not determine whether both datasets are in agreement to each other. Thus, the B&A agreement method serves to determine the agreement between the pair of datasets. This method gives a percentage, A , of samples in the datasets that are within the agreement range of ± 2 standard deviations (S.D.). The variation, V , is a percentage of samples in the datasets that are out of this agreement range and thus can be calculated as follows:

$$V = 100 - A \tag{5.1}$$

Therefore, the variation forms a theoretical level of discrepancies between two datasets.

By computing variations of datasets between each pair of four force distributions, I obtained theoretical variation levels of visual displacement and force feedback, respectively, under one-finger palpation and two-finger palpation.

	RMSE [cm]	ANOVA		B&A agreement	
		F	p	S.D. [cm]	V [%]
1 vs. 2	0.9611	2.99	0.1004	0.0667	14.14
1 vs. 3	0.4274	3.01	0.0921	0.0298	13.79
1 vs. 4	0.3974	2.11	0.1853	0.0284	13.23
2 vs. 3	0.5340	1.78	0.2231	0.0369	6.43
2 vs. 4	0.6493	2.59	0.1256	0.0455	6.46
3 vs. 4	0.2183	2.5	0.2241	0.0166	5.55

Table 5.1: Comparisons of visual displacement under one-finger palpation.

	RMSE [N]	ANOVA		B&A agreement	
		F	p	S.D. [N]	V [%]
1 vs. 2	1.0150	0.85	0.3063	0.3041	5.54
1 vs. 3	0.5816	0.32	0.5523	0.8416	5.99
1 vs. 4	0.3617	0.21	0.6201	0.9214	4.03
2 vs. 3	0.3021	0.16	0.6215	0.1214	3.98
2 vs. 4	0.7514	0.34	0.6012	0.2147	3.54
3 vs. 4	0.1254	0.12	0.7410	0.6032	2.55

Table 5.2: Comparisons of force feedback under one-finger palpation.

5.2.4 Results

Under one-finger palpation, Table 5.1 and Table 5.2 present the comparison results of visual displacement and force feedback, respectively. As indicated earlier, there were six pairs of comparison among the four force distributions. That is, the notation “1 vs. 2” in Table 1 and Table 2 denotes the comparison under force distributions of Distribution 1 and Distribution 2. Similar notations apply to the comparison of other force distributions.

As indicated in Table 5.1, the paired comparisons of visual displacement produced RMSE values, roughly ranging from 0.22 cm to 0.96 cm. The minimum RMSE value of 0.22 cm was yielded by “3 vs. 4”. These two distributions were multi-node contact with respective centered and off-centered 2D Gaussian distributions of applying force. In contrast, the RMSE value of 0.96 cm was produced by “1 vs. 2” - comparison between the single-node contact (Distribution 1) and the homogenous multi-node contact (Distribu-

tion 2). Further ANOVA analysis revealed p -values greater than 0.05 (a threshold value) for all pairs of comparison, as indicated in Table 5.1. These p -values demonstrated that the two datasets of visual displacement in each pair of comparison could not be statistically differentiated from each other. Then, the B&A agreement method determined the variation level between these two datasets. As presented in Table 5.1, the variation levels ranged from 5.55% (for “3 vs. 4”) to 14.14% (for “1 vs. 2”). In addition, a gap of variation levels existed, from the paired comparisons between single-node contact and multi-node contact (13.23%-14.14%) to those between multi-node contacts (5.55%-6.46%). This gap indicates that visual displacement produced by single-node contact of Distribution 1 was consistently apart from that yielded by multi-node of Distribution 2, Distribution 3 and Distribution 4.

Table 5.2 illustrates outcomes derived from the paired comparisons of force feedback. The RMSE values of these comparisons had a range from 0.12 N (for “3 vs. 4”) to 1.01 N (for “1 vs. 2”). This trend is similar to that observed in the paired comparisons of visual displacement. Moreover, the analysis of using ANOVA found that p -values for all paired comparisons were over the threshold of 0.05, agreeing with the observations from the paired comparison of visual displacement. Finally, the B&A agreement method yielded variation levels, ranged from 2.55% (for “3 vs. 4”) to 5.99% (for “1 vs. 3”). It is worth to observe that this range was narrower than that for visual displacement; so did the maximum value of the variation levels.

Under two-finger palpation, Table 5.3 and Table 5.4 illustrate the results of data processing for visual displacement and force feedback, respectively. For visual displacement, RSME values varied from 0.31 cm (for “3 vs. 4”) to 1.05 cm (for “1 vs. 2”), as shown in Table 5.3. These two RMSE values gave a range, which was similar to that found under one-finger palpation. As indicated in Table 5.3, the p -values computed by using ANOVA were consistently over the threshold of 0.05. Consequently, the B&A agreement method

	RMSE [cm]	ANOVA		B&A agreement	
		F	p	S.D. [cm]	V [%]
1 vs. 2	1.0521	2.24	0.1982	0.0325	11.08
1 vs. 3	0.8111	2.65	0.1127	0.0564	10.95
1 vs. 4	0.9577	1.49	0.2314	0.0425	11.18
2 vs. 3	0.9103	1.25	0.2649	0.0627	8.66
2 vs. 4	0.3281	1.44	0.2451	0.0165	4.38
3 vs. 4	0.3047	1.87	0.2185	0.0768	5.26

Table 5.3: Comparisons of visual displacement under two-finger palpation.

	RMSE [N]	ANOVA		B&A agreement	
		F	p	S.D. [N]	V [%]
1 vs. 2	1.1054	0.06	0.8012	0.2458	4.03
1 vs. 3	0.7951	0.10	0.7852	0.3362	6.26
1 vs. 4	0.7218	0.26	0.5812	0.2017	6.06
2 vs. 3	0.5893	0.16	0.6214	0.1920	3.34
2 vs. 4	0.2954	0.09	0.7915	0.0815	4.46
3 vs. 4	0.1849	0.50	0.4745	0.0521	3.31

Table 5.4: Comparisons of force feedback under two-finger palpation.

yielded variation levels, ranging from 5.26% (for “3 vs. 4”) to 11.18% (for “1 vs. 4”). A gap of variation levels existed from the paired comparisons between single-node contact and multi-node contact (10.95%-11.18%) to those between multi-node contacts (5.26%-8.66%). This range was narrower than its counterpart under one-finger palpation. So did the gap variation levels.

Table 5.4 reveals the results of analyzing force feedback under two-finger palpation. The RMSE values ranged from 0.18 N (for “3 vs. 4”) to 1.10 N (for “1 vs. 2”). These values were comparable to those found under one-finger palpation. Moreover, the p -values yielded by using ANOVA were consistent with those under one-finger palpation. Furthermore, the B&A agreement method generated variation levels, ranging from 3.31% (for “3 vs. 4”) to 6.26% (for “1 vs. 3”). This range was comparable to that under one-finger palpation too.

5.2.5 Discussion

Theoretically, the above variation computation determined variation levels of visual displacement and force feedback that are related to object softness. Based on the real-time viscoelastic model of a virtual phantom, the computation was undertaken over a force profile of a 4-second period. This computation departs largely from existing empirical studies on the human ability of discriminating compliance levels of object softness [82, 83]. Importantly, the theoretical outcomes of this computation might anticipate human perception of object softness in the following three aspects.

At first, a gap of variation levels indicates that visual displacement produced by single-node contact was consistently apart from that yielded by multi-node contacts with various force distributions. This is true for both types of palpation: one-finger palpation and two-finger palpation. However, there is no gap of variation levels for force feedback under both types of palpation. The gap for visual displacement might suffice for humans to discriminate object softness under single-node and multi-node contact.

Secondly, there are a difference and a similarity between these two types of palpation. One-finger palpation produced averagely larger variation levels for visual displacement, compared to two-finger palpation. In contrast, both types of palpation yielded comparable variation levels for force feedback. This might indicate that variation levels for force feedback are less subject to the size discrepancy of the contact area than their counterparts for visual displacement.

Lastly, the computation for force feedback produced smaller variation levels than the computation for visual displacement. This is true under both types of palpation. In addition, it is observed that the variation levels for force feedback were always much smaller than 15% – just noticeable difference (JND) for discriminating object softness under only force feedback [82]. This permits a postulation that humans might be unable to differentiate object softness between single-node contact and multi-node contact by

relying only on force feedback.

Indeed, the analysis of variation computation yielded theoretical variation levels for both visual displacement and force feedback. Nevertheless, a human study is needed to verify whether these theoretical outcomes anticipate human perception of object softness.

5.3 Human Study

As a complementary analysis, a human study examined the hypothesis that the human perception of object softness is insensitive to some of the theoretical variation levels resulting from the variation computation. I conducted the study following the within-subject design of repeated measures. Via a stylus-style haptic device, a human participant palpated a virtual breast phantom (a largely deformable object) to discriminate its softness. The palpation was under either one index finger (one-finger palpation) or both index and middle fingers (two-finger palpation), as introduced in Chapter 3. The study had an approved ethic clearance, according to the Canadian Tri-Council Ethics Guidelines.

5.3.1 Methodology

Participants

Applying within-subject design of repeated measures to my study, I determined the total of 15 participants according to a method of computing sample size [84]. These participants were 6 females and 9 males, aged between 20 and 30. All participants, with normal or corrected-to-normal vision, were naive to the purpose of the study and had given their consent prior to their participation. As pre-screening, each participant was tested for his/her stereo acuity of at least 40" of arc, determined by the Randot Stereotest (Stereo Optical, Inc). His/her color blindness was also verified using an Ishihara color test, because various colors were used in visual stimuli (described below) of the study.

In addition, the handedness of each participant was examined by employing a modified version of the Edinburgh handedness inventory [77]. Each participant in the study was strongly right-handed.

Apparatus

I used a “same-location” VR apparatus as introduced in Chapter 4 for the study. This apparatus aligns visual and haptic stimuli onto one spatial location, resulting in reduced physical workload for a participant during interacting with soft objects as explained in Chapter 4. This apparatus was composed of a facing-down CRT monitor, a first surface mirror, and a haptic device PHANTOM 1.5/6DOF (stylus-style). The mirror was placed horizontally in front of the participant. Under the mirror, the stylus-style haptic device was located so that its haptic reference point could move according to the visual stimuli in the mirror. Sitting in front of the apparatus, the participant held the stylus of the haptic device and could not view both hand and haptic device. Refracted from the mirror, the visual stimuli on the CRT screen were visible to the participant at the same location as the reference point of the haptic device. A forehead rest restrained the head location and orientation of the participant. This maintained a consistent view of the stimuli for all participants.

Stimuli

During palpation, each participant viewed virtual breast phantoms (as visual stimuli) and his/her hand received force feedback (as haptic stimuli) by maneuvering the haptic device to undertake palpation on the virtual phantoms. The visual stimuli used in this study were two virtual breast phantoms as described in Section 5.2 (Variation Computation). In a trial, each phantom could be viewed from its top, as illustrated in Fig. 5.1b and Fig. 5.1c, with a randomly assigned color of either blue or purple. The colors of the phantoms had same intensity of luminance, in order to eliminate the use of luminance as a visual cue. Both phantoms were applied a pair of force distributions for palpa-

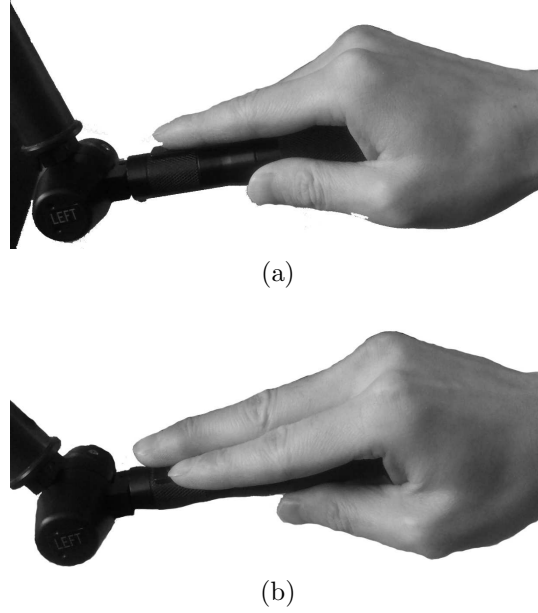


Figure 5.3: Finger position and holding posture on the stylus of the haptic device for palpation. (a) Under one-finger palpation; (b) Under two-finger palpation.

tion. These force distributions were the same as those introduced in Chapter 3. During palpation, the deformation of each phantom was governed by the real-time viscoelastic model presented in Chapter 3. For both types of palpation (one-finger palpation and two-finger palpation), the participant could view the finger(s) on the top of the phantom and the deformation of the phantom. This deformation produced visual displacement of all meshed nodes on the surface of the phantom and force feedback from the nodes within the contact area of the finger(s).

Force feedback was rendered to the finger(s) of the participant via the haptic device. Under one-finger palpation, the participant used their hand to hold the stylus of the haptic device by placing the index finger on the top of the stylus, as illustrated in Fig. 5.3a. This holding mimicked applying force through a contact area of $2\text{ cm} \times 2.84\text{ cm}$, as depicted in Fig. 5.2. Under two-finger palpation, the participant placed both index and middle fingers on the top of the stylus of the haptic device for holding the stylus, as shown in Fig. 5.3b. This holding covered a contact area of twice large as its counterpart

under one-finger palpation, as depicted in Fig. 5.2.

For applying force, there were a total of 4 force distributions as described in Subsection 5.2.2. For each force distribution, I capped the maximum resultant of force feedback at 3.5 N (the maximum sustainable force of the haptic device). Thus, I scaled force feedback derived from the real-time viscoelastic model described in Chapter 3 by the number of contact nodes as follows:

$$\vec{F}_{avg} = \frac{1}{n} \sum_{i=1}^n \vec{F}_i \quad (5.2)$$

where \vec{F}_{avg} represents the vector of force fed back to the hand of the participant; n corresponds to the number of nodes within the contact area of the finger (or fingers); \vec{F}_i is the vector of force computed on contact node i . Under one-finger palpation, there were 23 nodes within the contact area. A total of 46 nodes existed within the contact area under two-finger palpation. For all force distributions, this scaling permitted to maintain the same variation levels of force feedback among paired comparisons as those presented in Table 5.2 and Table 5.4.

For each force distribution, I verified that the force feedback rendered by the haptic device was comparable with the scaled force feedback yielded by both real-time model and Eq. (5.2). This verification employed the same method reported in Chapter 4. To warrant a consistent fashion of palpation among all participants, I instructed the participants to apply force vertically on the top of the phantom.

Both visual and haptic stimuli were produced by using OpenGL and OpenHaptic in C++ programming. I rendered these stimuli on a Dell Precision 690 with 2 dual-core processors at 3.2 GHz and 4 GB of RAM.

Procedures

After pre-screening, each participant was explained that there was a safety threshold of force set to protect the haptic device. The participant was instructed to palpate two

deformable breast phantoms one after another and to select the harder one among them in each trial. The palpation was the finger motion of pressing on a deformable surface and then releasing from it. There was no constraint on how many times this finger motion should have taken place. The selection of a harder phantom was forced as the 2-Alternative-Forced-Choice utilized in psychophysics studies [85].

During both types of palpation, each participant interacted with the virtual phantoms under the following three testing conditions:

- Active palpation (V+H): When palpating one virtual phantom via the haptic device, the participant saw the deformation of the phantom and felt force fed back on his/her hand. Thus, both visual and haptic stimuli were available to the participant. This mimicked a common palpating scenario in practice.
- Passive palpation (Vonly): When interacting with the phantom, the participant could see the deformation of the phantom but could not feel force feedback. Therefore, only visual stimuli were available to the participant. This simulated palpation via a robotic arm without force feedback.
- Hidden palpation (Honly): The participant could feel force feedback through the haptic device but could not view the phantom during palpation. Consequently, only haptic stimuli were available to the participant. This was palpation under obstacles which block the view of a palpated object.

Each participant underwent 6 blocks of trials (2 types of palpation \times 3 testing conditions). Each block of trials had a practice session of 10 trials, prior to a testing session of 30 trials (6 catching trials and 24 testing trials: 6 comparisons \times 4 repetitions). The practice session allowed the participant to familiarize with the palpation task of the block. The trials in this session randomly derived from those in the testing session, covering both catching and testing trials. Catching trials featured two virtual breast

phantoms, whose softness levels and force distributions as applying force differed from each other. The softness levels of the two phantoms varied from each other significantly at about 50% - much higher than 15% (the Just-Noticeable-Difference [82]). Thus, the two phantoms possessed two largely different sets of physical parameters, respectively, for the real-time viscoelastic model. In contrast, testing trials had two phantoms with the identical softness levels (i.e., the same set of physical parameters for the real-time model) to be palpated under two different force distributions, respectively.

The order of the 6 blocks was randomized and counterbalanced among all participants. So did the trials of both practice and testing sessions. Each participant took about 1.5 hours to complete all blocks of trials, with a 5-minute break between two blocks of trials.

Data Analysis

In each trial, I recorded two performance parameters for data analysis: subjective perception and objective measurements. These parameters were identical to those in Chapter 4. Under a paired comparison of force distributions, subjective perception was the participant's selection of the harder phantom between the two presented. This performance parameter indicates the participant's perception of object softness. Objective measurements included maximum pressing depth and maximum force applied on each phantom during a trial. This performance parameter allows examining the consistency of the participant's palpating behavior.

I computed the objective measurements from the visual displacement of meshed nodes on each phantom under palpation. When the phantom deformed, the maximum pressing depth was the longest distance between the original surface within the contact area and its depressed surface. The maximum force corresponded to the peak value of the force that the participant supposed to feel from each phantom. The maximum pressing depth and force were not directly correlated to each other due to the real-time

model. Under the testing condition of active palpation (V+H), there were both maximum pressing depth and force computed. The maximum force was always zero under the testing condition of passive palpation (Vonly), due to the absence of force feedback to the participant's hand. Although the participant could not view the deformed phantom under the testing condition of hidden palpation (Honly), the maximum pressing depth existed because the participant could feel force feedback from the phantom.

For each participant, subjective perception of all catching trials was used to verify whether the participant could correctly feel the different levels of object softness. Once the verification was positive, both performance parameters of all testing trials were considered in data analysis. However, the parameters of the catching trials were not included in this analysis.

Consequently, the performance parameters from all participants were used in within-subject-design ANOVA. If an ANOVA resulted in significance, further analysis was conducted by utilizing pairwise contrasts of Bonferroni correction. The Bonferroni correction is responsible to offset errors of performing multiple contrast comparisons [86]. Thus, I investigated the effect of paired comparison of force distributions and testing conditions on both performance parameters. As well, I examined the effect between two types of palpation.

5.3.2 Results and Discussion

Subjective Perception

Under one-finger palpation, a two-way ANOVA (paired comparisons of force distributions \times testing conditions) revealed that subjective perception of object softness was significantly affected by the paired comparisons of force distributions [$F(5, 14)=6.694$, $p < 0.001$]. As well, participants perceived object softness differently among all testing conditions [$F(2, 14)=3.683$, $p < 0.05$]. Furthermore, there was a significant interaction between the paired comparison of force distributions and the testing conditions [$F(10,$

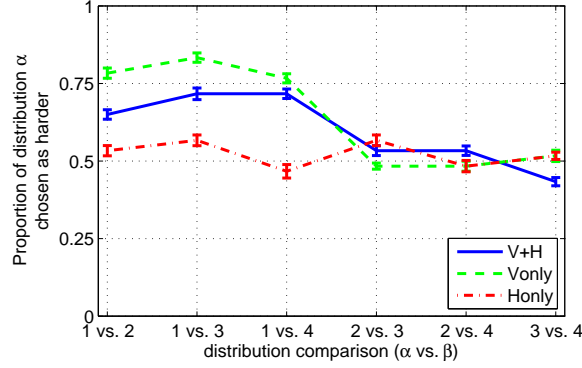


Figure 5.4: Subjective perception of object softness during one-finger palpation. [Error bars represent standard errors.]

14)=2.381, $p < 0.05$]. For subjective perception, Fig. 5.4 illustrates general trends among paired comparisons of force distributions. The notation of the horizontal axis “ α vs. β ” in Fig. 5.4 denotes the comparison under force distributions of Distribution α and Distribution β . This is the same as that described in the Subsection 5.2.4. The vertical axis indicates the proportion of virtual phantoms palpated under Distribution α chosen harder than under Distribution β . For example, the virtual phantoms under Distribution 1 were perceived harder than under Distribution 3 in about 74% of the trials, when under the testing condition V+H.

Following the significant observations of the above two-way ANOVA, further investigation was conducted by using two one-way ANOVA and pairwise contrasts of Bonferroni correction. Table 5.5 shows the results of a one-way ANOVA (paired comparisons of force distributions) under all testing conditions and subsequent pairwise contrasts for each testing condition. One-way ANOVA confirmed significant differences among paired comparisons of force distributions under the testing conditions V+H and Vonly. The same significance did not appear under the testing condition Honly. Thus, further pairwise contrasts were undertaken under the testing conditions V+H and Vonly. These pairwise contrasts revealed that virtual phantoms palpated through the single-node force distribution (Distribution 1) were selected harder than through the multi-node force dis-

	One-way ANOVA $F(5,14)$	Pairwise Contrast (Bonferroni)	
Vonly	$F = 7.506,$ $p < 0.01$	1 vs. 2 < - > 2 vs. 3	$p < 0.01$
		1 vs. 2 < - > 2 vs. 4	$p < 0.05$
		1 vs. 2 < - > 3 vs. 4	$p < 0.05$
		1 vs. 3 < - > 2 vs. 3	$p < 0.01$
		1 vs. 3 < - > 2 vs. 4	$p < 0.01$
		1 vs. 3 < - > 3 vs. 4	$p < 0.01$
		1 vs. 4 < - > 2 vs. 3	$p < 0.01$
		1 vs. 4 < - > 2 vs. 4	$p < 0.01$
		1 vs. 4 < - > 3 vs. 4	$p < 0.05$
V+H	$F = 4.709,$ $p < 0.01$	1 vs. 2 < - > 3 vs. 4	$p < 0.05$
		1 vs. 3 < - > 2 vs. 3	$p < 0.05$
		1 vs. 3 < - > 2 vs. 4	$p < 0.05$
		1 vs. 3 < - > 3 vs. 4	$p < 0.01$
		1 vs. 4 < - > 2 vs. 3	$p < 0.01$
		1 vs. 4 < - > 2 vs. 4	$p < 0.01$
		1 vs. 4 < - > 3 vs. 4	$p < 0.01$
Honly	$F = 0.719, p > 0.05$	-	-

Table 5.5: Results of One-Way ANOVA and Pairwise Contrasts for the effect of paired comparison of force distributions on subjective perception under One-Finger palpation.

	One-way ANOVA $F(2,14)$	Pairwise Contrast (Bonferroni)	
1 vs. 2	$F = 4.561, p < 0.05$	Vonly < - > Honly	$p < 0.05$
1 vs. 3	$F = 5.437, p < 0.01$	Vonly < - > Honly	$p < 0.05$
1 vs. 4	$F = 5.271, p < 0.05$	Vonly < - > Honly	$p < 0.05$
2 vs. 3	$F = 1.123, p > 0.05$	-	-
2 vs. 4	$F = 0.225, p > 0.05$	-	-
3 vs. 4	$F = 0.579, p > 0.05$	-	-

Table 5.6: Results of one-way ANOVA and pairwise contrasts for the effect of testing conditions on subjective perception of object softness under one finger palpation.

tributions (Distributions 2, 3 and 4). This observation was stronger under the testing condition Vonly than the testing condition V+H. All pairwise contrasts were significant under the testing condition Vonly, whereas two pairwise contrasts between single-node and multi-node contacts (“1 vs. 2 < - > 2 vs. 3”; “1 vs. 2 < - > 2 vs. 4”) did not yield significance under the testing condition V+H.

Table 5.6 shows the results of a one-way ANOVA of testing conditions, followed

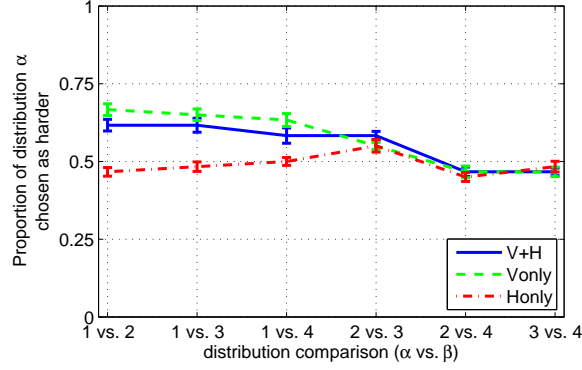


Figure 5.5: Subjective perception under two-finger palpation. [Error bars represent standard errors.]

by pairwise contrasts. A significant difference of subjective perception existed between single-node and multi-node contacts. Furthermore, this significant difference was contributed by the contrast between the testing condition Vonly and the testing condition Honly. No significant effect was observed among multi-node contacts using one-way ANOVA. This reinforces the observation that object softness under single-node contact is perceived harder than under multi-node contacts, when visual stimuli were available.

Under two-finger palpation, Fig. 5.5 depicts the subjective perception of object softness under all paired comparisons of force distributions and testing conditions. A two-way ANOVA (paired comparisons of force distributions \times testing conditions) confirmed that there was no significant difference of subjective perception among all sign-node and multi-node contacts. Paired comparisons of force distributions did not affect the perception of object softness [$F(2,14)=3.421$, $p > 0.05$] and neither did testing conditions [$F(5,14)=2.056$, $p > 0.05$]. There was no interaction effect between the paired comparisons of force distributions and testing conditions [$F(10,14)=0.787$, $p > 0.05$]. These observations indicate that single-node and multi-node contacts under two-finger palpation do not affect the perception of object softness. This is in contrast to the findings under one-finger palpation.

Consequently, a one-way ANOVA was performed to examine the effect of the types of

palpation (one-finger palpation vs. two-finger palpation) on subjective perception. This analysis revealed that subjective perception of object softness under one-finger palpation was significantly different from under two-finger palpation [$F(1,14)=8.749, p < 0.01$].

In short, I observed that subjective perception of object softness under single-node contact was significantly different from under multi-node contacts, when applying force by one finger with visual stimuli. However, this observation was not true under two-finger palpation.

Objective Measurements

There were two objective measurements: maximum pressing depth and maximum force. These measurements were computed for each force distribution under each type of palpation. Under one-finger palpation, Fig. 5.6 illustrates the objective measurement of maximum pressing depth for all 4 force distributions under 3 testing conditions. A two-way ANOVA (force distributions \times testing conditions) revealed no significance of maximum pressing depth among all force distributions [$F(3, 14)=1.198, p > 0.05$]. Neither were maximum pressing depth among all testing conditions [$F(2, 14)=3.662, p > 0.05$] and interaction between force distributions and testing conditions [$F(6, 14)=0.081, p > 0.05$].

Fig. 5.7 depicts the objective measurement of maximum force for all force distributions under all testing conditions. A two-way ANOVA (force distributions \times testing conditions) indicated that force distributions did not affect significantly maximum force [$F(3, 14)=0.488, p > 0.05$]. However, there was a significant difference of maximum force among testing conditions [$F(2, 14)=1250, p > 0.001$]. Moreover, there is no interaction effect [$F(6, 14)=2.438, p > 0.05$]. Because the testing condition Vonly had always a force feedback of 0 N, further one-way ANOVA discarded this testing condition and analyzed effect between both testing conditions V+H and Honly. This ANOVA did not show significant difference of maximum force between these testing conditions [$F(1, 14)=1.441, p > 0.05$].

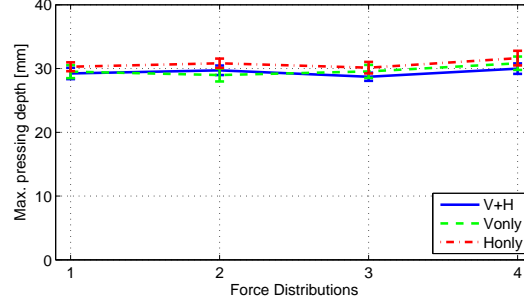


Figure 5.6: Objective measurement of maximum pressing depth under one-finger palpation. [Error bars represent standard errors.]

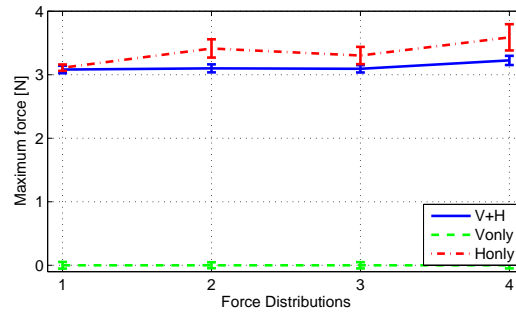


Figure 5.7: Objective measurement of maximum force under one-finger palpation. [Error bars represent standard errors.]

Under two-finger palpation, Fig. 5.8 and Fig. 5.9 illustrate the objective measurements of maximum pressing depth and maximum force, respectively. A two-way ANOVA revealed that the objective measurements of maximum pressing depth was not affected by the force distributions [$F(3, 14)=1.565$, $p > 0.05$] and the testing conditions [$F(2, 14)=1.838$, $p > 0.05$]. No interaction between both force distributions and testing conditions was found either [$F(6, 14)=1.072$, $p > 0.05$]. In discarding the testing condition Vonly, a two-way ANOVA on the objective measurement of maximum force showed no significant difference among force distributions [$F(3, 14)=2.188$, $p > 0.05$]. However, a significant difference of maximum force was observed between the testing conditions V+H and Honly [$F(1, 14)=13.881$, $p < 0.001$]. No interaction effect was found between the force distributions and testing conditions [$F(3, 14)=0.490$, $p > 0.05$]. Further one-way ANOVA examined how each force distribution contributed to the significant

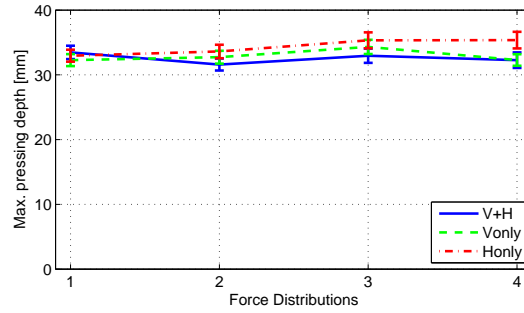


Figure 5.8: Objective measurement of maximum pressing depth under two-finger palpation. [Error bars represent standard errors.]

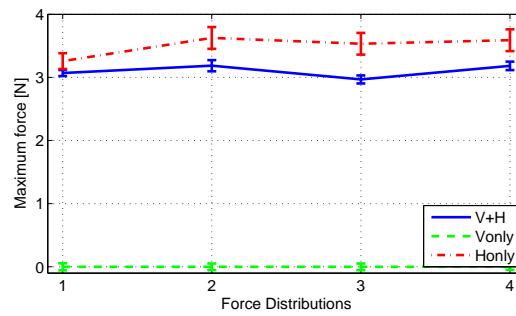


Figure 5.9: Objective measurement of maximum force under two-finger palpation. [Error bars represent standard errors.]

	One-way ANOVA $F(1,14)$
Distr. 1	$F = 3.003, p > 0.05$
Distr. 2	$F = 4.313, p < 0.05$
Distr. 3	$F = 10.219, p < 0.01$
Distr. 4	$F = 4.151, p < 0.05$

Table 5.7: Results of one-way ANOVA and pairwise contrast for the effect of force distribution on objective measurement of maximum force under two-finger contact.

difference of maximum force between the testing conditions V+H and Honly. This significant difference appeared for multi-node contacts (Distribution 2 to 4), as indicated in Table 5.7 under two-finger palpation.

From Fig. 5.6 to Fig. 5.9, it is interesting to observe that the objective measurement of maximum pressing depth was always larger without visual stimuli (Honly) than with visual stimuli (V+H and Vonly); so was the objective measurement of maximum

force. Nevertheless, significant difference of objective measurements between the testing condition Honly and other testing conditions (V+H and Vonly) was evident only for maximum force under two-finger palpation. In addition, Appendix B shows similar results when 15 other participants palpated the phantom on the side. The main difference between palpation on the top of the phantom and palpation on the side of the phantom is the reduced maximum pressing depth available on the side of the phantom.

Discussion

The above results from the human study revealed some interesting findings. Under one-finger palpation, the participants perceived the phantom significantly harder under single-node contact than under multi-node contacts, when visual information of the phantom was available. In contrast, this did not hold under two-finger palpation. These observations of subjective perception might result from two factors. First, humans rely dominantly on visual information of objects for their perception [52, 87]. The single-node contact under one-finger palpation might yield less meshed nodes undergoing large displacement than multi-node contacts, due to the number of meshed nodes in the contact area directly receiving applying force. Further evidence of support is the relative flatness at about 0.5 of selecting a harder phantom for all paired comparisons of force distributions, under the testing condition of hidden palpation (Honly) depicted in Fig. 5.4 and Fig. 5.5 under both types of palpation. Secondly, one-finger palpation covered all meshed nodes in the contact area undergoing large displacement. This contact area was only half of that under two-finger palpation. That is, less meshed nodes undergoing large displacement were visually occluded under one-finger palpation than under two-finger palpation.

Conversely, objective measurements of both maximum pressing depth and maximum force were, respectively, indifferent among all force distributions. This was true for both types of palpation. Although there was no instruction on how many times the finger

motion of palpation should be, all participants performed averagely the finger motion about 2 to 3 times. This was noticed during the computation of maximum pressing depth. All these observations imply two consistencies. First, the participants would behave relatively consistent in the way of palpating each phantom under all single-node and multi-node contacts. Secondly, the palpating behavior would be consistent between two types of palpation, unlike subjective perception of object softness. Thus, the difference of subjective perception between two types of palpation would not be related to their respective palpating behavior. Consequently, other factors such as visual displacement of the visible meshed nodes might play an important role for subjective perception.

Overall, the outcomes of this human study confirm my postulation in Introduction. That is, visual information of objects affects the perception of object softness, even though haptic information of these objects is not discernible. However, all discrepancies of visual information do not contribute equally to this perception. This confirms my hypothesis that the human perception of object softness is insensitive to some of theoretical variation levels.

5.4 General Discussion

In order to determine what theoretical variation levels affect the human perception of object softness, this section discusses observations from the analyses of both variation computation and human study. In addition, I introduced some possible applications of this determination.

5.4.1 Variation Computation vs. Human Perception

Similarities arise in the results from variation computation and human study, based upon the same real-time viscoelastic model for the breast phantom. In variation computation,

a gap of variation levels in visual displacement appeared for paired comparisons of force distributions. Under one-finger palpation, this gap decreased from around 13.2% (the smallest for the comparisons between single-node and multi-node contacts) to roughly 6.5% (the largest for the comparisons between multi-node contacts). Under two-finger palpation, the gap was smaller and reduced from about 11.0% to 8.7%. There is no such a gap in force feedback under both types of palpation.

Likewise, the results of human study reveal that the participants perceived the softness of the phantom significantly harder under single-node contact than under multi-node contacts, when the phantom was under one-finger palpation with visual information of the phantom. This observation was not true under two-finger palpation however. Due to the scaling of force feedback used for the stylus-style haptic device, the variation levels of force feedback in the human study were kept in a relatively similar way as in variation computation for both types of palpation.

Consequently, the variation level of visual displacement at about 13.2% is related to the difference of perceiving object softness between single-node and multi-node contacts. In contrast, there is no difference of perceiving object softness at the variation level about 11.0% of visual displacement. In other words, the threshold of visual displacement that affects the perception of object softness might be within the range from 11.0% to 13.2%.

The maximum variation level of force feedback under both types of palpation was about 6.3%, much smaller than the JND of 15% [82]. This might underlie the perceptual indifference of object softness, when the haptic information was the sole source for the perception (the testing condition Honly). Although this maximum played a role in influencing the perception of object softness when both visual and haptic information were available (the testing condition V+H), the influence was too subtle to be significant. That is, force feedback at the variation level of less than or equal to 6.3% could not affect the perception of object softness.

5.4.2 Relation to Existing Human Studies

For the perception of object softness, there are some human studies on discriminating the softness of actual/virtual objects with various degrees of compliance. For example, LaMotte and Srinivasan revealed that their human participants were always able to discriminate the softer one among two actual objects that processed degrees of compliance apart at least 15% from each other [82]. Other studies reported findings in agreement with this differentiable degree of compliance [88, 89, 90]. However, my current investigation of perceiving object softness departs from these studies in three aspects: the model to govern the deformation of soft objects, the methods to compute variation levels, and the comparison between contact definitions.

As the first aspect, a degree of compliance in the above existing studies is defined as the ratio of a finger traveling distance over applied force. The compliance could be regarded as a one-dimensional (1D) linear model to govern the deformation of soft objects in terms of force feedback. Thus, this 1D linear model of compliance cannot describe the deformation as visual displacement and force feedback of meshed nodes, covering a virtual object (e.g., a breast phantom) on its three-dimensional (3D) surface. Consequently, my real-time viscoelastic model introduced in Chapter 3 that governs the 3D deformation of the breast phantom is more complex and proper for describing object softness than the 1D model of compliance.

The second aspect is the way of computing variation levels derived from these models. In the existing studies, the degrees of compliance were discretized as pre-defined ratios under one contact definition. These degrees of compliances served well for their human studies. In contrast, my variation computation considered a period of a force profile under two contact definitions (with four force distributions). This computation was complex for actual 3D objects. Therefore, the variation levels yielded by this computation are better suited for investigating the perception of object softness under palpation

than the degrees of compliance.

The last aspect is represented by the novelty in the fact that my investigation found the perceptual difference of object softness between single-node and multi-node contact definitions. This difference was yielded by visual displacement of the meshed nodes on the phantom, rather than force feedback. Being much less than the JND of 15% [82], my maximum variation level of force feedback yielded outcomes in agreement with those related to force feedback from the existing studies. Nevertheless, my investigation on perceiving object softness separates the influence of variation levels of visual information from haptic information. This separation highlights the distinct influence of visual information on active and passive palpation. The implication of the influence is that robot-assisted surgical systems rendering no force feedback (alike passive palpation) would produce similar perceptual outcomes as active palpation between single-node and multi-node contact definitions.

5.4.3 Applications

The findings in this current investigation could imply two applications. On one hand, I observed that the human perception of object softness is insensitive to small visual discrepancies up to a variation level in the order of 11.0%. Taking account of this insensitivity opens a new avenue of developing VR training systems for palpation, by utilizing simplified physical models of soft objects for real-time interaction at a computational rate of 100Hz (or higher). On another hand, it is known that a stylus-style haptic device of using single-node contact diverges from actual palpation of requiring multi-node contact. However, the device might be sufficient for simulating palpation, if the simulation renders multi-node contact for active (and/or passive) palpation and the discrepancies of force feedback are up to 6.3%. Nevertheless, further effort is needed to develop haptic devices with multi-node contact for palpation.

5.5 Summary

In this chapter, I presented the investigation on human perception of object softness when interacting with virtual breast phantoms palpated through four different force distributions under different conditions. This investigation included two complementary analyses to verify whether human perception of object softness is insensitive to small discrepancies of visual and/or haptic information. In the first analysis, I computed variation levels of visual displacement on meshed nodes on the phantom and force feedback derived from the phantom, respectively, among paired comparisons of four force distributions under two contact definitions. In the second analysis, I undertook a human study to determine a variation level of insensitivity under the same force distributions. Both analyses revealed that the perception of object softness is insensitive up to a variation level of 11.0% for visual displacement and of 6.3% for force feedback. These levels of insensitivities show that it would be possible to relax design criteria when developing real-time model used in VR training systems for palpation.

Chapter 6

Conclusion and Future Work

6.1 Summary and Contribution

The objective of this thesis was to investigate a new approach that considers the constraints of human perception of object softness to relax design criteria for real-time models used in a VR training system for palpation. To reach this objective, the contributions of this thesis focused on the four following challenges:

1. Development of a new evaluation method to assess the feasibility of a real-time model to be used for user interaction in a VR system considering human constraints.
2. Development of a real-time model to be used as an example to demonstrate the evaluation method.
3. Investigation of the effect of different alignments between a visual display and a haptic device on the perception of object softness.
4. Investigation of the effect of statistical variation of visual displacement and force feedback on the perception of object softness.

Based on these challenges, this thesis aimed at describing the development and verification of an evaluation method for assessing a real-time model simulating an actual breast phantom by considering human constraints perceiving of object softness. Three major chapters covered the research work as follows:

1. **Evaluation Method and Real-Time Model (Chapter 3)** – This chapter presented an evaluation method designed to assess the behavior of a real-time model

in comparison with an offline FEM model. Based on evidences that human perception is not very sensitive to small differences in a real-time simulation, this evaluation take a statistical approach to check the level of agreement between the real-time model and its FEM counterpart. To show the benefit of this evaluation, we apply it to a breast phantom real-time model used in VR palpation training system. The real-time model shows an agreement level over 95% for all distributions in the two conditions involving only one-finger contact. However, the agreement level is not as high when using a two-finger contact.

The main innovations introduced in this chapter are: (1) the evaluation considering this limitation of human perception, (2) the comparison of visual displacement and force feedback at all time steps of a quantized force profile, (3) the usage of force distributions in different testing conditions involving one or two fingers, and (4) the modification of a real-time model to simulate an highly viscoelastic soft tissue.

2. **Effects of Hardware Alignments on Perception of Object Softness (Chapter 4)** – This chapter described a study investigating the effect of three different widely used hardware alignments on human perception of objects softness. Although the three different alignment yielded similar subjective perception of objects softness, this study showed the advantage of a “same-location” alignment. This particular alignment allows a user to have the same subjective feeling while using less force to discriminate objects softness.
3. **Human Constraints for Softness Perception during Real-Time Palpation (Chapter 5)** – Virtual Reality (VR) systems could offer alternative simulations for training palpation. An issue of such training systems is to assess contact definitions between the finger(s) and a virtual phantom of an organ (e.g. the breast) during real-time palpation, because contact definitions might affect the softness perception of the phantom. Considering visual and haptic information

derived from the phantom, I hypothesized that the human perception of object softness is insensitive to small discrepancies of the information. I conducted two complementary analyses to verify this hypothesis. In the first analysis, I computed variation levels of visual displacement on meshed nodes on the phantom and force feedback derived from the phantom, respectively, among paired comparisons of four force distributions under two contact definitions. In the second analysis, I undertook a human study to determine a variation level of insensitivity under the same force distributions. Both analyses revealed that the perception of object softness is insensitive up to a variation level of 11.0% for visual displacement and of 6.3% for force feedback.

In summary, the overall results of this thesis reveal small insensitivity of human perception of object softness. This has implications for the development of a VR training system for palpation. For example, a simpler real-time model can be implemented in such a system. As introduced in Chapter 3, the real-time model featuring a surface mesh and a inside gel may be enough to simulate an actual breast phantom showing a difference of visual displacement of less than 11% compared to a FEM model governed by equations using actual breast phantom softness parameters in most palpation conditions. In addition, the force feedback difference between the real-time model and its FEM counterpart is always below the haptic threshold of 15% [82]. Based on these observations, the feasibility of a VR training system for palpation is quite high if the VR training system uses the real-time model introduced in Chapter 3 and the “same-location” alignment between a visual display and an haptic device introduced in Chapter 4.

6.2 Future Work

Exploring a new evaluation method, this thesis lays some foundations to assess real-time models considering human perception of object softness. However, such a method needs improvements to be fully applicable to assess real-time models. From these results, some areas can be considered as future work as described in the following subsections.

6.2.1 Incorporation of Other Human Constraints

In this thesis, I focused on human constraints during perception of object softness. Considering these constraints alone, my work showed that it is possible to ease design criteria for real-time models of soft objects. Based on this observation, other human constraints could affect interaction in a VR system. There are many sensory illusions affecting humans. For example, the visual system is known to be subject to the Ponzo effect using the depth perception. In the field of haptic, Lecuyer *et al.* demonstrated that haptic texture could be simulated without haptic device by dynamically changing the motion speed of the user [91]. Therefore, a study can investigate other constraints that can be considered to improve interaction within a VR system. A deep understanding of the different human constraints can lead to adaptations either to ease or though design criteria for the development of a VR system to achieve immersion during interaction.

6.2.2 New Haptic Device for Palpation

Chapter 5 showed some limitations of a stylus-style haptic device (e.g PHaMTOM Sensable) for palpation tasks. Such a device lacks in providing force feedback on a surface as an actual palpation would. Some research groups have added tactile pad on existing haptic device. For example, Kuchenbecker *et al.* proposed a mechanical attachment for a PHaMTOM haptic device allowing the user to feel different shapes of solid objects [92]. As limitation, this attachment allows only one finger to feel contact feedback in opposi-

tion to a two-finger contact for normal palpation. Adding a pad for two fingers, Ullrich and Kuhlen developed another attachment made of static rubber to a PHaMTOM haptic device [93]. However the static nature of the rubber does not allow dynamically changing the softness of an object. These two types of attachments are good candidate for an enhanced haptic feedback for a VR training system for palpation task but need some improvements to be effective for such a task. Well designed, a haptic device able to offer multiple precise forces over a surface could enhance virtual palpation training.

6.2.3 VR Training System for Clinical Breast Examination

The roots of the new approach to ease design criteria of a real-time model used in a VR training system considering constraints of human perception come from the idea for developing of a VR training system for Clinical Breast Examination. To achieve such VR training system, a real-time model must include harder lumps within the shape of the breast phantom. Therefore, the addition of lumps of varying degrees of softness within the virtual breast phantom can be possible by inserting harder virtual objects within the virtual breast phantom controlled by the same governing equations as those used in the virtual breast phantom. Adjusting the size, depth and softness parameters of these harder objects will allow the model to simulate different cases of a diseased breast. Nevertheless, the evaluation method presented in Chapter 3 would be able to take in account a viscoelastic breast phantom with embedded harder lumps by only changing the real-time model and its FEM counterpart. However, new human studies would be needed to investigate how human participants perceive the difference of level of softness within one virtual phantom.

6.3 Final Remarks

This thesis presented the work done to develop a new evaluation method to assess real-time model of soft tissue considering human perception of object softness. The method was based on statistical tools and was verified through human studies. These studies investigated two different aspects of a VR system simulating a palpation task. The first aspect investigated the preferred choice of an alignment between a visual display and force feedback device. The second aspect concerned the effect of statistical variations among visual displacements and force feedbacks on perception of object softness. In this thesis, I found that human participant were insensitive to small discrepancies up to a level of 11% of variation for visual displacement. Nevertheless, the development presented in this thesis is a preliminary work. This work showed encouraging results and promising potential for developing VR systems that take advantage of human constraints to train palpation.

Bibliography

- [1] A. Alaraj, M. G. Lemole, J. H. Finkle, R. Yudkowsky, A. Wallace, C. Luciano, P. P. Banerjee, S. H. Rizzi, and F. T. Charbel, “Virtual reality training in neurosurgery: Review of current status and future applications,” *Surgical neurology international*, vol. 2, no. 2, p. 52, 2011. [Online]. Available: <http://www.ncbi.nlm.nih.gov/pubmed/21697968>
- [2] S. Mangione, *Physical diagnosis secrets*. Mosby/Elsevier, 2008.
- [3] W. W. M. Lam, C. P. Chan, C. F. Chan, C. C. C. Mak, C. F. Chan, K. W. H. Chong, M. H. J. Leung, and M. H. Tang, “Factors affecting the palpability of breast lesion by self-examination,” *Singapore Medical Journal*, vol. 49, pp. 228–232, 2008.
- [4] G. C. Burdea and P. Coiffet, *Virtual Reality Technology*. John Wiley & Sons Inc., 2003.
- [5] S. Misra, K. T. Ramesh, and A. M. Okamura, “Modelling of non-linear elastic tissues for surgical simulation.” *Computer Methods in Biomechanics and Biomedical Engineering*, vol. 13, no. 6, pp. 811–818, 2010. [Online]. Available: <http://www.pubmedcentral.nih.gov/articlerender.fcgi?artid=3050496&tool=pmcentrez&rendertype=abstract>
- [6] J. R. Pomerantz, *Perception: Overview*. John Wiley & Sons, Ltd, 2006. [Online]. Available: <http://dx.doi.org/10.1002/0470018860.s00589>
- [7] C. O’sullivan and J. Dingliana, “Collisions and perception,” *ACM Trans. Graph.*, vol. 20, no. 3, pp. 151–168, 2001.
- [8] A. Widmer and Y. Hu, “The role of viewing angle in integrating the senses of vision and touch for perception of object softness,” *Canadian Journal of Electrical and*

- Computer Engineering*, vol. 32, no. 4, pp. 193–198, Fall 2007.
- [9] J.-M. Schwartz, M. Denninger, D. Rancourt, C. Moisan, and D. Laurendeau, “Modelling liver tissue properties using a non-linear visco-elastic model for surgery simulation,” *Medical Image Analysis*, vol. 9, no. 2, pp. 103 – 112, 2005, medical Simulation - Delingette, Medical Simulation - Delingette. [Online]. Available: <http://www.sciencedirect.com/science/article/B6W6Y-4DXT7K3-1/2/347d14f61a9f91c55ca03ce62bc6ad47>
- [10] A. E. Kerdok, S. M. Cotin, M. P. Ottensmeyer, A. M. Galea, R. D. Howe, and S. L. Dawson, “Truth cube: Establishing physical standards for soft tissue simulation,” *Medical Image Analysis*, vol. 7, no. 3, pp. 283 – 291, 2003, functional Imaging and Modeling of the Heart. [Online]. Available: <http://www.sciencedirect.com/science/article/B6W6Y-48FSTG9-4/2/a2c840760f74a5fe474ef00951c00691>
- [11] B. Wu, R. L. Klatzky, D. Shelton, and G. D. Stetten, “Psychophysical evaluation of in-situ ultrasound visualization,” *IEEE Transactions on Visualization and Computer Graphics*, vol. 11, no. 6, pp. 684–693, Nov.–Dec. 2005.
- [12] B. Unger, A. Nicolaidis, P. Berkelman, A. Thompson, S. Lederman, R. Klatzky, and R. Hollis, “Virtual peg-in-hole performance using a 6-dof magnetic levitation haptic device: comparison with real forces and with visual guidance alone,” *Haptic Interfaces for Virtual Environment and Teleoperator Systems, 2002. HAPTICS 2002. Proceedings. 10th Symposium on*, pp. 263–270, 2002.
- [13] J. M. Bland and D. G. Altman, “Statistical methods for assessing agreement between two methods of clinical measurement,” *Lancet*, vol. 1, no. 8476, pp. 307–310, Feb. 1986, PMID: 2868172. [Online]. Available: <http://www.ncbi.nlm.nih.gov/pubmed/2868172>

- [14] M. Dinsmore, N. Langrana, G. Burdea, and J. Ladeji, "Virtual reality training simulation for palpation of subsurface tumors," in *Proc. Virtual Reality Annual International Symposium IEEE 1997*, N. Langrana, Ed., 1997, pp. 54–60.
- [15] H. Chen and H. Sun, "Body-based haptic interaction model for touch-enabled virtual environments," *Presence: Teleoper. Virtual Environ.*, vol. 15, no. 2, pp. 186–203, 2006.
- [16] V. Daniulaitis, M. Alhalabi, H. Kawasaki, and Y. Tanaka, "Medical palpation of deformable tissue using physics-based model for haptic interface robot (hiro)," in *Proc. IEEE/RSJ International Conference on Intelligent Robots and Systems (IROS 2004)*, M. Alhalabi, Ed., vol. 4, 2004, pp. 3907–3911 vol.4.
- [17] M. Sedef, E. Samur, and C. Basdogan, "Real-time finite-element simulation of linear viscoelastic tissue behavior based on experimental data," *Computer Graphics and Applications, IEEE*, vol. 26, no. 6, pp. 58–68, Nov.-Dec. 2006.
- [18] F. Dogan and M. S. Celebi, "Real-time deformation simulation of non-linear viscoelastic soft tissues," *SIMULATION*, vol. 87, no. 3, pp. 179–187, 2010. [Online]. Available: <http://sim.sagepub.com/content/early/2010/04/08/0037549710364532.abstract>
- [19] W. Mollemans, F. Schutyser, N. Nadjmi, F. Maes, and P. Suetens, "Predicting soft tissue deformations for a maxillofacial surgery planning system: From computational strategies to a complete clinical validation," *Medical Image Analysis*, vol. 11, no. 3, pp. 282 – 301, 2007.
- [20] M. Marchal, J. Allard, C. Duriez, and S. Cotin, "Towards a framework for assessing deformable models in medical simulation," in *ISBMS*, 2008, pp. 176–184.
- [21] W. Mollemans, F. Schutyser, J. V. Cleynenbreugel, and P. Suetens, "Tetrahedral

- mass spring model for fast soft tissue deformation,” in *Surgery Simulation and Soft Tissue Modeling*, 2003, pp. 1002–1003.
- [22] T. Cui, A. Song, and J. Wu, “Simulation of a mass-spring model for global deformation,” *Frontiers of Electrical and Electronic Engineering in China*, vol. 4, no. 1, pp. 78–82, Mar. 2009. [Online]. Available: <http://dx.doi.org/10.1007/s11460-009-0001-6>
- [23] J. Berkley, G. Turkiyyah, D. Berg, M. Ganter, and S. Weghorst, “Real-time finite element modeling for surgery simulation: An application to virtual suturing,” *IEEE Transactions on Visualization and Computer Graphics*, vol. 10, no. 3, pp. 314–325, 2004.
- [24] B. A. Lloyd, G. Szkely, and M. Harders, “Identification of spring parameters for deformable object simulation,” *Visualization and Computer Graphics, IEEE Transactions on*, vol. 13, no. 5, pp. 1081–1094, September 2007.
- [25] S. Cotin, H. Delingette, and N. Ayache, “A hybrid elastic model for real-time cutting, deformations, and force feedback for surgery training and simulation,” *The Visual Computer*, vol. 16, pp. 437–452, Dec. 2000. [Online]. Available: <http://dx.doi.org/10.1007/PL00007215>
- [26] G. Sela, J. Subag, A. Lindblad, D. Albocher, S. Schein, and G. Elber, “Real-time haptic incision simulation using fem-based discontinuous free-form deformation,” *Computer Aided Design*, vol. 39, no. 8, pp. 685–693, 2007.
- [27] M. Alhalabi, V. Daniulaitis, H. Kawasaki, and T. Hori, “Medical training simulation for palpation of subsurface tumor using hiro,” in *Proc. First Joint Eurohaptics Conference and Symposium on Haptic Interfaces for Virtual Environment and Teleoperator Systems World Haptics 2005*, V. Daniulaitis, Ed., 2005, pp. 623–624.

- [28] X. Guo and H. Qin, “Meshless methods for physics-based modeling and simulation of deformable models,” *Science in China Series F: Information Sciences*, vol. 52, no. 3, pp. 401–417, Mar. 2009. [Online]. Available: <http://dx.doi.org/10.1007/s11432-009-0069-x>
- [29] S. A. Gottschalk, “Collision queries using oriented bounding boxes,” Ph.D. dissertation, University of North Carolina at Chapel Hill, 2000, director-Manocha Dinesh and Director-Lin Ming C.
- [30] M. A. Otaduy and M. C. Lin, “A modular haptic rendering algorithm for stable and transparent 6-dof manipulation,” *IEEE Transactions on Robotics*, vol. 22, no. 4, pp. 751–762, Aug. 2006.
- [31] S. Redon, A. Kheddar, and S. Coquillart, “Fast continuous collision detection between rigid bodies,” in *Proc. of Eurographics (Computer Graphics Forum)*, vol. 21, no. 3, 2002, pp. 279–288.
- [32] W. A. McNeely, K. D. Puterbaugh, and J. J. Troy, “Six degree-of-freedom haptic rendering using voxel sampling,” in *SIGGRAPH ’99: Proceedings of the 26th annual conference on Computer graphics and interactive techniques*. New York, NY, USA: ACM Press/Addison-Wesley Publishing Co., 1999, pp. 401–408.
- [33] J. Barbič and D. L. James, “Six-dof haptic rendering of contact between geometrically complex reduced deformable models,” *IEEE Transactions on Haptics*, vol. 1, no. 1, pp. 39–52, 2008.
- [34] D. A. Bernstein, *Essentials of Psychology*. Cengage Learning, Mar. 2010.
- [35] M. Srinivasan, G. Beauregard, and D. Brock, “The impact of visual information on the haptic perception of stiffness in virtual environments,” in *Proc. ASME DSC Division*, vol. 58, 1996, pp. 555–559.

- [36] W.-C. Wu, C. Basdogan, and M. A. Srinivasan, “Visual, haptic, and bimodal perception of size and stiffness in virtual environments,” in *Proc. ASME DSC Division*, vol. 67, 1999, pp. 19–26.
- [37] M. A. Heller, J. A. Calcaterra, S. L. Green, and L. Brown, “Intersensory conflict between vision and touch: the response modality dominates when precise, attention-riveting judgments are required.” *Percept Psychophys*, vol. 61, no. 7, pp. 1384–1398, Oct 1999.
- [38] M. O. Ernst and M. S. Banks, “Humans integrate visual and haptic information in a statistically optimal fashion.” *Nature*, vol. 415, no. 6870, pp. 429–433, 2002.
- [39] M. Kuschel, M. Buss, F. Freyberger, B. Farber, and R. Klatzky, “Visual-haptic perception of compliance: Fusion of visual and haptic information,” in *Haptic interfaces for virtual environment and teleoperator systems, 2008. haptics 2008. symposium on*, March 2008, pp. 79–86.
- [40] K. Drewing, A. Ramisch, and F. Bayer, “Haptic, visual and visuo-haptic softness judgments for objects with deformable surfaces,” in *EuroHaptics conference, 2009 and Symposium on Haptic Interfaces for Virtual Environment and Teleoperator Systems. World Haptics 2009. Third Joint*, March 2009, pp. 640–645.
- [41] W. M. B. Tiest and A. M. Kappers, “Haptic and visual perception of roughness,” *Acta Psychologica*, vol. 124, no. 2, pp. 177 – 189, 2007.
- [42] M. Reiner, “The role of haptics in immersive telecommunication environments,” *IEEE Transactions on Circuits and Systems for Video Technology*, vol. 14, no. 3, pp. 392–401, March 2004.
- [43] C. Chase, P. Chenoweth, R. Larsen, T. Olson, A. Hammond, M. Menchaca, R. Randel, M. Srinivasan, and C. Basdogan, “Haptics in virtual environments: taxonomy,

research status, and challenges,” *Computers and Graphics*, vol. 21, 1997.

- [44] R. B. Welch and D. H. Warren., *Handbook of Perception and Human Performance*. New York: Wiley, 1986, ch. Intersensory Interactions.
- [45] G. Poling, J. Weisenberger, and T. Kerwin, “The role of multisensory feedback in haptic surface perception,” *Haptic Interfaces for Virtual Environment and Teleoperator Systems, 2003. HAPTICS 2003. Proceedings. 11th Symposium on*, pp. 187–194, 22-23 March 2003.
- [46] D. R. Stevenson, K. A. Smith, J. P. McLaughlin, C. J. Gunn, J. P. Veldkamp, and M. J. Dixon, “Haptic workbench: a multisensory virtual environment,” in *Stereoscopic Displays and Virtual Reality Systems VI*, J. O. Merritt, M. T. Bolas, and S. S. Fisher, Eds., vol. 3639, no. 1. SPIE, 1999, pp. 356–366.
- [47] R. Komerska and C. Ware, “Haptic state surface interactions,” *Computer Graphics and Applications, IEEE*, vol. 24, no. 6, pp. 52–59, 2004.
- [48] R. W. Webster, D. I. Zimmerman, B. J. Mohler, M. G. Melkonian, and R. S. Haluck, “A prototype haptic suturing simulator.” *Stud Health Technol Inform*, vol. 81, pp. 567–569, 2001.
- [49] M. O. Ernst, M. S. Banks, and H. H. Blthoff, “Touch can change visual slant perception.” *Nat Neurosci*, vol. 3, no. 1, pp. 69–73, Jan 2000.
- [50] L. Bouguila, M. Ishii, and M. Sato, “Effect of coupling haptics and stereopsis on depth perception in virtual environment,” in *Proceedings of the 1st Workshop on Haptic Human Computer Interaction*, Glasgow, Scotland, 31st August - 1st September, 2000, 2000, pp. 54–63.
- [51] D. Swapp and V. P. C. Loscos, “Interaction with co-located haptic feedback in virtual reality,” *Virtual Reality*, vol. 10, pp. 24–30, 2006.

- [52] N. Gurari, K. Kuchenbecker, and A. Okamura, “Stiffness discrimination with visual and proprioceptive cues,” in *EuroHaptics conference, 2009 and Symposium on Haptic Interfaces for Virtual Environment and Teleoperator Systems. World Haptics 2009. Third Joint*, march 2009, pp. 121–126.
- [53] C. Duriez, C. Andriot, and A. Kheddar, “A multi-threaded approach for deformable/rigid contacts with haptic feedback,” in *Proc. 12th International Symposium on Haptic Interfaces for Virtual Environment and Teleoperator Systems HAPTICS '04*, 27–28 March 2004, pp. 272–279.
- [54] P. Manousopoulos, V. Drakopoulos, T. Theoharis, and P. Stavrou, “Virtual reality systems modelling haptic two-finger contact with deformable physical surfaces,” in *Cyberworlds, 2007. CW '07. International Conference on*, oct. 2007, pp. 292–299.
- [55] A. Widmer and Y. Hu, “A viscoelastic model of a breast phantom for real-time palpation,” in *Engineering in Medicine and Biology Society, EMBC, 2011 Annual International Conference of the IEEE*, 30 2011-sept. 3 2011, pp. 4546–4549.
- [56] S. A. Cholewiak, S. A. Cholewiak, H. Z. Tan, and D. S. Ebert, “Haptic identification of stiffness and force magnitude,” in *Proc. Symposium on Haptic Interfaces for Virtual Environment and Teleoperator Systems HAPTICS 2007*, H. Z. Tan, Ed., 2008, pp. 87–91.
- [57] R. H. LaMotte, “Softness discrimination with a tool,” *J Neurophysiol*, vol. 83, no. 4, pp. 1777–1786, 2000.
- [58] S. J. Lederman and R. L. Klatzky, “Sensing and displaying spatially distributed fingertip forces in haptic interfaces for teleoperator and virtual environment systems,” *Presence: Teleoper. Virtual Environ.*, vol. 8, pp. 86–103, February 1999.
[Online]. Available: <http://portal.acm.org/citation.cfm?id=1246796.1246803>

- [59] S. J. Lederman, R. L. Klatzky, A. Abramowicz, K. Salsman, R. Kitada, and C. Hamilton, "Haptic recognition of static and dynamic expressions of emotion in the live face," *Psychological Science*, vol. 18, no. 2, pp. 158–164, 2007.
- [60] A. Law, *Simulation Modeling and Analysis*, 4th ed. McGraw Hill Higher Education, Aug. 2006.
- [61] A. Widmer and Y. Hu, "Statistical comparison between a real-time model and a fem counterpart for visualization of breast phantom deformation during palpation," in *Electrical and Computer Engineering (CCECE), 2010 23rd Canadian Conference on*, may 2010, pp. 1 –4.
- [62] H. Chen, W. Wu, H. Sun, and P.-A. Heng, "Dynamic touch-enabled virtual palpation," *Computer Animation and Virtual Worlds*, vol. 18, pp. 339–348, 2007. [Online]. Available: <http://dx.doi.org/10.1002/cav.194>
- [63] H. Barreto and F. Howland, *Introductory Econometrics: Using Monte Carlo Simulation with Microsoft Excel*, 1st ed. Cambridge University Press, Dec. 2005.
- [64] E. Basafa and F. Farahmand, "Real-time simulation of the nonlinear viscoelastic deformations of soft tissues." *International journal of computer assisted radiology and surgery*, vol. 6, no. 3, pp. 297–307, 2011. [Online]. Available: <http://sim.sagepub.com/cgi/doi/10.1177/0037549710364532>
- [65] S. E. Maxwell and H. D. Delaney, *Designing Experiments and Analyzing Data: A Model Comparison Perspective, Second Edition*, 2nd ed. Routledge Academic, Sept. 2003.
- [66] W. G. Cochran, *Sampling Techniques, 3rd Edition*, 3rd ed. Wiley, Jan. 1977.
- [67] M. Sridhar and M. Insana, "Ultrasonic measurements of breast viscoelasticity," *Med Phys.*, vol. 12, pp. 4757–4767, 2007.

- [68] N. N. Mohsenin, *Physical properties of plant and animal materials: structure, physical characteristics, and mechanical properties*. Taylor & Francis, 1986.
- [69] J. Stewart, *Calculus: Early Transcendentals*, 5th ed. Brooks Cole, Dec. 2002.
- [70] H. Mehrabian and A. Samani, “An iterative hyperelastic parameters reconstruction for breast cancer assessment,” in *Proceedings of the SPIE, Medical Imaging 2008: Physiology, Function, and Structure from Medical Images*, X. P. Hu and A. V. Clough, Eds., vol. 6916, 2008, pp. 69 161C–69 161C–9.
- [71] W. N. Findley, J. S. Lai, and K. Onaran, *Creep and relaxation of nonlinear viscoelastic materials: with an introduction to linear viscoelasticity*. Courier Dover Publications, June 1989.
- [72] G. van den Bergen, “Efficient collision detection of complex deformable models using aabb trees,” *J. Graph. Tools*, vol. 2, no. 4, pp. 1–13, Jan. 1998. [Online]. Available: <http://dl.acm.org/citation.cfm?id=763345.763346>
- [73] T. M. Greiner, “Hand anthropometry of US army personnel,” DTIC Document, Tech. Rep., 1991. [Online]. Available: <http://oai.dtic.mil/oai/oai?verb=getRecord&metadataPrefix=html&identifier=ADA244533>
- [74] A. Widmer and Y. Hu, “Effects of the alignment between a haptic device and visual display on the perception of object softness,” *Systems, Man and Cybernetics, Part A: Systems and Humans, IEEE Transactions on*, pp. 1 –10, 2010.
- [75] L. Renier, C. Laloyaux, O. Collignon, D. Tranduy, A. Vanlierde, R. Bruyer, and A. G. D. Volder, “The ponzo illusion with auditory substitution of vision in sighted and early-blind subjects.” *Perception*, vol. 34, no. 7, pp. 857–867, 2005.
- [76] A. Widmer and Y. Hu, “Integration of the senses of vision and touch in perceiving object softness,” in *Electrical and Computer Engineering, 2007. CCECE 2007*.

- Canadian Conference on*, april 2007, pp. 1353 –1356.
- [77] R. C. Oldfield, “The assessment and analysis of handedness: The Edinburgh inventory,” *Neuropsychologia*, vol. 9, no. 1, pp. 97–113, 1971.
 - [78] M. Matyka and M. Ollila, “A pressure model for soft body simulation,” in *Proc. of SIGRAD*, Umea, 2003.
 - [79] K. Hinkelmann and O. Kempthorne, *Design and Analysis of Experiments. I and II*. Wiley, 2008.
 - [80] J. Liu and A. Song, “Discrimination and memory experiments on haptic perception of softness,” *Perceptual and Motor Skills*, vol. 106, pp. 295–306, Feb. 2008.
 - [81] R. M. Bracewell, A. S. Wimperis, and A. M. Wing, “Brain mechanisms of haptic perception,” *Springer Tracts in Advanced Robotics*, vol. 45 STAR, pp. 25 – 37, 2008.
 - [82] M. A. Srinivasan and R. H. LaMotte, “Tactual discrimination of softness.” *J Neurophysiol*, vol. 73, no. 1, pp. 88–101, Jan 1995.
 - [83] R. M. Friedman, K. D. Hester, B. G. Green, and R. H. LaMotte, “Magnitude estimation of softness,” *Exp. Brain Res*, vol. 191, no. 2, pp. 133–142, 2008.
 - [84] J. M. Bland and D. G. Altman, “Statistics notes: Measurement error,” *BMJ*, vol. 313, no. 7059, p. 744, 9 1996.
 - [85] G. Gescheider, *Psychophysics: the fundamentals*, 3rd ed. Lawrence Erlbaum Associates, 1997.
 - [86] J. P. Shaffer, “Multiple hypothesis testing,” *Ann. Rev. Psych.*, vol. 46, pp. 561–584, 1995.

- [87] M. Kuschel, M. Di Luca, M. Buss, and R. Klatzky, “Combination and integration in the perception of visual-haptic compliance information,” *Haptics, IEEE Transactions on*, vol. 3, no. 4, pp. 234–244, oct.-dec. 2010.
- [88] H. Z. Tan, N. I. Durlach, G. L. Beauregard, and M. A. Srinivasan, “Manual discrimination of compliance using active pinch grasp: the roles of force and work cues,” *Perception & psychophysics*, vol. 57, no. 4, pp. 495–510, May 1995, PMID: 7596747. [Online]. Available: <http://www.ncbi.nlm.nih.gov/pubmed/7596747>
- [89] L. A. Jones and I. W. Hunter, “A perceptual analysis of stiffness,” *Experimental brain research. Experimentelle Hirnforschung. Experimentation crbrale*, vol. 79, no. 1, pp. 150–156, 1990, PMID: 2311691. [Online]. Available: <http://www.ncbi.nlm.nih.gov/pubmed/2311691>
- [90] V. Varadharajan, R. Klatzky, B. Unger, R. Swendsen, and R. Hollis, “Haptic rendering and psychophysical evaluation of a virtual Three-Dimensional helical spring,” *2008 Symposium on Haptic Interfaces for Virtual Environment and Teleoperator Systems*, pp. 57–64, 2008.
- [91] A. Lécuyer, J.-M. Burkhardt, and L. Etienne, “Feeling bumps and holes without a haptic interface: the perception of pseudo-haptic textures,” in *Proceedings of the SIGCHI conference on Human factors in computing systems*, ser. CHI ’04. New York, NY, USA: ACM, 2004, pp. 239–246. [Online]. Available: <http://doi.acm.org/10.1145/985692.985723>
- [92] K. J. Kuchenbecker, D. Ferguson, M. Kutzer, M. Moses, and A. M. Okamura, “The touch thimble: Providing fingertip contact feedback during point-force haptic interaction,” in *Proceedings of the 2008 Symposium on Haptic Interfaces for Virtual Environment and Teleoperator Systems*, ser. HAPTICS ’08. Washington,

DC, USA: IEEE Computer Society, 2008, pp. 239–246. [Online]. Available: <http://dx.doi.org/10.1109/HAPTICS.2008.4479950>

- [93] S. Ullrich and T. Kuhlen, “Haptic palpation for medical simulation in virtual environments,” *IEEE Transactions on Visualization and Computer Graphics*, vol. 18, pp. 617–625, 2012.

Appendix A

Requirements in VR Systems: The REVIR Approach and its Preliminary Evaluation*

A.1 Introduction

As a side project during the research for the main part of the thesis, I participated to a paper about the usage of requirements engineering needed for the creation of VR training system for medical procedures. This paper was published and presented at IEEE Virtual Reality 2010 Workshop on Software Engineering and Architectures for Real-Time Interactive Systems (SEARIS).

A.2 Abstract

Virtual reality (VR) has become a widely used concept to implement medical planning and simulation systems. However, developing such systems is challenging as we lack suitable guidelines for effectively integrating resource-consuming computations and interaction techniques, such as haptic devices. Therefore, this paper outlines a method that utilizes concepts from software requirements engineering and supports software developers when building medical VR systems. The presented approach is the result of performing “action research” when implementing a VR system to study the integration of the senses of vision and touch for perceiving the softness of human tissue. The approach focuses on performance, usability and the correctness of physical models in VR

*This appendix is published. Galster, M. and Widmer, A. “Requirements in a Virtual Environment: The REVIR Approach and a Preliminary Evaluation”, *IEEE Virtual Reality 2010 Workshop on Software Engineering and Architectures for Real-Time Interactive Systems (SEARIS)*, Waltham, MA, USA, March, 2010.

applications. A case study of developing a surgical planning system (which provides haptic and visual information simultaneously) is presented as a preliminary evaluation of our approach. Even though this paper focuses on medical VR systems, we believe that the approach can be generalized and is also applicable to other types of VR systems.

Appendix B

Results of The Second Experiment with Force Application on The Side

B.1 Introduction

This appendix summarizes results of a second variation computation and a second experiment as human study performed in the context of the investigation on insensitivity of human perception during perceiving object softness. Following the methodology introduced in Chapter 3, the variation computation and the second experiment focus on palpation on the side of the phantom. First, the variation computation explored visual displacement and force feedback comparison between a real-time model and its FEM counterpart. Second, the experiment used the same stimuli, apparatus, procedure, and data analysis as described in Chapter 5 but with 15 different participants. These participants applied force on the side of the phantom under one-finger or two-finger palpation as shown in Fig. B.1b and Fig. B.1c, respectively. The results of this experiment are similar to those presented in Chapter 5. The main difference from the results presented in Chapter 5 arises from the objective measurement of maximum pressing depth. In the second experiment, the maximum pressing depth applied by the participants always corresponded to the height of the phantom at the palpation location as illustrated in Fig. B.1a. This seemed to affect perception of object softness. For details on the methodology used in both variation computation and second experiment, please refer to Chapter 5.

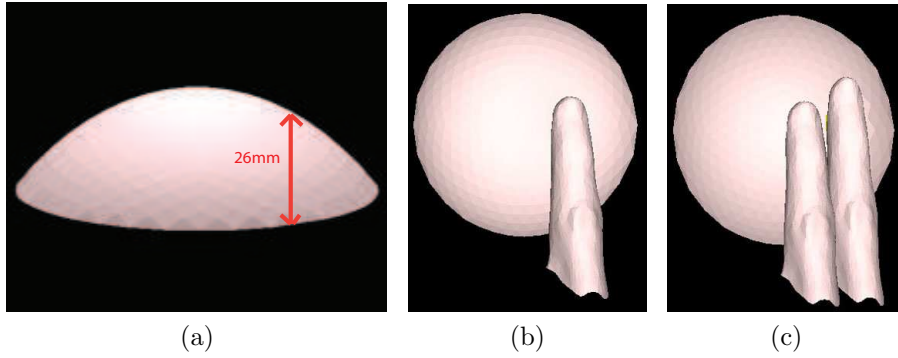


Figure B.1: Representation of a virtual breast phantom and palpation scenarios: (a) side view of the virtual phantom; (b) one-finger palpation using the index finger; (c) two-finger palpation using both index and middle fingers.

B.2 Variation Computation Results

B.2.1 One-Finger Palpation

Table B.1 shows results for visual displacement comparison computed under one-finger palpation. Under this palpation, the RMSE values ranged from 0.22 cm (Distribution 3 vs. Distribution 4) to 0.91 cm (Distribution 1 vs. Distribution 2). A low RSME value of 0.34 cm was found under the comparison between Distribution 1 and Distribution 4. As shown in Chapter 5, the nodes at the tail of the Gaussian curve in Distribution 4 did not render force, similarly to the same nodes in Distribution 1. These observations were similar to those I made under one-finger palpation applied on the top of the phantom. In addition, ANOVA did not yield significant difference for visual displacement among any two distributions. This was illustrated by p -values greater than the 0.05 threshold. In agreement with other palpation scenarios, this shows that every two datasets included in each pair for comparison are not statistically different from each other. The variation values computed through the Bland and Altman agreement method varied from 4.62% (Distribution 3 vs. Distribution 4) to 13.93%. Two groups of values are visible. The comparisons including only multi-node contact produced variation between 4.62% and 6.35%, whereas comparisons including the single-node contact compared to multi-node

	RMSE [cm]	ANOVA		B&A agreement	
		F	p	S.D. [cm]	V [%]
1 vs. 2	0.9084	3.15	0.0698	0.0639	13.93
1 vs. 3	0.3813	2.23	0.1312	0.0271	13.2
1 vs. 4	0.3430	2.11	0.1852	0.0250	13.11
2 vs. 3	0.5317	1.98	0.2015	0.0372	6.35
2 vs. 4	0.6613	2.59	0.1015	0.0469	6.48
3 vs. 4	0.2246	2.36	0.1244	0.0171	4.62

Table B.1: Visual displacement comparison computed under one-finger palpation on the side of the phantom.

contacts have variations comprise values from 13.11% to 13.93%. Similarly to one-finger palpation on the top of the phantom, a gap of 6.63% was visible between the two groups. This gap illustrates the difference of visual displacement produced by the single-node contact in comparison to multi-node contacts.

Table B.2 illustrates comparisons of force feedback under one-finger palpation on the side of the phantom. Under this palpation, RMSE results fluctuated from 0.45 N () to 0.88 N (Distribution 1 vs. Distribution 2). This observation shows that the range of RMSE values under one-finger palpation on the side of the phantom is similar to one-finger or two-finger palpation on the top of the phantom as described in Chapter 5. Using ANOVA, I demonstrate that force feedbacks produced by force distributions are not statistically differentiable. This was shown by p -values computed among comparisons over the 0.05 threshold. Variation results derived from the Bland and Altman agreement method ranged from 1.88% (Distribution 3 vs. Distribution 4) to 4.82% (Distribution 1 vs. Distribution 2). In agreement with results found under one-finger palpation on the top of the phantom, the range of variation was small in comparison to the variations found for visual displacement and no variation was higher than 5%. This may be due to the limited number of nodes taken in account during the analysis of force feedback.

	RMSE [N]	ANOVA		B&A agreement	
		F	p	S.D. [N]	V [%]
1 vs. 2	0.8787	1.52	0.2310	0.1071	4.82
1 vs. 3	0.5274	1.78	0.2145	0.0924	3.39
1 vs. 4	0.3521	2.09	0.1745	0.1144	3.58
2 vs. 3	0.5145	2.45	0.1147	0.1256	2.64
2 vs. 4	0.4271	2.98	0.0985	0.1078	3.15
3 vs. 4	0.2871	1.50	0.2287	0.0574	1.88

Table B.2: Force feedback comparison computed under one-finger palpation on the side of the phantom.

B.2.2 Two-Finger Palpation

Under two-finger palpation on the side of the phantom, Table B.3 details the results produced by the visual displacement comparison. In this comparison, RMSE values ranged from 0.19 cm (Distribution 3 vs. Distribution 4) to 0.91 cm (Distribution 1 vs. Distribution 2). This is in agreement with other visual displacement comparisons found in Chapter 5. For significance testing, the results from ANOVA were consistent with those found under all other palpation scenarios. All p -values were above the 0.05 threshold. Therefore, no significant difference was found for any comparison. Based on the Bland and Altman agreement method, the variation levels varied from 4.33% (Distribution 3 vs. Distribution 4) to 11.06% (Distribution 1 vs. Distribution 3). The highest value (11.06%) is close to the highest values observed under one-finger palpation on the side of the phantom. The gaps found between distribution comparisons including single-node force distribution and those including only multi-node force distributions in previous palpation scenarios is less visible under two-finger palpation on the side of the phantom.

Table B.4 shows the results from the analysis of force feedback under two-finger palpation. RMSE values were ranging from 0.12 N (Distribution 3 vs. Distribution 4) to 0.86 N (Distribution 1 vs. Distribution 2). These values were in agreement with those found in other palpation scenarios. In addition, p -values computed by ANOVA were all

	RMSE [cm]	ANOVA		B&A agreement	
		F	p	S.D. [cm]	V [%]
1 vs. 2	0.9148	3.11	0.0798	0.0162	10.15
1 vs. 3	0.7958	2.05	0.1752	0.0285	11.06
1 vs. 4	0.3045	2.56	0.1285	0.0307	8.92
2 vs. 3	0.4682	1.48	0.2356	0.0332	5.81
2 vs. 4	0.2563	1.35	0.2452	0.0196	6.77
3 vs. 4	0.1965	1.89	0.2132	0.0397	4.33

Table B.3: Visual displacement comparison computed under two-finger palpation on the side of the phantom.

	RMSE [N]	ANOVA		B&A agreement	
		F	p	S.D. [N]	V [%]
1 vs. 2	0.8693	2.39	0.1185	0.0914	4.77
1 vs. 3	0.7851	2.47	0.1014	0.1285	3.98
1 vs. 4	0.8544	1.95	0.1954	0.1365	3.48
2 vs. 3	0.6284	1.89	0.2154	0.0987	3.14
2 vs. 4	0.5214	1.64	0.2265	0.0821	3.86
3 vs. 4	0.1278	1.98	0.1547	0.0685	2.85

Table B.4: Force feedback comparison computed under two-finger palpation on the side of the phantom.

above the 0.05 threshold and therefore did not show significant difference between the two datasets compared in each pair. Variation values computed through the Bland and Altman agreement method varied from 2.85% (Distribution 3 vs. Distribution 4) to 4.77% (Distribution 1 vs. Distribution 2). These results were in agreement with those found in other palpation scenarios.

B.3 Human Study Results

B.3.1 Subjective Perception

One-Finger Palpation

Different from the experiment described in Chapter 5, the second experiment features one or two fingers applying force on the side of the virtual phantom. To investigate subjective measurements recorded during palpation using 1 finger, I performed a two-way

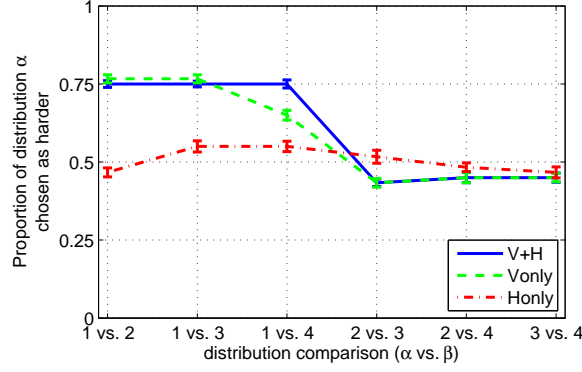


Figure B.2: Subjective perception of object softness under one-finger palpation on the side of the phantom. Error bars represent standard errors.

	One-way ANOVA $F(5,14)$	Pairwise Contrast (Bonferroni)	
Vonly	$F = 25.18,$ $p < 0.001$	1 vs. 2 < - > 2 vs. 3	$p < 0.01$
		1 vs. 2 < - > 2 vs. 4	$p < 0.01$
		1 vs. 2 < - > 3 vs. 4	$p < 0.05$
		1 vs. 3 < - > 2 vs. 3	$p < 0.01$
		1 vs. 3 < - > 2 vs. 4	$p < 0.01$
		1 vs. 3 < - > 3 vs. 4	$p < 0.01$
		1 vs. 4 < - > 2 vs. 3	$p < 0.01$
		1 vs. 4 < - > 2 vs. 4	$p < 0.01$
		1 vs. 4 < - > 3 vs. 4	$p < 0.01$
V+H	$F = 10.96,$ $p < 0.001$	1 vs. 2 < - > 2 vs. 3	$p < 0.01$
		1 vs. 2 < - > 2 vs. 4	$p < 0.05$
		1 vs. 2 < - > 3 vs. 4	$p < 0.05$
		1 vs. 3 < - > 2 vs. 3	$p < 0.01$
		1 vs. 3 < - > 2 vs. 4	$p < 0.01$
		1 vs. 3 < - > 3 vs. 4	$p < 0.01$
		1 vs. 4 < - > 2 vs. 3	$p < 0.01$
		1 vs. 4 < - > 2 vs. 4	$p < 0.05$
		1 vs. 4 < - > 3 vs. 4	$p < 0.05$
Honly	$F = 1.225, p > 0.05$	-	-

Table B.5: Results of One-way ANOVA and pairwise contrasts for the effect of force distributions on subjective perception of object softness palpated under one-finger palpation on the side of the phantom.

ANOVA (testing conditions x force distributions comparisons). The two-way ANOVA displays mixed results as illustrated in Fig. B.2. For example, there is no indication that the three conditions did affect the subjective perception of object softness among

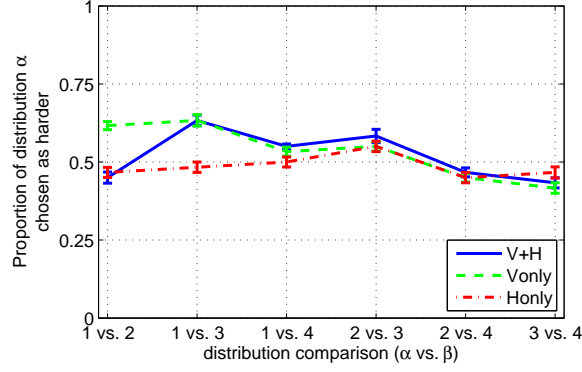


Figure B.3: Subjective perception of object softness under two-finger palpation on the side of the phantom. Error bars represent standard errors.

	One-way ANOVA $F(5,14)$	Pairwise Contrast (Bonferroni)	
V+H	$F = 2.431, p < 0.05$	-	-
Vonly	$F = 3.226, p < 0.05$	1 vs. 2 < - > 2 vs. 3	$p < 0.05$
Honly	$F = 0.277, p > 0.05$	-	-

Table B.6: Results of One-way ANOVA and pairwise contrasts for the effect of force distribution on subjective perception of object softness palpated under two-finger palpation on the side of the phantom.

distribution comparisons [$F(2, 14)=1.821$ $p > 0.05$]. However, a significant effect among the six force distributions was observed on this subjective perception [$F(5, 14)=20.704$, $p < 0.001$]. Moreover, an interaction between testing conditions and force distributions comparisons was significant [$F(10, 14)=2.704$ $p < 0.05$]. The difference of perception between Condition Honly and the two other Conditions Vonly and V+H might be the source of this significance.

As further analysis to investigate the significant effect of force distributions, Table B.5 displays the results of one-way ANOVA. In these results, I observed that participants perceived phantoms differently through a single-node force distribution and multi-node force distributions under Conditions Vonly and V+H. These observations are similar to those made using one-finger palpation on the top of the phantom in Chapter 5. However, Conditions Vonly, Honly and V+H did not significantly affect the subjective perception

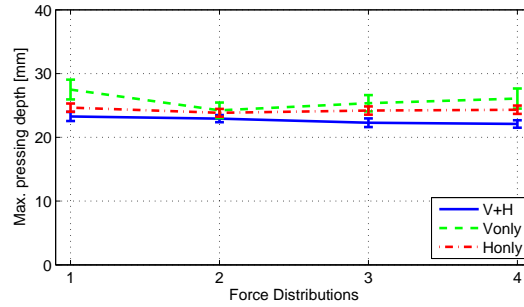


Figure B.4: Objective measurement of maximum pressing depth under one-finger palpation on the side of the phantom. Error bars represent standard errors.

of object softness in opposition to the results described in Chapter 5.

Two-Finger Palpation

Under two-finger palpation, Fig. B.3 displays the proportion of distribution α chosen as harder when comparing a distribution α and distribution β . A two-way ANOVA (testing conditions x force distributions comparisons) found that testing condition did not affect the subjective perception of object softness [$F(2,14)=0.137$, $p > 0.05$]. However, different force distributions comparisons yields significant different subjective perception [$F(5,14)=4.380$, $p < 0.01$]. No interaction effect was found [$F(10,14)=0.809$, $p > 0.05$]. One-way ANOVA analyses revealed that distribution comparisons are significant only in Condition Vonly as illustrated in Table B.6.

Following the same methodology as presented in Chapter 5, a one-way ANOVA revealed that there was no significant difference of subjective perception of softness yielded by one-finger palpation compared to two-finger palpation [$F(1,14)=1.673$, $p > 0.05$]. In summary, the second experiment shows similar results as those presented in Chapter 5 under one-finger palpation.

	One-way ANOVA $F(5,14)$	Pairwise Contrast (Bonferroni)	
Distr. 1	$F = 4.679, p < 0.05$	V+H < - > Vonly	$p < 0.05$
Distr. 2	$F = 0.728, p > 0.05$	-	-
Distr. 3	$F = 3.180, p < 0.05$	V+H < - > Vonly	$p < 0.05$
Distr. 4	$F = 3.958, p < 0.05$	V+H < - > Vonly	$p < 0.05$

Table B.7: Results of One-way ANOVA and pairwise contrasts for the effect of testing conditions on maximum pressing depth palpated under one-finger palpation on the side of the phantom.

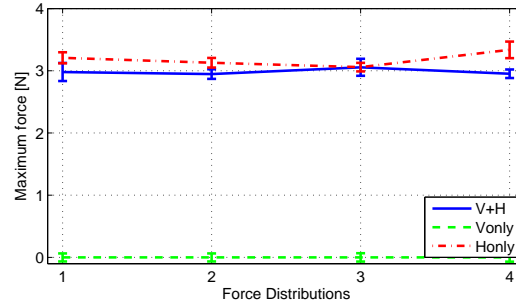


Figure B.5: Objective measurement of maximum force under one-finger palpation on the side of the phantom. Error bars represent standard errors.

B.3.2 Objective Measurements

One-Finger Palpation

Under one-finger palpation on the side of the phantom, a two-way ANOVA (testing conditions x force distributions) yielded different results than its counterpart in Chapter 5. In the second experiment, maximum pressing depth is affected by the three testing conditions [$F(2, 14)=6.510, p < 0.01$] as shown in Fig. B.4. However the two-way ANOVA did not show any significant effect of force distribution on maximum pressing depth [$F(3, 14)=2.085, p > 0.05$]. Similarly, there was no interaction effect between testing conditions and force distributions on maximum pressing depth [$F(6, 14)=0.851, p > 0.05$]. Table B.7 shows the results yielded by one-way ANOVA analyses for testing conditions. Precisely, maximum pressing depth was affected by the testing conditions only under Distribution 1 and Distribution 4.

For objective measurement of maximum force, a two-way ANOVA showed that test-

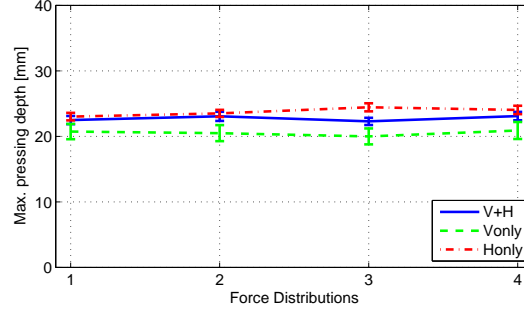


Figure B.6: Objective measurement of maximum pressing depth under two-finger palpation on the side of the phantom. Error bars represent standard errors.

ing conditions significantly affect maximum force [$F(1, 14)=7.569, p < 0.001$] as shown in Fig. B.5. However, maximum force was not affected by the different force distributions [$F(3, 14)= 0.444, p > 0.05$]. In addition, ANOVA did not find a significant interaction effect for maximum force [$F(3, 14)=1.336, p > 0.05$].

Two-Finger Palpation

Under two-finger palpation on the side of the phantom, Fig. B.6 shows the objective measurement of maximum pressing depth applied under each of the four force distributions. The results produced by a two-way ANOVA (testing conditions x force distributions) showed that testing conditions affected the maximum pressing depth [$F(2, 14)=8.306, p < 0.001$]. However force distributions did not affect this objective measurement [$F(3, 14)=0.344, p > 0.05$]. No interaction effect between testing conditions x force distributions was present [$F(6, 14)=0.520, p > 0.05$]. Investigating the significant effect of testing condition on maximum pressing depth, Table B.8 lists the results produced by a one-way ANOVA per distribution.

Under two-finger palpation on the side of the phantom, another two-way ANOVA showed a significant difference of maximum force applied under the four force distributions between the conditions V+H and Honly (Discarding the data from the condition Vonly) [$F(1, 14)=23.496, p < 0.001$]. However, no significant difference was found among force distributions [$F(3, 14)=0.545, p > 0.05$] and no interaction effect was found [$F(3,$

	One-way ANOVA $F(5,14)$	Pairwise Contrast (Bonferroni)	
Distr. 1	$F = 2.223, p > 0.05$	-	-
Distr. 2	$F = 3.644, p < 0.05$	Vonly < - > Honly	$p < 0.05$
Distr. 3	$F = 7.506, p < 0.05$	Vonly < - > Honly	$p < 0.05$
Distr. 4	$F = 3.427, p < 0.05$	Vonly < - > Honly	$p < 0.05$

Table B.8: Results of One-way ANOVA and pairwise contrast for the effect of testing conditions on maximum pressing depth palpated under two-finger palpation on the side of the phantom.

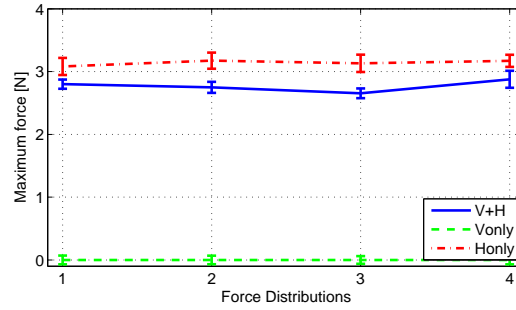


Figure B.7: Objective measurement of maximum force under two-finger palpation on the side of the phantom. Error bars represent standard errors.

	One-way ANOVA $F(1,14)$
Distr. 1	$F = 3.961, p < 0.05$
Distr. 2	$F = 10.579, p < 0.001$
Distr. 3	$F = 13.385, p < 0.001$
Distr. 4	$F = 4.291, p < 0.05$

Table B.9: Results of One-way ANOVA for the effect of force distribution on subjective perception of object softness palpated under two-finger palpation on the side of the phantom.

14)=0.549, $p > 0.05$]. Further analysis was performed to investigate the significance found by the two-way ANOVA. As illustrated in Fig. B.7 and Table B.9, participants constantly applied more force when visual information was not available among all force distributions.

B.4 Summary

Overall, these results confirm the observations made in Chapter 5: Both analyses revealed that the perception of object softness is insensitive up to a variation level of 11.0% for visual displacement and of 6.3% for force feedback, respectively. These levels of insensitivities show that it would be possible to ease design criteria when developing real-time model used in VR training systems for palpation.

Appendix C

Sample Size for a Within-Subject Human Study

This appendix describes how to choose the sample size to estimate the within subject standard deviation, s_w . This is described in a Statistics Note in the BMJ *. The assumptions are as follow:

- The distribution of observations is normal.
- Equal numbers of observations on each participant.
- Multiple repetitions of the same test.

The equation to compute the number of participants is as follow:

$$n = \frac{1.96^2}{2(m-1)s_w^2}, \quad (\text{C.1})$$

where s_w is the standard error of the within-subject standard deviation, n is the number of participants and m is the number of repetitions.

*J Martin Bland and Douglas G Altman, Statistics Notes: “Measurement error,” *BMJ*, vol. 313, pp. 744, 1996

Appendix D

University of Calgary Ethics Approval



CERTIFICATION OF INSTITUTIONAL ETHICS REVIEW

This is to certify that the Conjoint Faculties Research Ethics Board at the University of Calgary has examined the following research proposal and found the proposed research involving human subjects to be in accordance with University of Calgary Guidelines and the Tri-Council Policy Statement on *"Ethical Conduct in Research Using Human Subjects"*. This form and accompanying letter constitute the Certification of Institutional Ethics Review.

File no: **4314**
Applicant(s): **Yaoping Hu**
Department: **Electrical & Computer Engineering**
Project Title: **The Development of a 3-D Preoperative Planning System for Surgical Treatment of Lung Cancer**
Sponsor (if applicable): **NSERC**

Restrictions:

This Certification is subject to the following conditions:

1. Approval is granted only for the project and purposes described in the application.
2. Any modifications to the authorized protocol must be submitted to the Chair, Conjoint Faculties Research Ethics Board for approval.
3. A progress report must be submitted 12 months from the date of this Certification, and should provide the expected completion date for the project.
4. Written notification must be sent to the Board when the project is complete or terminated.

Janice Dickin, Ph.D, LL.B.
Chair
Conjoint Faculties Research Ethics Board

14 Nov 2005
Date:

Distribution: (1) Applicant, (2) Supervisor (if applicable), (3) Chair, Department/Faculty Research Ethics Committee, (4) Sponsor, (5) Conjoint Faculties Research Ethics Board (6) Research Services.



CERTIFICATION OF INSTITUTIONAL ETHICS REVIEW


This is to certify that the Conjoint Faculties Research Ethics Board at the University of Calgary has examined the following research proposal and found the proposed research involving human subjects to be in accordance with University of Calgary Guidelines and the Tri-Council Policy Statement on "Ethical Conduct in Research Using Human Subjects". This form and accompanying letter constitute the Certification of Institutional Ethics Review.

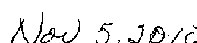
File no: 4314
 Applicant(s): Yaoping Hu
 Bob A. Menelas
 Christopher Millette
 Qiao Wei
 Kan Lo
 Antoine Widmer
 Department: Electrical & Computer Engineering
 Project Title: The Development of a 3-D Preoperative Planning System for Surgical Treatment of Lung Cancer
 Sponsor (if applicable): NSERC

Restrictions:

This Certification is subject to the following conditions:

1. Approval is granted only for the project and purposes described in the application.
2. Any modifications to the authorized protocol must be submitted to the Chair, Conjoint Faculties Research Ethics Board for approval.
3. A progress report must be submitted 12 months from the date of this Certification, and should provide the expected completion date for the project.
4. Written notification must be sent to the Board when the project is complete or terminated.


 Kathleen Oberle, PhD
 Chair
 Conjoint Faculties Research Ethics Board


 Revised Date:
 March 14th 2005
 Original Signed Date:

Distribution: (1) Applicant, (2) Supervisor (if applicable), (3) Chair, Department/Faculty Research Ethics Committee, (4) Sponsor, (5) Conjoint Faculties Research Ethics Board (6) Research Services.

Appendix E

Copyright Transfers

IEEE COPYRIGHT FORM

To ensure uniformity of treatment among all contributors, other forms may not be substituted for this form, nor may any wording of the form be changed. This form is intended for original material submitted to the IEEE and must accompany any such material in order to be published by the IEEE. Please read the form carefully and keep a copy for your files.

TITLE OF PAPER/ARTICLE/REPORT/PRESENTATION/SPEECH INCLUDING ALL CONTENT IN ANY FORM, FORMAT, OR MEDIA (hereinafter, "the Work"): **Subjective perception and objective measurements in perceiving object softness for VR surgical systems**

COMPLETE LIST OF AUTHORS: **Antoine Widmer; Yaoping Hu**

IEEE PUBLICATION TITLE (Journal, Magazine, Conference, Book): **IEEE Virtual Reality 2009**

COPYRIGHT TRANSFER

The undersigned hereby assigns to the Institute of Electrical and Electronics Engineers, Incorporated (the "IEEE") all rights under copyright that may exist in and to the above Work, any revised or expanded derivative works submitted to the IEEE by the undersigned based on the Work, and any associated written, audio and/or visual presentations or other enhancements accompanying the Work. The undersigned hereby warrants that the Work is original and that he/she is the author of the Work; to the extent the Work incorporates text passages, figures, data or other material from the works of others, the undersigned has obtained any necessary permissions. See Retained Rights, below.

See Retained Rights below.

AUTHOR RESPONSIBILITIES

The IEEE distributes its technical publications throughout the world and wants to ensure that the material submitted to its publications is properly available to the readership of those publications. Authors must ensure that their Work meets the requirements as stated in section 8.2.1 of the IEEE PSPB Operations Manual, including provisions covering originality, authorship, author responsibilities and author misconduct. More information on IEEE's publishing policies may be found at <http://www.ieee.org/web/publications/pubtoolsandpolicy/info/index.html>. Authors are advised especially of IEEE PSPB Operations Manual section 8.2.1.B.12: "It is the responsibility of the authors, not the IEEE, to determine whether disclosure of their material requires the prior consent of other parties and, if so, to obtain it." Authors are also advised of IEEE PSPB Operations Manual section 8.1.1B: "Statements and opinions given in work published by the IEEE are the expression of the authors."

RETAINED RIGHTS/TERMS AND CONDITIONS

1. Authors/employers retain all proprietary rights in any process, procedure, or article of manufacture described in the Work.
2. Authors/employers may reproduce or authorize others to reproduce The Work, material extracted verbatim from the Work, or derivative works to the extent permissible under United States law for works authored by U.S. Government employees, and for the author's personal use or for company or organizational use, provided that the source and any IEEE copyright notice are indicated, the copies are not used in any way that implies IEEE endorsement of a product or service of any employer, and the copies themselves are not offered for sale.
3. Authors/employers may make limited distribution of all or portions of the Work prior to publication if they inform the IEEE in advance of the nature and extent of such limited distribution.
4. In the case of a Work performed under a U.S. Government contract or grant, the IEEE recognizes that the U.S. Government has royalty-free permission to reproduce all or portions of the Work, and to authorize others to do so, for official U.S. Government purposes only, if the contract/grant so requires.
5. For all uses not covered by items 2, 3, and 4, authors/employers must request permission from the IEEE Intellectual Property Rights office to reproduce or authorize the reproduction of the Work or material extracted verbatim from the Work, including figures and tables.
6. Although authors are permitted to re-use all or portions of the Work in other works, this does not include granting third-party requests for reprinting, republishing, or other types of re-use. The IEEE Intellectual Property Rights office must handle all such third-party

requests.

INFORMATION FOR AUTHORS

IEEE Copyright Ownership

It is the formal policy of the IEEE to own the copyrights to all copyrightable material in its technical publications and to the individual contributions contained therein, in order to protect the interests of the IEEE, its authors and their employers, and, at the same time, to facilitate the appropriate re-use of this material by others. The IEEE distributes its technical publications throughout the world and does so by various means such as hard copy, microfiche, microfilm, and electronic media. It also abstracts and may translate its publications, and articles contained therein, for inclusion in various compendiums, collective works, databases and similar publications.

Author/Employer Rights

If you are employed and prepared the Work on a subject within the scope of your employment, the copyright in the Work belongs to your employer as a work-for-hire. In that case, the IEEE assumes that when you sign this Form, you are authorized to do so by your employer and that your employer has consented to the transfer of copyright, to the representation and warranty of publication rights, and to all other terms and conditions of this Form. If such authorization and consent has not been given to you, an authorized representative of your employer should sign this Form as the Author.

Reprint/Replication Policy

The IEEE requires that the consent of the first-named author and employer be sought as a condition to granting reprint or republication rights to others or for permitting use of a Work for promotion or marketing purposes.

GENERAL TERMS

1. The undersigned represents that he/she has the power and authority to make and execute this assignment.
2. The undersigned agrees to indemnify and hold harmless the IEEE from any damage or expense that may arise in the event of a breach of any of the warranties set forth above.
3. In the event the above work is not accepted and published by the IEEE or is withdrawn by the author(s) before acceptance by the IEEE, the foregoing copyright transfer shall become null and void and all materials embodying the Work submitted to the IEEE will be destroyed.
4. For jointly authored Works, all joint authors should sign, or one of the authors should sign as authorized agent for the others.

Yaoping Hu

Author/Authorized Agent For Joint Authors

19-12-2008

Date(dd-mm-yy)

PLEASE DIRECT ALL QUESTIONS ABOUT THIS FORM TO:

Manager, IEEE Intellectual Property Rights Office, 445 Hoes Lane, P.O. Box 1331, Piscataway, NJ 08855-1131.
Telephone +1 (732) 562-3966

IEEE COPYRIGHT AND CONSENT FORM

To ensure uniformity of treatment among all contributors, other forms may not be substituted for this form, nor may any wording of the form be changed. This form is intended for original material submitted to the IEEE and must accompany any such material in order to be published by the IEEE. Please read the form carefully and keep a copy for your files.

TITLE OF PAPER/ARTICLE/REPORT, INCLUDING ALL CONTENT IN ANY FORM, FORMAT, OR MEDIA (hereinafter, "The Work"): **Effects of the Alignment between a Haptic Device and Visual Display on the Perception of Object Softness**

COMPLETE LIST OF AUTHORS: **Widmer, Antoine; Hu, Yaoping**

IEEE PUBLICATION TITLE (Journal, Magazine, Conference, Book): **Transactions on Systems, Man, and Cybernetics—Part A: Systems and Humans**

COPYRIGHT TRANSFER

1. The undersigned hereby assigns to The Institute of Electrical and Electronics Engineers, Incorporated (the IEEE) all rights under copyright that may exist in and to: (a) the above Work, including any revised or expanded derivative works submitted to the IEEE by the undersigned based on the Work; and (b) any associated written or multimedia components or other enhancements accompanying the Work.

See Retained Rights below.

CONSENT AND RELEASE

2. In the event the undersigned makes a presentation based upon the Work at a conference hosted or sponsored in whole or in part by the IEEE, the undersigned, in consideration for his/her participation in the conference, hereby grants the IEEE the unlimited, worldwide, irrevocable permission to use, distribute, publish, license, exhibit, record, digitize, broadcast, reproduce and archive, in any format or medium, whether now known or hereafter developed: (a) his/her presentation and comments at the conference; (b) any written materials or multimedia files used in connection with his/her presentation; and (c) any recorded interviews of him/her (collectively, the Presentation). The permission granted includes the transcription and reproduction of the Presentation for inclusion in products sold or distributed by IEEE and live or recorded broadcast of the Presentation during or after the conference.

3. In connection with the permission granted in Section 2, the undersigned hereby grants IEEE the unlimited, worldwide, irrevocable right to use his/her name, picture, likeness, voice and biographical information as part of the advertisement, distribution and sale of products incorporating the Work or Presentation, and releases IEEE from any claim based on right of privacy or publicity.

4. The undersigned hereby warrants that the Work and Presentation (collectively, the Materials) are original and that he/she is the author of the Materials. To the extent the Materials incorporate text passages, figures, data or other material from the works of others, the undersigned has obtained any necessary permissions. Where necessary, the undersigned has obtained all third party permissions and consents to grant the license above and has provided copies of such permissions and consents to IEEE.

[] Please check this box if you do not wish to have video/audio recordings made of your conference presentation.

AUTHOR RESPONSIBILITIES

The IEEE distributes its technical publications throughout the world and wants to ensure that the material submitted to its publications is properly available to the readership of those publications. Authors must ensure that their Work meets the requirements as stated in section 8.2.1 of the IEEE PSPB Operations Manual, including provisions covering originality, authorship, author responsibilities and author misconduct. More information on IEEE's publishing policies may be found at <http://www.ieee.org/web/publications/pubtoolsandpolicyinfo/index.html>. Authors are advised especially of IEEE PSPB Operations Manual section 8.2.1.B.12: "It is the responsibility of the authors, not the IEEE, to determine whether disclosure of their material requires the prior consent of other parties and, if so, to obtain it." Authors are also advised of IEEE PSPB Operations Manual section 8.1.1B: "Statements and opinions given in work published by the IEEE are the expression of the authors."

RETAINED RIGHTS/TERMS AND CONDITIONS

1. Authors/employers retain all proprietary rights in any process, procedure, or article of manufacture described in the Work.
2. Authors/employers may reproduce or authorize others to reproduce The Work, material extracted verbatim from the Work, or derivative works to the extent permissible under United States law for works authored by U.S. Government employees, and for the author's personal use or for company or organizational use, provided that the source and any IEEE copyright notice are indicated, the copies are not used in any way that implies IEEE endorsement of a product or service of any employer, and the copies themselves are not offered for sale.
3. Authors/employers may make limited distribution of all or portions of the Work prior to publication if they inform the IEEE in advance of the nature and extent of such limited distribution.
4. In the case of a Work performed under a U.S. Government contract or grant, the IEEE recognizes that the U.S. Government has royalty-free permission to reproduce all or portions of the Work, and to authorize others to do so, for official U.S. Government purposes only, if the contract/grant so requires.
5. For all uses not covered by items 2, 3, and 4, authors/employers must request permission from the IEEE Intellectual Property Rights office to reproduce or authorize the reproduction of the Work or material extracted verbatim from the Work, including figures and tables.
6. Although authors are permitted to re-use all or portions of the Work in other works, this does not include granting third-party requests for reprinting, republishing, or other types of re-use. The IEEE Intellectual Property Rights office must handle all such third-party requests.

INFORMATION FOR AUTHORS

IEEE Copyright Ownership

It is the formal policy of the IEEE to own the copyrights to all copyrightable material in its technical publications and to the individual contributions contained therein, in order to protect the interests of the IEEE, its authors and their employers, and, at the same time, to facilitate the appropriate re-use of this material by others. The IEEE distributes its technical publications throughout the world and does so by various means such as hard copy, microfiche, microfilm, and electronic media. It also abstracts and may translate its publications, and articles contained therein, for inclusion in various compendiums, collective works, databases and similar publications.

Author/Employer Rights

If you are employed and prepared the Work on a subject within the scope of your employment, the copyright in the Work belongs to your employer as a work-for-hire. In that case, the IEEE assumes that when you sign this Form, you are authorized to do so by your employer and that your employer has consented to the transfer of copyright, to the representation and warranty of publication rights, and to all other terms and conditions of this Form. If such authorization and consent has not been given to you, an authorized representative of your employer should sign this Form as the Author.

Reprint/Republishing Policy

The IEEE requires that the consent of the first-named author and employer be sought as a condition to granting reprint or republication rights to others or for permitting use of a Work for promotion or marketing purposes.

GENERAL TERMS

1. The undersigned represents that he/she has the power and authority to make and execute this assignment.
2. The undersigned agrees to indemnify and hold harmless the IEEE from any damage or expense that may arise in the event of a breach of any of the warranties set forth above.
3. In the event the above work is not accepted and published by the IEEE or is withdrawn by the author(s) before acceptance by the IEEE, the foregoing copyright transfer shall become null and void and all materials embodying the Work submitted to the IEEE will be destroyed.
4. For jointly authored Works, all joint authors should sign, or one of the authors should sign as authorized agent for the others.

Yaoping Hu

26-01-2010

IEEE COPYRIGHT AND CONSENT FORM

To ensure uniformity of treatment among all contributors, other forms may not be substituted for this form, nor may any wording of the form be changed. This form is intended for original material submitted to the IEEE and must accompany any such material in order to be published by the IEEE. Please read the form carefully and keep a copy for your files.

TITLE OF PAPER/ARTICLE/REPORT, INCLUDING ALL CONTENT IN ANY FORM, FORMAT, OR MEDIA (hereinafter, "The Work"): **A Viscoelastic Model of a Breast Phantom for Real-Time Palpation**

COMPLETE LIST OF AUTHORS: **Antoine Widmer, Yaoping Hu**

IEEE PUBLICATION TITLE (Journal, Magazine, Conference, Book): **33rd Annual International IEEE EMBS Conference, August 30 - September 3, 2011, Boston Marriott Copley Place, Boston, MA, USA**

COPYRIGHT TRANSFER

1. The undersigned hereby assigns to The Institute of Electrical and Electronics Engineers, Incorporated (the "IEEE") all rights under copyright that may exist in and to: (a) the above Work, including any revised or expanded derivative works submitted to the IEEE by the undersigned based on the Work; and (b) any associated written or multimedia components or other enhancements accompanying the Work.

CONSENT AND RELEASE

2. In the event the undersigned makes a presentation based upon the Work at a conference hosted or sponsored in whole or in part by the IEEE, the undersigned, in consideration for his/her participation in the conference, hereby grants the IEEE the unlimited, worldwide, irrevocable permission to use, distribute, publish, license, exhibit, record, digitize, broadcast, reproduce and archive, in any format or medium, whether now known or hereafter developed: (a) his/her presentation and comments at the conference; (b) any written materials or multimedia files used in connection with his/her presentation; and (c) any recorded interviews of him/her (collectively, the "Presentation"). The permission granted includes the transcription and reproduction of the Presentation for inclusion in products sold or distributed by IEEE and live or recorded broadcast of the Presentation during or after the conference.

3. In connection with the permission granted in Section 2, the undersigned hereby grants IEEE the unlimited, worldwide, irrevocable right to use his/her name, picture, likeness, voice and biographical information as part of the advertisement, distribution and sale of products incorporating the Work or Presentation, and releases IEEE from any claim based on right of privacy or publicity.

4. The undersigned hereby warrants that the Work and Presentation (collectively, the "Materials") are original and that he/she is the author of the Materials. To the extent the Materials incorporate text passages, figures, data or other material from the works of others, the undersigned has obtained any necessary permissions. Where necessary, the undersigned has obtained all third party permissions and consents to grant the license above and has provided copies of such permissions and consents to IEEE.

☐ Please check this box if you do not wish to have video/audio recordings made of your conference presentation.

See below for Retained Rights/Terms and Conditions, and Author Responsibilities.

AUTHOR RESPONSIBILITIES

The IEEE distributes its technical publications throughout the world and wants to ensure that the material submitted to its publications is properly available to the readership of those publications. Authors must ensure that their Work meets the requirements as stated in section 8.2.1 of the IEEE

PSPB Operations Manual, including provisions covering originality, authorship, author responsibilities and author misconduct. More information on IEEE's publishing policies may be found at http://www.ieee.org/publications_standards/publications/rights/pub_tools_policies.html. Authors are advised especially of IEEE PSPB Operations Manual section 8.2.1.B12: "It is the responsibility of the authors, not the IEEE, to determine whether disclosure of their material requires the prior consent of other parties and, if so, to obtain it." Authors are also advised of IEEE PSPB Operations Manual section 8.1.1B: "Statements and opinions given in work published by the IEEE are the expression of the authors."

RETAINED RIGHTS/TERMS AND CONDITIONS

General

1. Authors/employers retain all proprietary rights in any process, procedure, or article of manufacture described in the Work.
2. Authors/employers may reproduce or authorize others to reproduce the Work, material extracted verbatim from the Work, or derivative works for the author's personal use or for company use, provided that the source and the IEEE copyright notice are indicated, the copies are not used in any way that implies IEEE endorsement of a product or service of any employer, and the copies themselves are not offered for sale.
3. In the case of a Work performed under a U.S. Government contract or grant, the IEEE recognizes that the U.S. Government has royalty-free permission to reproduce all or portions of the Work, and to authorize others to do so, for official U.S. Government purposes only, if the contract/grant so requires.
4. Although authors are permitted to re-use all or portions of the Work in other works, this does not include granting third-party requests for reprinting, republishing, or other types of re-use. The IEEE Intellectual Property Rights office must handle all such third-party requests.
5. Authors whose work was performed under a grant from a government funding agency are free to fulfill any deposit mandates from that funding agency.

Author Online Use

6. **Personal Servers.** Authors and/or their employers shall have the right to post the accepted version of IEEE-copyrighted articles on their own personal servers or the servers of their institutions or employers without permission from IEEE, provided that the posted version includes a prominently displayed IEEE copyright notice and, when published, a full citation to the original IEEE publication, including a link to the article abstract in IEEE Xplore. Authors shall not post the final, published versions of their papers.
7. **Classroom or Internal Training Use.** An author is expressly permitted to post any portion of the accepted version of his/her own IEEE-copyrighted articles on the authors personal web site or the servers of the authors institution or company in connection with the authors teaching, training, or work responsibilities, provided that the appropriate copyright, credit, and reuse notices appear prominently with the posted material. Examples of permitted uses are lecture materials, course packs, e-reserves, conference presentations, or in-house training courses.
8. **Electronic Preprints.** Before submitting an article to an IEEE publication, authors frequently post their manuscripts to their own web site, their employers site, or to another server that invites constructive comment from colleagues. Upon submission of an article to IEEE, an author is required to transfer copyright in the article to IEEE, and the author must update any previously posted version of the article with a prominently displayed IEEE copyright notice. Upon publication of an article by the IEEE, the author must replace any previously posted electronic versions of the article with either (1) the full citation to the IEEE work with a Digital Object Identifier (DOI) or link to the article abstract in IEEE Xplore, or (2) the accepted version only (not the IEEE-published version), including the IEEE copyright notice and full citation, with a link to the final, published article in IEEE Xplore.

INFORMATION FOR AUTHORS

IEEE Copyright Ownership

It is the formal policy of the IEEE to own the copyrights to all copyrightable material in its technical publications and to the individual contributions contained therein, in order to protect the interests of the IEEE, its authors and their employers, and, at the same time, to facilitate the appropriate re-use of this material by others. The IEEE distributes its technical publications throughout the world and does so by various means such as hard copy, microfiche, microfilm, and electronic media. It also abstracts and may translate its publications, and articles contained therein, for inclusion in various compendiums, collective works, databases and similar publications.

Author/Employer Rights

If you are employed and prepared the Work on a subject within the scope of your employment, the copyright in the Work belongs to your employer as a work-for-hire. In that case, the IEEE assumes that when you sign this Form, you are authorized to do so by your employer and that your employer has consented to the transfer of copyright, to the representation and warranty of publication rights, and to all other terms and conditions of this Form. If such authorization and consent has not been given to you, an authorized representative of your employer should sign this Form as the Author.

GENERAL TERMS

1. The undersigned represents that he/she has the power and authority to make and execute this form.
2. The undersigned agrees to indemnify and hold harmless the IEEE from any damage or expense that may arise in the event of a breach of any of the warranties set forth above.
3. In the event the above work is not accepted and published by the IEEE or is withdrawn by the author(s) before acceptance by the IEEE, the foregoing grant of rights shall become null and void and all materials embodying the Work submitted to the IEEE will be destroyed.
4. For jointly authored Works, all joint authors should sign, or one of the authors should sign as authorized agent for the others.

Y. Hu

Author/Authorized Agent For Joint Authors

15-06-2011

Date(dd-mm-yy)

THIS FORM MUST ACCOMPANY THE SUBMISSION OF THE AUTHOR'S MANUSCRIPT.

Questions about the submission of the form or manuscript must be sent to the publication's editor. Please direct all questions about IEEE copyright policy to:

IEEE Intellectual Property Rights Office, copyrights@ieee.org, +1-732-562-3966 (telephone)

IEEE COPYRIGHT AND CONSENT FORM

To ensure uniformity of treatment among all contributors, other forms may not be substituted for this form, nor may any wording of the form be changed. This form is intended for original material submitted to the IEEE and must accompany any such material in order to be published by the IEEE. Please read the form carefully and keep a copy for your files.

TITLE OF PAPER/ARTICLE/REPORT, INCLUDING ALL CONTENT IN ANY FORM, FORMAT, OR MEDIA (hereinafter, "The Work"): **An evaluation method for real-time soft-tissue model used for multi-vertex palpation**

COMPLETE LIST OF AUTHORS: **Antoine Widmer, Yaoping Hu**

IEEE PUBLICATION TITLE (Journal, Magazine, Conference, Book): **Proceedings of the 2011 IEEE International Conference on Systems, Man, and Cybernetics**

COPYRIGHT TRANSFER

1. The undersigned hereby assigns to The Institute of Electrical and Electronics Engineers, Incorporated (the "IEEE") all rights under copyright that may exist in and to: (a) the above Work, including any revised or expanded derivative works submitted to the IEEE by the undersigned based on the Work; and (b) any associated written or multimedia components or other enhancements accompanying the Work.

CONSENT AND RELEASE

2. In the event the undersigned makes a presentation based upon the Work at a conference hosted or sponsored in whole or in part by the IEEE, the undersigned, in consideration for his/her participation in the conference, hereby grants the IEEE the unlimited, worldwide, irrevocable permission to use, distribute, publish, license, exhibit, record, digitize, broadcast, reproduce and archive, in any format or medium, whether now known or hereafter developed: (a) his/her presentation and comments at the conference; (b) any written materials or multimedia files used in connection with his/her presentation; and (c) any recorded interviews of him/her (collectively, the "Presentation"). The permission granted includes the transcription and reproduction of the Presentation for inclusion in products sold or distributed by IEEE and live or recorded broadcast of the Presentation during or after the conference.

3. In connection with the permission granted in Section 2, the undersigned hereby grants IEEE the unlimited, worldwide, irrevocable right to use his/her name, picture, likeness, voice and biographical information as part of the advertisement, distribution and sale of products incorporating the Work or Presentation, and releases IEEE from any claim based on right of privacy or publicity.

4. The undersigned hereby warrants that the Work and Presentation (collectively, the "Materials") are original and that he/she is the author of the Materials. To the extent the Materials incorporate text passages, figures, data or other material from the works of others, the undersigned has obtained any necessary permissions. Where necessary, the undersigned has obtained all third party permissions and consents to grant the license above and has provided copies of such permissions and consents to IEEE.

☐ Please check this box if you do not wish to have video/audio recordings made of your conference presentation.

See below for Retained Rights/Terms and Conditions, and Author Responsibilities.

AUTHOR RESPONSIBILITIES

The IEEE distributes its technical publications throughout the world and wants to ensure that the material submitted to its publications is properly available to the readership of those publications. Authors must ensure that their Work meets the requirements as stated in section 8.2.1 of the IEEE

PSPB Operations Manual, including provisions covering originality, authorship, author responsibilities and author misconduct. More information on IEEE's publishing policies may be found at http://www.ieee.org/publications_standards/publications/rights/pub_tools_policies.html. Authors are advised especially of IEEE PSPB Operations Manual section 8.2.1.B12: "It is the responsibility of the authors, not the IEEE, to determine whether disclosure of their material requires the prior consent of other parties and, if so, to obtain it." Authors are also advised of IEEE PSPB Operations Manual section 8.1.1B: "Statements and opinions given in work published by the IEEE are the expression of the authors."

RETAINED RIGHTS/TERMS AND CONDITIONS

General

1. Authors/employers retain all proprietary rights in any process, procedure, or article of manufacture described in the Work.
2. Authors/employers may reproduce or authorize others to reproduce the Work, material extracted verbatim from the Work, or derivative works for the author's personal use or for company use, provided that the source and the IEEE copyright notice are indicated, the copies are not used in any way that implies IEEE endorsement of a product or service of any employer, and the copies themselves are not offered for sale.
3. In the case of a Work performed under a U.S. Government contract or grant, the IEEE recognizes that the U.S. Government has royalty-free permission to reproduce all or portions of the Work, and to authorize others to do so, for official U.S. Government purposes only, if the contract/grant so requires.
4. Although authors are permitted to re-use all or portions of the Work in other works, this does not include granting third-party requests for reprinting, republishing, or other types of re-use. The IEEE Intellectual Property Rights office must handle all such third-party requests.
5. Authors whose work was performed under a grant from a government funding agency are free to fulfill any deposit mandates from that funding agency.

Author Online Use

6. **Personal Servers.** Authors and/or their employers shall have the right to post the accepted version of IEEE-copyrighted articles on their own personal servers or the servers of their institutions or employers without permission from IEEE, provided that the posted version includes a prominently displayed IEEE copyright notice and, when published, a full citation to the original IEEE publication, including a link to the article abstract in IEEE Xplore. Authors shall not post the final, published versions of their papers.
7. **Classroom or Internal Training Use.** An author is expressly permitted to post any portion of the accepted version of his/her own IEEE-copyrighted articles on the authors personal web site or the servers of the authors institution or company in connection with the authors teaching, training, or work responsibilities, provided that the appropriate copyright, credit, and reuse notices appear prominently with the posted material. Examples of permitted uses are lecture materials, course packs, e-reserves, conference presentations, or in-house training courses.
8. **Electronic Preprints.** Before submitting an article to an IEEE publication, authors frequently post their manuscripts to their own web site, their employers site, or to another server that invites constructive comment from colleagues. Upon submission of an article to IEEE, an author is required to transfer copyright in the article to IEEE, and the author must update any previously posted version of the article with a prominently displayed IEEE copyright notice. Upon publication of an article by the IEEE, the author must replace any previously posted electronic versions of the article with either (1) the full citation to the IEEE work with a Digital Object Identifier (DOI) or link to the article abstract in IEEE Xplore, or (2) the accepted version only (not the IEEE-published version), including the IEEE copyright notice and full citation, with a link to the final, published article in IEEE Xplore.

INFORMATION FOR AUTHORS

IEEE Copyright Ownership

It is the formal policy of the IEEE to own the copyrights to all copyrightable material in its technical publications and to the individual contributions contained therein, in order to protect the interests of the IEEE, its authors and their employers, and, at the same time, to facilitate the appropriate re-use of this material by others. The IEEE distributes its technical publications throughout the world and does so by various means such as hard copy, microfiche, microfilm, and electronic media. It also abstracts and may translate its publications, and articles contained therein, for inclusion in various compendiums, collective works, databases and similar publications.

Author/Employer Rights

If you are employed and prepared the Work on a subject within the scope of your employment, the copyright in the Work belongs to your employer as a work-for-hire. In that case, the IEEE assumes that when you sign this Form, you are authorized to do so by your employer and that your employer has consented to the transfer of copyright, to the representation and warranty of publication rights, and to all other terms and conditions of this Form. If such authorization and consent has not been given to you, an authorized representative of your employer should sign this Form as the Author.

GENERAL TERMS

1. The undersigned represents that he/she has the power and authority to make and execute this form.
2. The undersigned agrees to identify and hold harmless the IEEE from any damage or expense that may arise in the event of a breach of any of the warranties set forth above.
3. In the event the above work is not accepted and published by the IEEE or is withdrawn by the author(s) before acceptance by the IEEE, the foregoing grant of rights shall become null and void and all materials embodying the Work submitted to the IEEE will be destroyed.
4. For jointly authored Works, all joint authors should sign, or one of the authors should sign as authorized agent for the others.

Yaoping Hu

Author/Authorized Agent For Joint Authors

04-07-2011

Date(dd-mm-yy)

THIS FORM MUST ACCOMPANY THE SUBMISSION OF THE AUTHOR'S MANUSCRIPT.

Questions about the submission of the form or manuscript must be sent to the publication's editor. Please direct all questions about IEEE copyright policy to:

IEEE Intellectual Property Rights Office, copyrights@ieee.org, +1-732-562-3966 (telephone)

IEEE COPYRIGHT AND CONSENT FORM

To ensure uniformity of treatment among all contributors, other forms may not be substituted for this form, nor may any wording of the form be changed. This form is intended for original material submitted to the IEEE and must accompany any such material in order to be published by the IEEE. Please read the form carefully and keep a copy for your files.

TITLE OF PAPER/ARTICLE/REPORT, INCLUDING ALL CONTENT IN ANY FORM, FORMAT, OR MEDIA (hereinafter, "The Work"): **Human Constraints for Softness Perception during Real-Time Palpation**

COMPLETE LIST OF AUTHORS: **Widmer, Antoine; Hu, Yaoping**

IEEE PUBLICATION TITLE (Journal, Magazine, Conference, Book): **Transactions on Haptics**

COPYRIGHT TRANSFER

1. The undersigned hereby assigns to The Institute of Electrical and Electronics Engineers, Incorporated (the "IEEE") all rights under copyright that may exist in and to: (a) the above Work, including any revised or expanded derivative works submitted to the IEEE by the undersigned based on the Work; and (b) any associated written or multimedia components or other enhancements accompanying the Work.

CONSENT AND RELEASE

2. In the event the undersigned makes a presentation based upon the Work at a conference hosted or sponsored in whole or in part by the IEEE, the undersigned, in consideration for his/her participation in the conference, hereby grants the IEEE the unlimited, worldwide, irrevocable permission to use, distribute, publish, license, exhibit, record, digitize, broadcast, reproduce and archive, in any format or medium, whether now known or hereafter developed: (a) his/her presentation and comments at the conference; (b) any written materials or multimedia files used in connection with his/her presentation; and (c) any recorded interviews of him/her (collectively, the "Presentation"). The permission granted includes the transcription and reproduction of the Presentation for inclusion in products sold or distributed by IEEE and live or recorded broadcast of the Presentation during or after the conference.

3. In connection with the permission granted in Section 2, the undersigned hereby grants IEEE the unlimited, worldwide, irrevocable right to use his/her name, picture, likeness, voice and biographical information as part of the advertisement, distribution and sale of products incorporating the Work or Presentation, and releases IEEE from any claim based on right of privacy or publicity.

4. The undersigned hereby warrants that the Work and Presentation (collectively, the "Materials") are original and that he/she is the author of the Materials. To the extent the Materials incorporate text passages, figures, data or other material from the works of others, the undersigned has obtained any necessary permissions. Where necessary, the undersigned has obtained all third party permissions and consents to grant the license above and has provided copies of such permissions and consents to IEEE.

☐ Please check this box if you do not wish to have video/audio recordings made of your conference presentation.

See below for Retained Rights/Terms and Conditions, and Author Responsibilities.

AUTHOR RESPONSIBILITIES

The IEEE distributes its technical publications throughout the world and wants to ensure that the material submitted to its publications is properly available to the readership of those publications. Authors must ensure that their Work meets the requirements as stated in section 8.2.1 of the IEEE PSPB Operations Manual, including provisions covering originality, authorship, author responsibilities and author misconduct. More information on

IEEE's publishing policies may be found at http://www.ieee.org/publications_standards/publications/rights/pub_tools_policies.html. Authors are advised especially of IEEE PSPB Operations Manual section 8.2.1.B12: "It is the responsibility of the authors, not the IEEE, to determine whether disclosure of their material requires the prior consent of other parties and, if so, to obtain it." Authors are also advised of IEEE PSPB Operations Manual section 8.1.1B: "Statements and opinions given in work published by the IEEE are the expression of the authors."

RETAINED RIGHTS/TERMS AND CONDITIONS

General

1. Authors/employers retain all proprietary rights in any process, procedure, or article of manufacture described in the Work.
2. Authors/employers may reproduce or authorize others to reproduce the Work, material extracted verbatim from the Work, or derivative works for the author's personal use or for company use, provided that the source and the IEEE copyright notice are indicated, the copies are not used in any way that implies IEEE endorsement of a product or service of any employer, and the copies themselves are not offered for sale.
3. In the case of a Work performed under a U.S. Government contract or grant, the IEEE recognizes that the U.S. Government has royalty-free permission to reproduce all or portions of the Work, and to authorize others to do so, for official U.S. Government purposes only, if the contract/grant so requires.
4. Although authors are permitted to re-use all or portions of the Work in other works, this does not include granting third-party requests for reprinting, republishing, or other types of re-use. The IEEE Intellectual Property Rights office must handle all such third-party requests.
5. Authors whose work was performed under a grant from a government funding agency are free to fulfill any deposit mandates from that funding agency.

Author Online Use

6. **Personal Servers.** Authors and/or their employers shall have the right to post the accepted version of IEEE-copyrighted articles on their own personal servers or the servers of their institutions or employers without permission from IEEE, provided that the posted version includes a prominently displayed IEEE copyright notice and, when published, a full citation to the original IEEE publication, including a link to the article abstract in IEEE Xplore. Authors shall not post the final, published versions of their papers.
7. **Classroom or Internal Training Use.** An author is expressly permitted to post any portion of the accepted version of his/her own IEEE-copyrighted articles on the authors personal web site or the servers of the authors institution or company in connection with the authors teaching, training, or work responsibilities, provided that the appropriate copyright, credit, and reuse notices appear prominently with the posted material. Examples of permitted uses are lecture materials, course packs, e-reserves, conference presentations, or in-house training courses.
8. **Electronic Preprints.** Before submitting an article to an IEEE publication, authors frequently post their manuscripts to their own web site, their employers site, or to another server that invites constructive comment from colleagues. Upon submission of an article to IEEE, an author is required to transfer copyright in the article to IEEE, and the author must update any previously posted version of the article with a prominently displayed IEEE copyright notice. Upon publication of an article by the IEEE, the author must replace any previously posted electronic versions of the article with either (1) the full citation to the IEEE work with a Digital Object Identifier (DOI) or link to the article abstract in IEEE Xplore, or (2) the accepted version only (not the IEEE-published version), including the IEEE copyright notice and full citation, with a link to the final, published article in IEEE Xplore.

INFORMATION FOR AUTHORS

IEEE Copyright Ownership

It is the formal policy of the IEEE to own the copyrights to all copyrightable material in its technical publications and to the individual contributions contained therein, in order to protect the interests of the IEEE, its authors and their employers, and, at the same time, to facilitate the appropriate re-

use of this material by others. The IEEE distributes its technical publications throughout the world and does so by various means such as hard copy, microfiche, microfilm, and electronic media. It also abstracts and may translate its publications, and articles contained therein, for inclusion in various compendiums, collective works, databases and similar publications.

Author/Employer Rights

If you are employed and prepared the Work on a subject within the scope of your employment, the copyright in the Work belongs to your employer as a work-for-hire. In that case, the IEEE assumes that when you sign this Form, you are authorized to do so by your employer and that your employer has consented to the transfer of copyright, to the representation and warranty of publication rights, and to all other terms and conditions of this Form. If such authorization and consent has not been given to you, an authorized representative of your employer should sign this Form as the Author.

GENERAL TERMS

1. The undersigned represents that he/she has the power and authority to make and execute this form.
2. The undersigned agrees to identify and hold harmless the IEEE from any damage or expense that may arise in the event of a breach of any of the warranties set forth above.
3. In the event the above work is not accepted and published by the IEEE or is withdrawn by the author(s) before acceptance by the IEEE, the foregoing grant of rights shall become null and void and all materials embodying the Work submitted to the IEEE will be destroyed.
4. For jointly authored Works, all joint authors should sign, or one of the authors should sign as authorized agent for the others.

Yaoping Hu

Author/Authorized Agent For Joint Authors

05-06-2012

Date(dd-mm-yy)

THIS FORM MUST ACCOMPANY THE SUBMISSION OF THE AUTHOR'S MANUSCRIPT.

Questions about the submission of the form or manuscript must be sent to the publication's editor. Please direct all questions about IEEE copyright policy to:

IEEE Intellectual Property Rights Office, copyrights@ieee.org, +1-732-562-3966 (telephone)